Research for Advanced Concept Development (RACeD)
Doctorate Programme Project on
Electromagnetic Test Framework for
Wireless Network Services in Vehicles

Detecting from in-vehicle at the physical layer a smart device spatial location via 2.4 GHz SRD RF services

Innovation Report

by

Vlad Alexandru Marsic

A thesis submitted in partial fulfilment of the requirements for the degree of Doctor of Engineering

WMG, University of Warwick

9th March 2022

Abstract

Detecting the position of a smartphone over a short range outside and inside a vehicle through its secondary radio frequency (RF) services is a difficult task, with various trials and tests employing Wi-Fi, Bluetooth Low Energy (BLE), and Near Field Communication (NFC) suggesting possible solutions using forthcoming services to be introduced, such as the ultra-wide band (UWB) radio or the IEEE 802.15.4 standard. This thesis addresses the modern radio location problem of inside-outside position location for a mobile RF source by proposing an empirical solution that is based on the 2.4 GHz IEEE 802.15.4 standard. For a proof-of-concept scenario involving a static vehicle with its side windows down and no passenger presence, this work derived an offline calculation based on empirical measurements demonstrating that four directive, inside-orientated sensors can be sufficient to produce a 100% successful inside-outside RF position discrimination. Furthermore, by adding four more RF directive sensors pointing towards outside, it was possible to detect on a radius of up to 5 m around the vehicle the variable location of a mobile RF source within a root mean square error (RMSE) of up to ±1.4 m outside and ±0.4 m inside the vehicle. The demonstrated experimental RF ranging is based solely on the received signal strength indicator (RSSI) and the individual sensor's directivity achieved through shielding. The results rely on an RSSI fingerprinting database derived from only empirical outdoor measurements, delivering a consistent performance inside the highly RF-reflective vehicle cabin by exploiting the sensor position and directivity and suggesting that a focus on the front of each seat may avoid future human interference. Moreover, a theoretical propagation model based on Friis' transmission equation constructed on system parameters shows a high correlation with the RSSI fingerprinting experimental model, thus supporting the consistency of the empirical model. The directive RF sensors used in the experimental work were refined based on ray tracing (RT) simulation suggestions so as to display an optimal discrimination of targets on a convex open volume such as a vehicle cabin.

To summarise, this EngD successfully demonstrated a 2.4 GHz RF location system based on the IEEE 802.15.4 standard with direct applications in RF detection, such as the restricted entrance scenario employed in vehicle and smart infrastructure industry.

Acknowledgements

I would like to thank my supervisors, Dr Matthew D. Higgins and Dr Erik Kampert, for their fantastic guidance and help through this project, combining their great technical knowledge with patience, inducing an enjoyable “can do” working environment.

A very special thank you goes to my supervisor Prof Paul Jennings for supporting and encouraging me in the EngD programme and beyond.

I am grateful to Dhadyalla Gunwant and Andrew D. Moore for their great advice and technical insights, to my colleague and friend Liz James for her brilliant knowledge sharing and sense of humour, and to everybody from the Research for Advanced Concept Development (RACeD) Doctorate Programme group, Rob, Joseph and Arun for being there when needed.

I would also like to thank my Jaguar Land Rover supervisory team, Tom Mizutani, Dr Joshi Harita, David Oxtoby and Dr Alex Mouzakitis for their help and tact throughout the EngD project. A special thanks goes to Dr Emma Kowalczuk for sharing FEKO technical simulation data, and to Mark Allen for providing CAD vehicle design insights.

I would like to thank my examination team, Dr Andrew McGordon, Dr Qasim Ahmed and Dr Jonathan Rigelsford, for their insightful observations and suggestions on the presentation, content and target delivery of this work.

I would also like to offer special thanks to Jaguar Land Rover, WMG and the University of Warwick for funding and supporting this project.

I am grateful to my wonderful parents Simona and Adrian Marsic, and my close family members, Crenguta and Bogdan Vasiliu, Ana and Adrian Radu, Maricica and Ionel Puscasu for their understanding and support.

Last but not least, I would like to thank my wonderful wife Georgiana Marsic, for her help, support, kindness and unconditional understanding, making the EngD possible and putting up with me as a student for so many years.

Declaration

I confirm that the work presented in this report is my own unless otherwise stated. This work has not been previously submitted for any other degree.

Vlad A. Marsic

9th March 2022

Table of Contents

Glossary of Terms

Abbreviation	Description
1D	One dimensional
2D	Two dimensional
3D	Three dimensional
ACA	Adaptive Cross Approximation
AIM	Adaptive Integral Method
ANT	Advanced and Adaptive Network Technology
AoA	Angle of Arrival
BEM	Boundary Element Method
BER	Bit Error Rate
BLE	Bluetooth Low Energy
BT	Bluetooth
CAD	Computer Aided Design
CEM	Computational Electromagnetic Methods
CFIE	Combined-Field Integral Equation
CFL	Courant–Friedrichs–Lewy
CG	Conjugate Gradient
CGFFT	Conjugate Gradient-Fast Fourier Transform
CNC	Computer Numerical Control
CPU	Central Processing Unit
CRC	Cyclic Redundancy Checks
DAE	Digital Asset Exchange
DoA	Direction of Arrival
DXF	Drawing Exchange Format
EFG	Element-Free Galerkin
EFIE	Electric-Field Integral Equation
E/H	Electric Field and Magnetic Field
EM	Electromagnetic
EngD	Engineering Doctorate
FDTD	Finite Differences Time Domain
FEA	Finite Element Analysis
FEC	Forward Error Corrections
FEM	Finite Element Method
FETI	Finite Element Tearing and Interconnecting
FFT	Fast Fourier Transform
FIT	Finite Integral Method
FMM	Fast Multipole Method
FVM	Finite Volume Method
GMRES	Generalized Minimal Residual
GO	Geometrical Optics
GPS	Global Positioning System
GPU	Graphics Processing Unit
GTD	Geometrical Theory of Diffraction
HF	High Frequency

Abbreviation	Description
IGES	Initial Graphics Exchange Specification
IoT	Internet of Things
IPS	Indoor Positioning Systems
JLR	Jaguar Land Rover
LAN	Local Area Network
LBS	Location-Based Service
LIDAR	Light Detection and Ranging
LF	Low Frequency
LOS	Line Of Sight
M2M	Machine-to-Machine
MATLAB	MATrix LABoratory
MFIE	Magnetic-Field Integral Equation
MLFMM	Multilevel Fast Multipole Method
MoM	Method of Moments
MVP	Minimum Viable Product
NFER	Near Field EM Ranging
NFER	Near Field
NLOS	No Line Of Sight
OBJ	Wavefront OBJect
OEM	Original Equipment Manufacturer
Ofcom	Office of Communications
OPS	Outdoor Positioning Systems
PCB	Printed Circuit Board
PD	Phase Difference
PDE	Partial Differential Equation
PEEC	Partial Element Equivalent Circuit
PER	Packet Error Rate
PO	Physical Optics
PoA	Phase of Arrival
PTD	Physical Theory of Diffraction
PVC	Polyvinyl Chloride
RACeD	Research for Advanced Concept Development
RADC	Ring Area Data Collection
RAM	Random Access Memory
RBF	Radial Basis Function
RF	Radio Frequency
RK	Runge-Kutta
RMSE	Root Mean Square Error
RSS	Received Signal Strength
RSSI	Received Signal Strength Index
RT	Ray Tracing
RTS	Real Time System
Rx	Receiver
SDR	Software Defined Radio
SIE	Surface Integral Equation

Abbreviation	Description
SMD	Surface-Mount Device
SPH	Smooth Particle Hydrodynamics
SRD	Short-Range Device
SVM	Support Vector Machines
SVG	Scalable Vector Graphics
STEP	Standard for the Exchange of Product Data
STL	STereoLithographic
TDoA	Time Difference of Arrival
TLM	Transmission Line Method
ToF	Time of Flight
Tx	Transmitter
TTW	Through-the-wall
UTD	Uniform Theory of Diffraction
UV	Ultra Violet
V2X	Vehicle Connected to Everything
VCU	Vehicle Control Unit
VNA	Vector Network Analyser
VRML	Virtual Reality Modelling Language
WMG	Warwick Manufacturing Group

List of Tables

List of Figures

1. Introduction

1.1 Low power RF-based location services in the automotive domain

The world's dynamics are pushing civilisation towards full automation and interconnectivity. RF communication services are playing a major role in connectivity, from remote control to voice and image transmission. A world of machines, interconnected to their own Internet of Things (IoT), derived from the industrial machine-to-machine (M2M) network, is ready to go to the next level of mobility with a vehicle connected to everything (V2X), e.g., smart infrastructure, buildings and facilities, being the next evolutionary step. Machines and vehicles also need sensing functions, preferably remote and nonintrusive, and this functionality can be provided by RF location-based services (LBSs), covering from basic ranging radars and network position detection to scanning and imaging technologies.

Since RF-based services are increasingly relevant and important for the modern automotive sector, Jaguar Land Rover, an emblematic name in the car industry and representing the industrial stakeholders of this work, are looking for the best use of this technology. Alongside the general trend of developing the smart car of tomorrow, equipping the vehicles with radars, LiDARs, cameras and proximity sensors, Jaguar Land Rover is showing an active interest in research of wireless technologies capable to be exploited in cooperative adaptive cruise control, roadwork assist, mind sense, driver wellness monitoring and safe pull away [1]. The Passive Keyless Entry (PKE), or Passive Entry Passive Start (PEPS), is another RF application which can be found currently inside the standard user's car key. Although the traditional vehicle key shape has morphed over the time, from the press-button RF remote to PEPS devices based on RFID and shaped like a Fitbit bracelet [2, 3], the next envisaged evolution step is anticipated as a software key app stored on the driver's smartphone.

Other major automotive brands are investigating the applications of a smartphone-based car-key, mainly by means of Near Field Communication (NFC) [4-7], Wi-Fi or Bluetooth Low Energy (BLE) [8-10] as illustrated in **Table 1.1**. Therefore,

Table 1.1 The commercially available smartphone PKE apps used by different representative automotive manufactures, RF services used and observations

Car manufacturer	RF technology	References	Observations
Mercedes Benz	NFC	[4]	Driver discovery range low (cm range), not easy to use as a keyless hands-free system as the system requires certain spatial spots to the doors to proceed with authentication.
BMW	NFC	[5]	Same as above for NFC
Audi	NFC	[6]	Same as above for NFC
Volkswagen	NFC	[7]	Same as above for NFC
Ford	Wi-Fi	[8]	Require subscription and, Wi-Fi along with Bluetooth, being designed for high data transfer, are power demanding (if the phone app needs to stay continuously On, this will have an impact on the car and phone battery)
Tesla	Bluetooth	[9]	Same as above for Wi-Fi. If the BLE is employed for the new phones then, as technology is still on testing stage (i.e., security, app uninterrupted connection required, blank detection spots, etc.), the RFID keys are recommended in the user manual, [11], to be carried along with the smartphone. The BLE car access is also paired with doorknob pressing.
Volvo	Bluetooth	[10]	Same as above for Wi-Fi. Designed with the car share service focus, the early 2016 advertised app is still required to be very close range and used with the touch sensors in the doorknob, [12]. Currently, used for car sharing in combination with another secured device, a "red key", [13].

depending on the requirements of the employed RF technology and benefits in terms of cost and detection position accuracy, Jaguar Land Rover is keen to add it to its toolset.

The migration from a vehicle hardware key sharable between different drivers to the user's smartphone provides various advantages: it delivers a less expensive implementation, reduces the number of devices that a user needs to carry, provides driver identification and monitoring for vehicle interior personalisation and telematics insurance, and constitutes a high-end vehicle interface, for instance potentially displaying the vehicle's status, position, diagnosis and infotainment data.

Future applications such as the self-driving car or smart taxi collecting passengers from different locations and adapting to their pre-set interior needs, thus addressing expectations for disabled persons and special needs, baby car seats, pets and large luggage may benefit as well from this hardware to software migration.

Nevertheless, to facilitate this car key transition to the future smartphone will require RF hardware support integration for the contactless location system, RF services like those relying on the current Bluetooth, BLE, Wi-Fi, NFC protocols, or future services to be embedded such as those relying on protocols based on IEEE 802.15.4 like ZigBee, THREAD or Ultra Wide Band (UWB).

To conclude, a great opportunity arose to study the potential implementation of a wireless low-power service integrated in a smart device such as a smartphone, to enable automotive applications like PKE or PEPS. Since various advantages of such technology exist, choosing the right technical candidate has been the first objective of this work.

1.2 2.4 GHz IEEE 802.15.4/ZigBee versus BLE and UWB

Various studies investigating the potential of short-range RF services currently integrated in smartphones such as Bluetooth, BLE, Wi-Fi and NFC for PEPS applications have been performed without indicating a convincing winner.

Wireless technologies potentially presenting a superior location accuracy than the 2.4 GHz transceivers used with BLE, IEEE 802.15.4/ZigBee or Wi-Fi may currently be perceived as better candidates to achieve this work's RF location goals from a technical point of view. The main representative of these technologies is UWB [14] which together with its 2.4 GHz IEEE 802.15.4 standard based rivals, is going to be accommodated by the future smartphone technology as illustrated in **Figure 1.1**.

There is no uncertainty in that UWB presents a better location accuracy than 2.4 GHz based services [15-17], however its qualities may be overshadowed by its

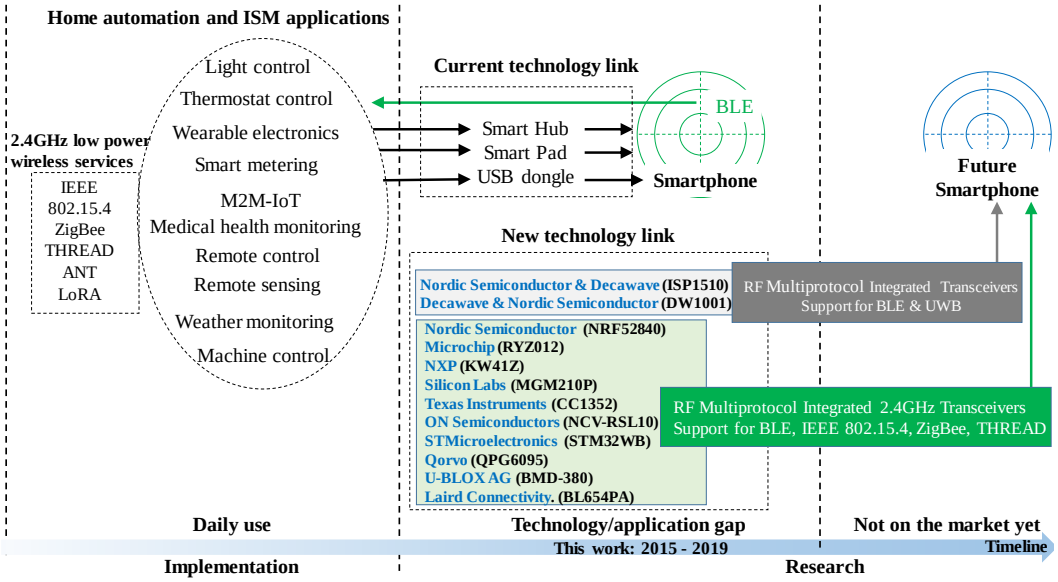

Figure 1.1 Research focus on future smartphone integrated technology for RF target location inside-outside vehicle reliant on IEEE 802.15.4 standard: 2.4 GHz multiprotocol transceiver chips, BLE, IEEE 802.15.4/ZigBee, THREAD compatible

predisposition to induce interference and get influenced by other wireless services operating in the same spectrum band [18-20]. On the network connectivity side, one may note indicators that important UWB-based projects like wireless USB (WUSB) have been officially stopped, with Linux formally depreciating the technology in its newest versions [21, 22], while Western Digital and Seagate adopted the Intel Thunderbolt standard [23] instead of UWB USB [24]. Based on an early Ofcom report prior to UWB adoption in the UK [25], it may be extrapolated that interferences with licensed and unlicensed operators represent the main problem of this technology. A December 2019 letter from Tim Harrington, the executive director of the Ultra Wide Band Alliance, to the Federal Communications Commission (FCC) reinforces this assumption, however this time the interference problems manifesting on the UWB side [26]. Since a smart vehicle accumulates wireless sensing technology vital for its telematics and infotainment, the interference between the technology and the applications for driver and passenger detection and monitoring may raise concerns for OEMs. Moreover, other important considerations include the fact that UWB is not widely spread and implemented, for instance only two main manufacturers Decawave and BlinkSight are representative for recent UWB technology [27], when compared with the mass integrated 2.4 GHz technology. Nevertheless, with UWB delivering a centimeter-scale RF position accuracy, the spatial positioning problem may lose its challenging appeal for current academic research, and become more interesting for development and deployment activities.

The market environment for short-range RF-based location services is challenging for BLE as well, however with BLE being currently integrated in smartphones and other general devices, it presents a notable advantage over UWB. At the same time, BLE actively competes on the home and industrial automation market where the UWB technology is still hesitant against current frontrunners such as IEEE 802.15.4/ZigBee, THREAD and ANT. Moreover, new challengers such as the 2.4 GHz LoRA protocol [28, 29] make this competition harder. The future of BLE and UWB is still unclear in the 5G landscape, with a good example supporting the observation regarding BLE uncertainty involving the case of Nordic Semiconductors, an iconic name for Bluetooth chip manufacturers, releasing the nRF528x series of system on chip (SoC) integrated circuits (ICs), enabling BLE, ANT, THREAD and IEEE 802.15.4/ZigBee protocols [30] that indicates a vote of confidence for IEEE 802.15.4 option rather than a separate BLE venture.

The 2.4 GHz IEEE 802.15.4 based services such as ZigBee, THREAD and ANT have proved their rugged and flexible functioning in home and industrial automation, large sensor networks, smart metering and parking occupancy detection [31]. The IEEE 802.15.4 standard is highly customisable and versatile, this property presenting an advantage against the in-house BLE protocol. Moreover, when the IEEE 802.15.4 standard will be included in smartphones, it will reinforce the direct access to currently connected smart infrastructure, making redundant the current smart hubs, such as the wireless hubs bridging the IEEE 802.15.4 based technology with Wi-Fi, Bluetooth or BLE [32, 33], smart pads such as screen integrated devices interfacing smart metering systems [34], and RF phone customised dongles [35].

To summarise, the 2.4 GHz IEEE 802.15.4 standard makes a strong candidate for the RF location study proposed by this work, delivering technological maturity while supported by a strong market [36, 37] pushing its way in the next generation of smartphones.

1.3 Limitations of implementing location-based services (LBSs) at 2.4 GHz

Although the 2.4 GHz based communication services attract a high interest, their limitations resulted from technology's substantial market penetration, inexpensive hardware and operating frequency in proximity to water molecule's natural oscillation make the LBS implementation a high challenge. The drawback arising from being widely utilised translates in a susceptibility to interferences from close functioning of similar systems. Another weakness results from the technology's inexpensive hardware, since the cost of a 2.4 GHz transceiver chip may decrease to being as low as $1.50 [38] or €1 [39] rivalling the cost of a common microcontroller, and on high volume orders representative for industry, the overall cost will reduce further. By conserving the overall low cost, the common 2.4 GHz implementations suffers from inaccurate timing induced by crystal oscillators [30] and noisy signal produced by the low noise amplifiers (LNAs) [40] since the designs present basic compensation for temperature drift. Therefore, extreme weather temperature may affect the functioning of the 2.4 GHz electronic equipment [41], in addition to the external influence of heat induced air ducting layers impacting the RF propagation [42]. Moreover, the fact that

2.4 GHz may induce resonant modes when incident on water molecules, makes this particular microwave-based technology sensible to atmospheric humidity, rain and snow [43, 44].

On the other hand, a general problem for LBSs is the dependency on infrastructure, the indoor positioning systems (IPS) best outlining the RF location service and construction relationship [15]. These characteristics of LBSs add subjectivity to any comparison between separate studies due to the specific structural factors present in each work.

An overall conclusion on limitations of LBS implementations at 2.4 GHz is that the experimental setup employed for the proof-of-concept empirical investigation of the above-mentioned technology will need to prevent data contamination resulted from the discussed factors. The countermeasures will require a short-range RF setup to prevent operations at the highest receiver sensitivity when any influence may translate in reception drop. Moreover, a careful selection of the outdoor environment for experiments will involve RF tests at similar temperatures, hours, avoiding high temperatures and atmospheric humidity. In addition, if building structures may not be avoided since they are representative for the modern city configuration of in-vehicle test scenarios, it will be recommended that their presence is at the limits of the pre-set short RF range, reducing their overall influence through this measure.

1.4 RF location accuracy and relevance of the proposed solution

1.4.1 RF location accuracy for 2.4 GHz low power independent services

Multi-sensor fusion incorporates a wide area of applications and domains, from fusions encountered at one system level such as a robot, to large communication networks such as IoT as a conglomerate of various domains like traffic and vehicles, industrial automation, metering, etc. [45-50]. Besides various classifications of sensor categories, fusion types, data sources, processing levels, etc., when investigating absolute accuracy [51], this RF location work refers to the main multiple-sensors data fusion classification: complementary, competitive and cooperative. In the complementary category, each sensor monitors a different region of an area, and the cumulative data produces the survey picture of the area. For competitive sensing, each

sensor measures the same target, with the combined data reducing the uncertainty of individual measurements, whereas in cooperative measurements, the data is combined to deliver new information, for instance multiple cameras providing 3D or stereoscopic perspectives. To determine the performance measurement for a certain technology involves investigating the data for an independent system representative of that technology, for instance a sensor node from a large network of identical nodes. This type of independent or non-cooperative measurement will be investigated for the 2.4 GHz low power services and placed in a general context to determine its performance. **Table 1.2** captures the state-of-the-art accuracy and range for the most common non-cooperative LBSs, based on latest evidence delivered by the research and industry domains [15, 16, 52, 53, 17]. The technologies currently integrated in smartphones are highlighted in grey. Despite of the ZigBee mesh protocol being widely utilised in IoT including smart home automation, its reference is not coloured with grey in **Table 1.2** since only some adapters [54] and special cases were noted [55] as applications on smartphones. In the table, Ultrasound technology is not highlighted since it is not part of the current smartphone technology as well.

Focusing more on the 2.4 GHz technology as delivered through Wi-Fi, IEEE 802.15.4/ZigBee, and BLE, the current state-of-the-art accuracy of LBSs without

Table 1.2 The LBS maximum range and minimum accuracy, for independent wireless services used by indoor/outdoor positioning systems, IPS/OPS

Service used in IPS	Range (m)	Accuracy (m)	References	Cost
Wi-Fi (IEEE 802.11.b, g, n)	100	±1-5	[15, 16, 52, 53, 17]	Low
ZigBee (IEEE 802.15.4)	10/100	±1-5	[15, 16, 52, 53, 17]	Low
Bluetooth, BT (IEEE 802.15.1)	1/10/100	±1-5	[16, 52, 53]	Low
Bluetooth Low Energy, BLE	40	±1-5	[53]	Low
Ultra wide band radio, UWB	1-50	±0.01-1	[15-17]	Medium
RFID	1-50	±1-5	[16, 52, 17]	Low
Infrared, IR	1-5	±0.01-1	[16, 52, 17]	Medium
Service used in OPS				
Ultrasound	2-10	±0.03-1	[16, 52, 17]	Medium
Galileo	global	± 1-5	[15]	High
GPS*	global	±5-10	[15, 52, 17]	High
2/2.5G (GSM/EDGE;GPRS)	large	±50-500	[15, 17]	High
3G (UMTS;UTRA)	large	±50-500	[15, 17]	High
3.5G (HSPA;LTE Rel. 8-9)	large	±20	[15]	High

*: some GPS systems may provide centimetre location accuracy; however, the high accuracy implies the adoption of a complex algorithm known as Real Time Kinematic, RTK, which involves extra calibration, real time error processing and correction from a ground-based network, making them bulky and expensive for general use [56]

using cooperative techniques or sensor fusion, for areas scaled in meters, enhances from the general interval presented in **Table 1.2** of ±1 to 5 m to a 2.4 GHz frequency specific of ±1 to 3 m [57, 58]. The values listed in **Table 1.2** illustrate wireless location technology's limitations and will be used as a further reference for the study's theoretical and experimental work.

Based on the above presented data it can be concluded that the current state-of-the-art RF location accuracy for non-cooperative services operating at 2.4 GHz belongs to the ±1 to 3 m interval. This thesis demonstrates that, by applying appropriately selected RF location methods in an experimental setup reflecting the testing conditions outlined above, the resulting RF location solution not only delivers improved accuracy performance, but also relevance for the automotive industrial partner.

1.4.2 RF detection system relevance for inside-outside vehicle location

Solving the RF location problem by using multiple-sensor fusion services based on different sensor technologies implies additional hardware, different data links and distinct data types, when compared with single sensor technology producing a network of identical nodes which are expanding the individual sensor capabilities. The additional hardware, links and data may not appeal to the OEM sector since it

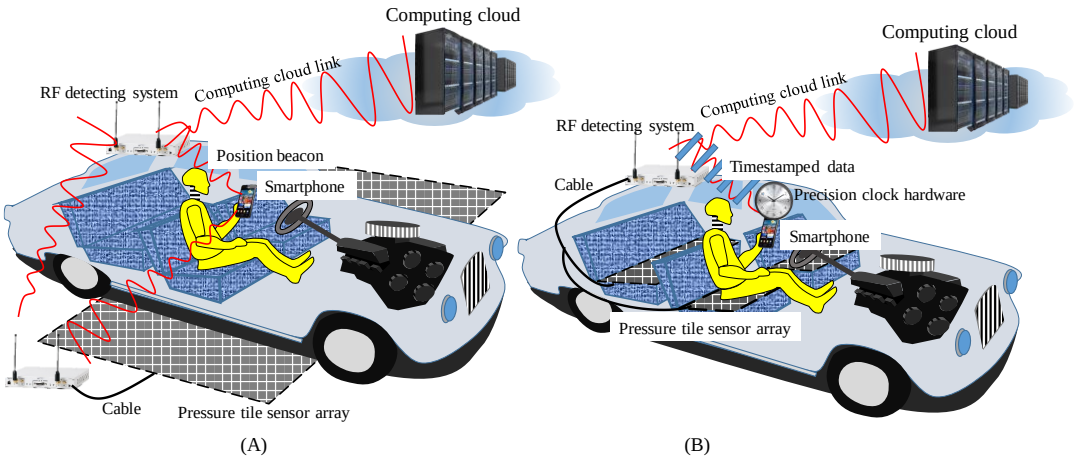

Figure 1.2 Cooperative detection of the smartphone position inside the car in a scenario where the pressure sensors are externally located on the outside parking infrastructure (A) versus a scenario where the pressure sensor array is on the seats located inside the car infrastructure (B)

transforms the solution into one that is infrastructure-dependent, while for the research community the problem's challenge diminishes proportional with the additional information sources enhancing the initial RF system. **Figure 1.2** illustrates the above statements exaggerating the sensors' sizes or shapes for explanatory clarity, delivering an overall view for the case of RF detection and location of a smartphone inside-outside a vehicle by using various data points such as data from pressure sensors like the ones in the car seats or door switches determining user presence and location by touch direct actuation. Moreover, advanced algorithmic processing, calculations and data filtering would require a powerful hardware added to the basic RF sensor or a constant link with one, for instance with a cloud computing service, potentially draining the vehicle battery, adding subscription expenses and exposing it to various cyberattacks.

Other approaches suggest that a low-profile alternative to the high-power computation and data link may be introduced by considering only the inclusion of a precision clock hardware used to transform the simple positioning beacon data exchanged between the smartphone and the RF detection system in timestamped data used for lateration time-based techniques. An RF signal beacon, such as the one used by BLE, is a short frame transmission broadcasted for spatial position identification purposes, analogue in functionality with a lighthouse light beacon. For instance, in **Figure 1.2** scenario B, additional hardware such as a precision clock needs to be present in the smart device or in the detection system to timestamp the data that is exchanged between the device and the detection system.

For instance, enhanced RF location accuracies of under ±1 m for inside vehicle have been recently reported by employing customised applications of 2.4 GHz BLE for location detection [59-63]. The conditions underlying this performance are restrictive [59, 60, 63] by utilising machine learning or Support Vector Machines (SVM) algorithms, in some cases requiring additional help [63] such as from the on-board car sensors, or manually timestamping data and using two RSSI fingerprint databases and switching between them based on the subjective timestamp [61, 62], whereas one of the reports does not account for the third dimension [61, 62] being susceptible to data loss due to simplification like schematically illustrated in **Figure 1.3**, where for long range distances the error is negligible, while for short ranges like 1.5 m inside or

outside the vehicle, the error between three-dimensional (3D) and two-dimensional (2D) distances may reach up to 80%.

To summarise, this study aims to overcome the above challenges by adopting a minimalistic resource approach for solving the RF location problem based on the low power 2.4 GHz technology, without any additional hardware, software, data links, data types than the ones provided by the default characteristics of the technology. Moreover, this work also generates an accurate 3D map for the RF empirical testing setup to avoid the errors resulted from 2D and 3D mismatches for short ranges.

1.4.3 Required RF detection system accuracy for inside vehicle location

Potential use cases for an RF location solution would require an accuracy of under 1 m for inside the car area. To this end, this study aims to deliver a solution superior to current state-of-the-art solutions for areas employing the meter as a representative metric. Due to various applications benefitting from driver and passenger identification inside the car, there is no official specific requirement on location accuracy encompassing all the scenarios. For certain applications requiring

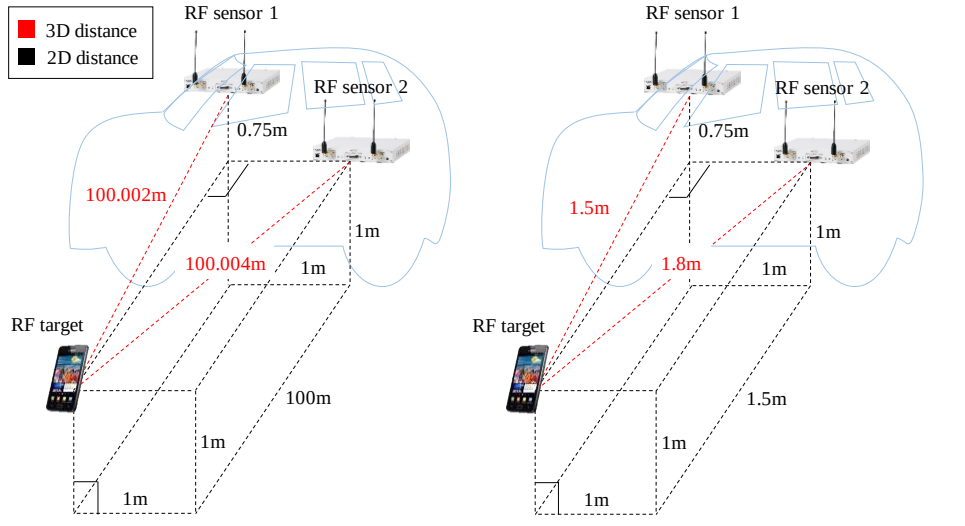

Errors between 2D and 3D long distances: up to 0.4%

Errors between 2D and 3D short distances: up to 80%

(A)

(B)

Figure 1.3 Three-dimensional (3D) distances versus two-dimensional (2D) measurements for long (A), and short ranges (B). The short distance scenario is characteristic for vehicle inside-outside detection and location of a smart device, while the long distance may be suitable for radar drone detection or remote control

smartphone user tagging as it is the case of telematics insurance, a minimum location accuracy of ±0.75 m, representing half the width of a passenger car is mentioned [64]. By considering that the seat width of a common passenger car ranges between 31-51cm excluding the cushion wings [65, 66], a higher location accuracy, down to a seat width of 0.5 m, may be required for life critical monitoring applications:

- monitor driver behaviour and phone usage, for instance determining if the driver asks one of the present passengers to answer or operate his phone [67].
- assisting passengers which do not possess a phone, mostly children, if they are left inside the car when the car is parked [68, 69], or involved in an accident and the smart car may be able to communicate automatically the distress call [70], however it will not be capable to assess the whole picture since the estimation will be based on the phone(s) left in the car or outside the vehicle when the event occurs. The reasoning is based on the vehicle's pressure sensors detecting passengers inside while detecting the driver's phone outside, or no movement while the phone is inside.

As outlined above, a detection mechanism with an accuracy of ±0.5 m may be a desirable feature. Since this target has been reported as tangible when using high computational methods, cooperative services, time stamping data and sensor fusion, the current work will advocate for a straightforward method capable to be supported by a minimalistic configuration low power system, towards achieving similar or higher RF location accuracies.

1.5 RF location methods suitable for signal's physical layer

Since this work investigates a possible solution for the low power 2.4 GHz LBS for vehicle applications such as PKE or PEPS, the adopted minimalistic approach requires selection of an RF location method that can be applied directly without hardware or software alterations. This option translates in signal parameter identification for 2.4 GHz low power IEEE 802.15.4 compatible transceivers, more precisely the parameters directly available to the user and exploited by the RF location methods. For instance, the received signal strength indicator (RSSI) and the link quality indicator (LQI) are both delivering information related to the transmission-reception

performance, the RSSI measuring the signal strength, whereas the LQI indicating the quality of received data. Other user accessible parameters capture information about the transmission frame rather than the RF link stability. When considering the signal's physical layer of 2.4 GHz IEEE 802.15.4 transceivers, besides RSSI and LQI, no other user accessible parameter delivers information related to signal transmission time, frequency, phase, nearest neighbour or transmission angle of arrival (AoA). Therefore, in the context of 2.4 GHz IEEE 802.15.4 transceivers we conclude that the only parameters useful in RF location techniques are the RSSI and LQI. The RSSI parameter is delivered in an 8bit numerical value and requires dBm transformation accordingly to its device's datasheet. Since its dBm values are truncated and derived by sampling the frame's preamble energy rather than the full received frame [71], the RSSI differs from the received signal strength (RSS), the later parameter generally being delivered by spectrum analysers and vector network analysers (VNAs).

When focusing on RF location at signal's physical layer, several localisation methods may become unavailable, such as the localisation via data timestamp used in time of flight (ToF) and time difference of arrival (TDoA). A similar logic is applied to exclude RF location methods that rely the received signal's amplitude, frequency or phase since they are not present in the 2.4 GHz IEEE 802.15.4 user's accessible default parameters. The signal's phase ranging and location methods are specific for dedicated LBSs such as radar systems where the phase of arrival (PoA) or phase difference (PD) techniques are mostly used. The phase-based methods apply for short RF range location systems such as near field EM ranging (NFER) employing near field phase difference or for more advanced communication equipment as found in dedicated LBS devices such as radars, custom scanners and detectors or software defined radios (SDRs). The RF location methods based solely on signal's parameters are often referred to as lateration techniques. Triangulation and multi-lateration techniques need at least three nodes to provide viable ranging values about the same target, therefore the methods may be applicable only occasionally within this study by adopting a minimalistic approach resulting in rare instances of sensors with overlapping detecting areas. However, since multi-lateration techniques may improve individual ranging estimates [72, 73], the technique will be used where applicable. On the other hand, the RSSI fingerprinting method relies on the process of associating the RSSI measured values at certain positions with the distance between the transmitter and receiver at

that location [74]. If the space is only a 1D line and not a 2D or 3D map, in order to construct a usable database for it, the individual fingerprinted values are in general collected successively with a constant progression step over the straight line separating the Rx from Tx by moving one of the units. The associated RSSI distances measured at the ranging-fingerprinting stage are paired with their RSSI counterparts in a two rows array or table. RSSI ranging-fingerprinting provides a fair accuracy for the outdoor environments and is unreliable indoors where multipath is ubiquitous [75]. Its accuracy relies, similarly to the RSS based cases, on its separation step between consecutive measurements, communication instruments' quality reflected in signal consistency and stability, and nonetheless on the data acquisition setup test condition [76, 77].

Other RF methods indirectly dependent of the signal's parameters employ proximity and angulation techniques, where the network's nodes know their instantaneous location and discover their nearest neighbour or the incoming incident transmission angle. Both methods may be applicable in this study. If a number of minimum three sensors with overlapping detection areas deliver valid ranging values, then triangulation or a multi-lateration technique may apply to enhance location accuracy by means of the nodes' cooperative decision. In cases where the time and phase parameters are missing and the general TDoA or PD schemes cannot be employed for an AoA method, the AoA may be accounted for by using the orientation of the receiver's antenna determined by the radiation pattern's null area for omnidirectional systems [78], or by the highest sensitivity area for directional antennas [79]. Since the proximity method requires a detecting network with redundancy that uses overlapping ranging area nodes, it will not represent a direct solution for this work, however, if applicable, it will be used for comparison reasons. On the other hand, the AoA method provides with a minimal configuration another useful parameter for the location problem, therefore it will be implemented based on antenna orientation and used accordingly in this study.

Figure 1.4 captures an overview of the general RF spatial location techniques, their parameters, their acronyms coined by specialised literature, and examples of system configurations [80-84]. The green coloured items represent the two detection methods selected for this study. Since after the ranging stage the data may be filtered further, the most general filtering methods associated with the RF location methods are

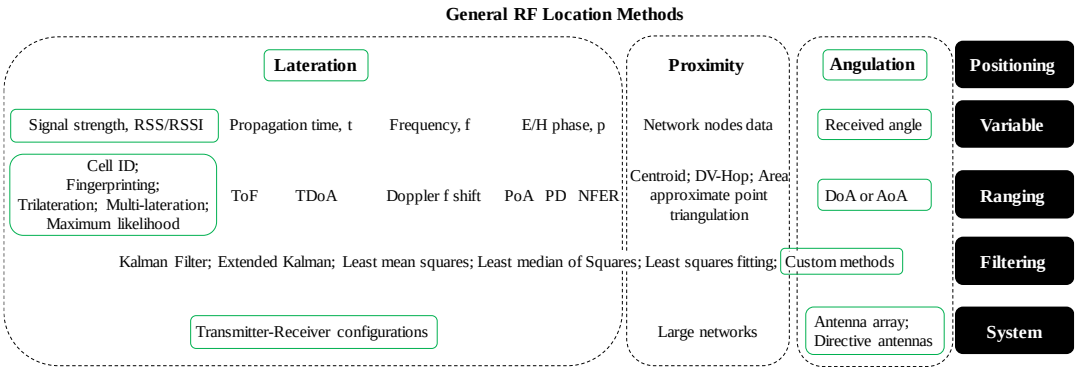

Figure 1.4 Current general RF location methods: classification and synthesis diagram (the techniques highlighted in green have been selected as applicable to this study)

illustrated as well. However, this work adopts a custom method that overcomes the algorithmic complexity linked to the other examples, making it suitable to be integrated in a low power inexpensive system. Moreover, as the LQI measures more the carrier modulation error induced in data packets rather than the RF link strength, the parameter is not represented in **Figure 1.4** and consequently not used in this study.

To summarise, this work has selected the RSSI and the receiving angle parameters to employ further within the RF location methods suitable for a low power 2.4 GHz IEEE 802.15.4 based transceiver at signal's physical layer, such as RSSI fingerprinting, AoA and multi-lateration which will be used when and if applicable.

1.6 Environmental RSSI influencing factors

The RSSI is very sensitive to the site location parameters. Some influencing parameters have an intermittent interaction, such as the noises induced by the high voltage discharges or moving objects inside the RF link space, whereas others are acting constantly, such the ones introduced by the communication or measuring equipment. In the category of constant RSSI influences, mainly derived from the outdoor environment, specific factors induce signal fading, such as the spatial propagating path, shadowing and multipath [85, 86]. **Figure 1.5** illustrates the three main signal fading effects, exaggerating some features for explanatory clarity.

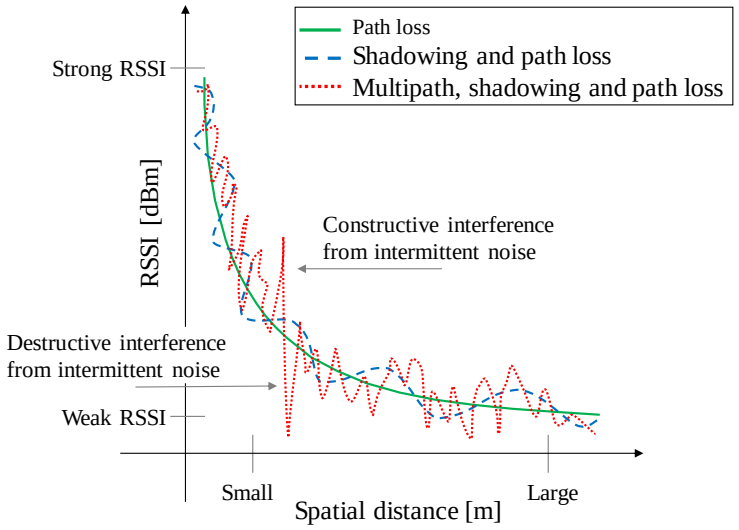

Figure 1.5 General RSSI fading factors: schematic representation for fading induced by signal path, shadowing and multipath encountered between transmitter and receiver positions

The RSSI parameter, especially for 2.4 GHz services, is highly sensitive to human presence in the measurement setup [87-89] supported by specific absorption rate (SAR) in vehicle studies [90], inferring signal's attenuation due to the body's water content, however the 2.4 GHz through-the-wall (TTW) radar, detecting human presence behind a screen suggests through its functioning a strong signal reflection produced by the human body [91, 92], another example supporting the signal reflection is based on the remote monitoring of heart rate and human breathing signal [93, 94]. More recently, smart clothes protecting from EMI [95, 96], or wearable sensor networks [97, 98] may induce reflection of RF as well due to their conductive fabrics. Therefore, human presence in the path of 2.4 GHz signal produces RSSI variation by reflecting and absorbing the signal depending on conditions specific to each scenario. In addition to the influence of the human body on the 2.4 GHz signal, other general influencing factors result from over the ground communication height [99, 100], temporal-spatial multipath [101, 102], equipment and measurement uncertainties [103], antenna polarisation and misalignment [104, 105], propagation through materials [106, 107], environmental temperature and humidity [108, 109], factors which are all reflected and captured in the RSSI measurements. When discussing the factors that influence signal propagation through materials, it is worth outlining the glass windows since they are present in all civilian vehicles. Studies suggest a low to medium impact at 2.4 GHz due their metallic UV glazing [110, 106],

however new technologies are aimed to produce passive or frequency selective microwave coatings to support automotive communication [111, 112].

Since the human presence in the RF measurement setup may influence results in various ways through a combination of signal absorption and reflection, the presence of any participants will be avoided as the position of the RF sensors used in ranging and location may be focusing on the empty space between passengers rather than on the mobile device user. The test vehicle's windows will be lowered down during the experiments to ensure unbiased results since due to their UV smart coatings they may enhance or reduce certain RF frequencies, whereas the front and rear windows will be avoided since besides coatings they may include metallic meshes used for heating or radio reception. When emulating the common placement for a smartphone, the size of an average person needs to be considered. Recent statistics indicate that in the transportation sector, male drivers are predominant representing 84% of transportation employees in Europe [113]. Since this study applies for Great Britain, the average height of an European male may be used as a reference to find the elevation for the mobile RF source test emulation in this study, with a measure between 1.68 and 1.83 m, according to [114]. However, in order to estimate the body parts dimensions, research branches of computer vision studying shape recognition or gait modelling adopted from arts [115] the "7-8 head model "of the human body [116-118], used as well in modern 3D clothing design [119]. Based on the above observations, the 0.9 m elevation from ground of the RF source emulating a smart device carried by its user around waist area, meets the criteria such as illustrated in **Figure 1.6**.

Acknowledging the RSSI measurement as a mandatory operation for RF spatial ranging and location implies that all the above discussed influencing factors will be encapsulated in the final result. Aside the control techniques that may limit some of the excess manifestations, a theoretical model and an electromagnetic (EM) simulation of the scenario may be required to introduce more information assessment in filtering and identifying the empirical outliers.

To summarise, this work will limit and reduce the RSSI influencing factors in measurements by selecting an appropriate test setup through conducting similar experiments on dry weather close to room temperature, using an RF short range to ensure a sufficient link budget over the noise floor.

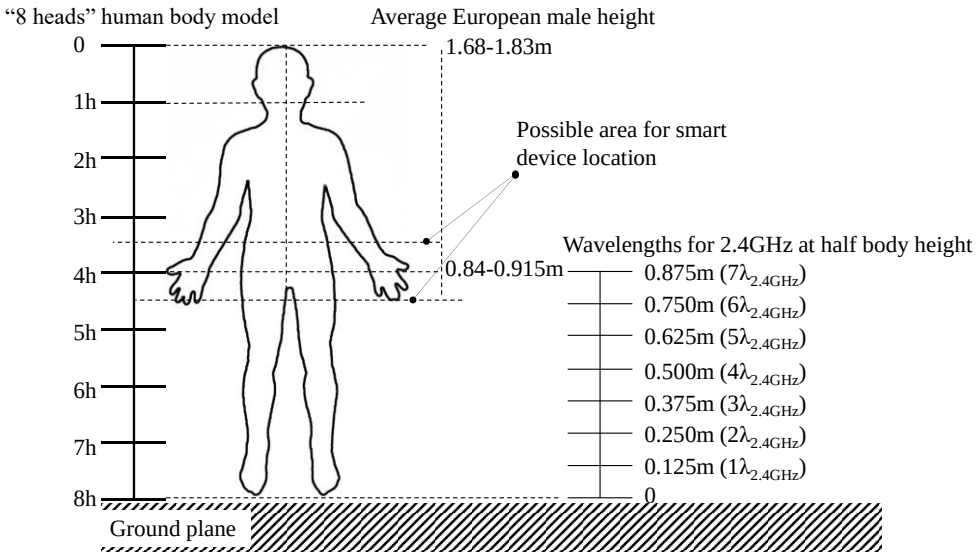

Figure 1.6 Possible location of the smart device, when carried by its user

Moreover, the RSSI measurement value at one test point will rely on an averaged value for a record of up to 100 received frames to combat the effects of possible intermittent intense interferences. The spatial setup will be selected and used avoiding obstacles and unique spaces, as much as possible. Human presence will be reduced and passengers will not participate in the tests, however their interference in the inside cabin RF detection will be anticipated and minimised by an RF sensor arrangement focusing on the empty space rather than the occupied spaces. Furthermore, since a theoretical propagation model and an EM simulation of the scenario may assist in this study by providing clear insightful information regarding the overall RSSI based results outliers, the methods will be considered further and included in this work.

1.7 EM simulation methods and RF propagation models

1.7.1 EM simulation software platform

The literature describing EM simulation techniques is extremely vast, encompassing a wide array of fields, from military to civilian. The main use of the EM simulation through professional specialised software [120], may be generalised in three objectives:

a) **To Prove** that specific electric field and magnetic field (E/H) spatial distributed values can exist under certain conditions, used in studies

hypothesising new theories or phenomena, for instance in physics [121], astronomy [122], and special materials like RF metamaterials engineering [123].

b) **To Validate** an engineering system functioning and design such as antenna [124], waveguide [125], transmission lines design [126], RF network planning [127], medical imagining [128], electric machines study [129], etc.

c) **To Determine** if a potential harm from RF exposure may be reached in biological tissues, such as SAR studies [130], medicine's RF based treatments and diagnoses [131], or in electronic victim systems, such as EMC/EMI studies [132].

Since for the purposes of this work the use of EM simulation may involve supporting assumptions related to the RF detection system's structure and validation for empirical experimentation, the use of a dedicated software package such as HFSS, CST or FEKO delivering off-the-shelf algorithmic solutions represents a reasonable solution. However, as previously stated, the main reason to employ EM simulation for this study would be to deliver information captured by the experimental data. To access the information correctly, a solid theoretical and practical knowledge of the simulation methods is necessary as each technique possesses unique advantages and limitations, and their software implementation may present a wide range of alternatives with specific optimisations. Since the dedicated EM simulation packages are the cumulated result of years of in-house software refinement delivering functionality at the press-of-a-button for an experienced user, they may not disclose the background functionality, providing a limited number of explanations and examples. Balancing the requirements necessary for the exploitation of such a simulation package, for instance the steep learning curve to reach the necessary experience and the cost linked to training and the allocated time, versus the desired research work outputs, suggested a different approach. To avoid the scenario of someone who wants to master the vehicle's mechanics and, based on the available evidence, buys a high-end car and then, out of the initial scope, spends all their time and resources attending racing tutorials, the decision was made to select a general scientific platform as an alternative to the dedicated EM simulation software. One of the best alternatives from a wide variety of programming environments is MATrix LABoratory (MATLAB) by providing a high-performance environment for engineering, scientific and technical computing, with a rich history of more than 30 years' experience in specialised

mathematical toolboxes, worldwide recognised both in academia and industry. Moreover, complete MATLAB books describing fundamental EM simulation methods such as the finite differences time domain (FDTD), the transmission line method (TLM) [133], the finite element method (FEM) or the finite element analysis (FEA) [134], the method of moments (MoM) [135] and geometrical optics (GO) [136] have been published unveiling the techniques' implementation details and assisting a vast cross-disciplinary community.

To conclude, the MATLAB platform is selected to support this work's RF location investigation via implementation of a suitable EM method, to provide insights of the implicit theoretical and empirical processes involved. The purpose of the MATLAB implementation is not to research new EM methods, optimisation algorithms or computational acceleration techniques since this is beyond the aim of this study, but to gain insight from innovative ways of combining classical methods and result analysis.

1.7.2 EM simulation methods

EM modelling displays an extended portfolio on simulating large areas similar with this study's RF location scenario. This work, due its nature, presents two components: outdoors, when the RF mobile source is outside the vehicle, and indoors, when the target is located inside the car. Since both components of this study are large enough to be habitable, each of them may use cross-disciplinary EM simulation perspectives such as large area network (LAN) planning [127], power plant analysis [137], inter-vehicle communication [138], antenna positioning on large structures and space exploration [139] for the outdoor domain, and learnings from previous work focusing on EM field in confined spaces such as in vehicles [140], tunnels [141] and buildings [142] for the indoor area. The above examples illustrate a small sample of the various approaches that may fit this RF location investigation through EM simulation, with a clear potential of delivering useful exploratory insights. However, due to the large diversity of perspectives and EM methods, a classification is required to filter the options and tailor the selection based on MATLAB and user resources in the context of optimal problem solving by investigating the most representative techniques used

in computational electromagnetic methods (CEM) [143]. Therefore, when emulating the RF problem via CEM, it may be divided in three areas and investigate its suitability to each of them:

1. **Problem formulation:** assessing the scenario by identifying its size, type and model type suitability, based on the properties of the electromagnetic signal and 3D geometry for a particular RF scenario.
2. **Problem domain:** evaluating the most well-known methods dealing with continuous and discrete domain variables in time or frequency, and also evaluating the problem's suitability to an analytical or numerical approach.
3. **Problem complexity:** investigates if any simplification may be available by investigating the possible geometry dimensionality and numerical solver algorithm for a particular RF problem.

Since all EM simulation methods are handling any scenario's materials and geometry, each in its specific way, the materials and geometry are not included in the ranking factors for the EM method selection.

The approach proposed in this thesis seeks to identify the balance between implementation complexity and RF problem solving while not aiming to develop new EM methods. The MATLAB simulation has an assistive role in the overall journey of identifying the most appropriate solution. The empirical and theoretical RF models, tests and analysis are delivering the solution, while the MATLAB EM methods are an assistive tool. Therefore, the selection of EM techniques described below will be based on their suitability and ability to accommodate the RF scenario, while selecting a straightforward MATLAB implementation.

1.7.2.1 Problem formulation

Problem formulation involves a preliminary estimation of the main factors generating the data: the electromagnetic signal and 3D geometry. The signal is characterised by its carrier's wavelength, λ, and the scenario's geometry by its domain metric, $a(x, y, z)$. The problem domain is represented in a discrete manner, an analogy of the Nyquist–Shannon sampling theorem (i.e., the discrete spatial grid resolution represents the problem domain's sampling rate). The theorem states that the sampling

Table 1.3 Maxwell electromagnetic field equations (1.1)-(1.4) and the constitutive relations (1.5)

Law name	Differential format	Integral format	No
Gauss	$\nabla \cdot \mathrm{E} = \frac{\rho}{\varepsilon_0} <=> \frac{\partial E_x}{\partial x} + \frac{\partial E_y}{\partial y} + \frac{\partial E_z}{\partial z} = \frac{\rho}{\varepsilon_0}$	$\oiint EdS = \frac{1}{\varepsilon_0}\iiint \rho dV$	(1.1)
Faraday	$\nabla \times E = -\frac{\partial B}{\partial t} <=> \begin{cases} \frac{\partial E_z}{\partial y} - \frac{\partial E_y}{\partial z} = -\frac{\partial B_x}{\partial t} \\ \frac{\partial E_x}{\partial z} - \frac{\partial E_z}{\partial x} = -\frac{\partial B_y}{\partial t} \\ \frac{\partial E_y}{\partial x} - \frac{\partial E_x}{\partial y} = -\frac{\partial B_z}{\partial t} \end{cases}$	$\oint Edl = -\frac{d}{dt}\iint BdS$	(1.2)
Gauss	$\nabla \cdot \mathrm{B} = 0 <=> \frac{\partial B_x}{\partial x} + \frac{\partial B_y}{\partial y} + \frac{\partial B_z}{\partial z} = 0$	$\oiint BdS = 0$	(1.3)
Ampere	$c^2 \nabla \times B = J + \frac{\partial E}{\partial t} <=> \begin{cases} c^2(\frac{\partial B_z}{\partial y} - \frac{\partial B_y}{\partial z}) = J_x + \frac{\partial E_x}{\partial t} \\ c^2(\frac{\partial B_x}{\partial z} - \frac{\partial B_z}{\partial x}) = J_y + \frac{\partial E_y}{\partial t} \\ c^2(\frac{\partial B_y}{\partial x} - \frac{\partial B_x}{\partial y}) = J_z + \frac{\partial E_z}{\partial t} \end{cases}$	$c^2 \oint Bdl = \iint JdS + \frac{d}{dt}\iint EdS$	(1.4)
Constitutive relations	$D = [\varepsilon] * E + P$ $B = [\mu] * H - M$		(1.5)

frequency (i.e., grid resolution) should be at least twice the maximum signal frequency, to be able to recover the transmitted information [144, 145]. The spatial discretisation of the problem accounts for the smallest resolution used on grid (i.e., unstructured grids have different element sizes), which, according to the minimum simulation accuracy required, may vary from six to ten signal wavelengths instead of two (i.e., $a \leq \lambda/6$ *or* $a \leq \lambda/10$) [146]. In the context of the present study, when considering that the problem investigation domain needs to enclose a vehicle of approximately 5 m x 2 m x 2 m, and the 2.4 GHz central frequency wavelength of approximatively 0.125 m, it can be observed that the primary focus moving forward should be on large problem size literature and methods [147].

Partial differential equations (PDEs) represent the class of equations encountered in the description of a large majority of physics phenomena. Theoretical electromagnetic exploration relies on Maxwell's equations. Oliver Heaviside generalised Maxwell's quaternion equations [148, 149] rewriting them in PDE format, and embedding the experimental work of Gauss and Faraday [150-152]. The general format of Maxwell's equation system is presented in **Table 1.3** (1.1)-(1.4), written in differential or integral format [153, 154], the constitutive equations (1.5), presenting the material interaction through the electric permittivity ε, and magnetic permeability, μ terms, with the electric E, and respective magnetic H fields. Maxwell's equations are generally presented as a multivariable PDE system in time domain. The constitutive equation is represented as the convolution product "*", between material tensor property

commonly expressed in array format and the field. The material's electric polarisation *P*, and magnetic polarisation *M*, are included to deliver the complete formulation. If the material is homogenous and isotropic, the convolution becomes a simple product and the tensor can be represented just by a single scalar value. Moreover, if the material does not polarise electrically or magnetically, the *P* and *M* may be considered as void values. For a frequency domain representation, the general path involves the Fourier transform substitution.

The PDEs can be solved and analysed using differential and integral formulation, derived from Newton-Leibniz calculus [155-157]. The calculus ideology is that everything can be decomposed or approximated via simple functions, like the algebraic base functions [158]. If the geometry is interpreted from an algebraic perspective, the same calculus principle can be applied by decomposing the spatial data relationships into simple geometrical shapes (i.e., shape functions) [159, 160]. In contrast to calculus there is chaos theory, where fractals are the simplest reduction shapes, the nonlinear equations such as polynomial degrees higher than one, generating them depending on data dimension, complexity and time evolution [161, 162]. The general classification of physical problems described by PDEs, according to [163, 164], indicates three major problem types: equilibrium (also known as steady state), eigenvalue, and propagation (also known as transient, unsteady state, marching or evolution). The 2.4 GHz RF localisation problem is a wave propagation problem: the RF source is generating the wave that propagates towards the receiving area.

The final core element of formulating the problem, in being able to define the model base construction, is often broadly described as modelling and simulation (M&S) [165]. In the scientific literature, the distinction between practical and theoretical based models is assumed to be common knowledge, the differentiations being briefly underlined in introductory lecture courses such as [166-168]. The problem modelling is dependent on the data provenance; therefore, three types of models are highlighted: practical models based on empirical data, theoretical models based on known physical laws, and semi-empirical models as a mix of empirical data and theoretical description. Since this work starts from theoretical premises, but empirical measurements will be used for result validation or for building empirical models, the simulation model for the spatial electromagnetic interaction and possible relationships between the 2.4 GHz RF source and the vehicle will be investigated via a mix model.

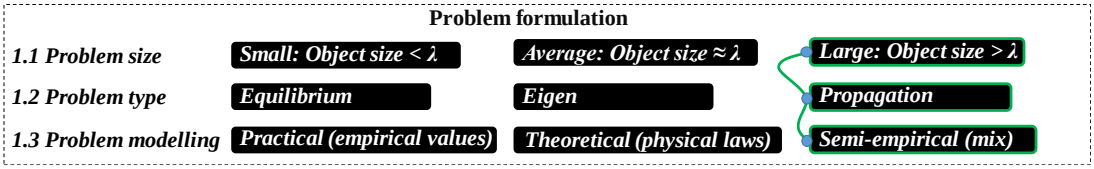

Figure 1.7 Summary diagram of the CEM problem formulation outlining this work's selected approach (green)

Figure 1.7 summarises the problem formulation conclusions regarding the electromagnetic relationship between the 2.4 GHz RF source and vehicle geometry, which may be derived via theoretical simulation and empirical validation of a large propagation problem.

1.7.2.2 Problem domain

Problem domain is concerned with assessing if the electromagnetic problem is suitable to an analytical or numerical approach, when considering the perspective of the mathematical equations. If a problem presents a continuous nature, analytical methods are the default tools used to formulate a solution. The Maxwell's PDEs are amenable to continuity, however, due to their complexity when applied to elaborate geometries like the in-vehicle scenario, only numerical approximate solution may be available since analytical solutions for Maxwell's PDEs are amenable only for simple geometries such as a sphere and an infinite circular cylinder [169, 170]. For this reason, the focus in the following will be placed on numerical techniques.

Numerical methods may be classified based on their data sampling approach into mesh and meshless methods, relative to the problem size, dictated by the signal wavelength into low frequency (LF) and high frequency (HF) methods, and, by considering the function representation into differential or integral format methods. The latter classification is important, as it relates to the format of the resulted PDE matrix used in CEM (i.e., the derivative methods are producing sparse matrix systems and the integral methods are producing dense matrix systems).

The finite differences time domain, FDTD, is a differential time domain method and it approximates via forward, backward or central differences the PDE's derivatives. For simulating an electromagnetic wave, a propagator (i.e., a time marching technique)

needs to be defined, in order to update the electric and magnetic field at a certain time step, Δt, conditioned by the grid time-space ratio, called the stability criterion and, referred in literature as the Courant–Friedrichs–Lewy (CFL) stability condition [171, 172]. The method was successfully used for the investigation of large electrical objects such as vehicles, [173-177], however, precaution needs to be taken as the unstructured grid introduces dispersion and, if classical FDTD is used (advanced FDTD approaches claim to overcome the CFL), grid elements equal or less than ten wavelengths need to be considered for solution convergence reasons [178]. Although it makes a good candidate for the vehicle scenario model, after several MATLAB tests, it was decided that due to its long running times given only one RF source position, it will necessitate additional resources such as parallelisation and domain decomposition, and for this reason other alternatives were considered.

The transmission line method, TLM, (also known as transmission-line-matrix method) has a very similar principle with FDTD (i.e., also discreet differential), nevertheless, the method links the field to the circuit theory by using equivalent electrical networks for spatial discretisation [178]. Although the TLM is mostly used in circuit analysis, by being a rigorous method, its usage in hybrid 3D discretisation scenarios involving large electrical structures presents an attractive simulation alternative [179-181]. Given that the present work involves producing a CAD geometry and importing it to MATLAB for analysis, and the fact that the TLM method does not provide a direct representation of real shapes such as the vehicle body, no further investigation of the technique was planned.

The finite element method, FEM, (also known as the finite element analysis, FEA) represents one of the most popular numerical techniques in physics, mathematics and engineering. The usual format for FEM is given by an array product relation [182, 183], where the stiffness matrix, usually found under the *K* notation, is representative for the method as it maps all the mesh's local points to the global simulation domain, this process being called assembly process [184]. The FEM includes two approaches in choosing the base function (i.e., for the mesh shape function discretisation): node-based (i.e., Lagrange finite element) and edge-based (i.e., Nedelec finite elements), the latter presenting better solution results when applied to electromagnetic problems [185]. FEM handles complex geometries without staircase approximations like FDTD, however, it requires additional computation (such as the stiffness matrix assembling and handling). The method is a volumetric technique just like FDTD, however, as it

has high resource requirements for a MATLAB implementation of a large scenario, it has not been further considered.

The method of moments, MoM (also known as the method of weighted residuals, or associated with the boundary element method, BEM) is one of the most popular numerical methods based on the integral form representation of the PDEs. The method is associated with Green's function [186]. When MoM is applied to solve electromagnetic problems involving surface integral equations, (SIE), three main integral approximations are used: electric-field integral equations (EFIE), magnetic-field integral equations (MFIE) or combined-field integral equations (CFIE) [135]. MoM is faster than FEM, however, by generating a dense matrix due to its integral form, solving the matrix for large sized problems is inefficient, requiring hybridisation with the fast multipole method (FMM), or the multilevel fast multipole method (MLFMM). The hybridisation is difficult, reducing the accuracy of the technique by implying further conditioning, therefore, after the method has been implemented in MATLAB and tested, it was decided that without additional optimisation algorithms, it will not be suitable for the vehicle scenario.

The finite integral method, FIT, represents another numerical method for solving Maxwell's equations in their integral form. The FIT deals better than FDTD with non-uniform and curve geometry, and a simplified ternary notation of -1, 0, 1 may be used in its topological matrix representations of the curl and divergence operators as shown in [187]. The FIT method is similar to FDTD in electromagnetics, where, electric field, *E*, and magnetic field, *H*, are staggered in Yee's grid [188], however, as this technique's advantages are hard to achieve given its MATLAB implementation complexity when compared with the former method, it has not been further investigated.

The finite volume method, FVM (also called box method), is a numerical integral method. Similar in approach to FDTD, the technique is considering at each discrete point of the mesh a non-overlapping surrounding volume, the volumes being called control volumes, CV, or cells. The integral conservation law is enforced for each volume [189]. Due to its similarity with FDTD, this method has not been further investigated.

The high frequency methods (also referred as asymptotic methods or optics) are represented by two main branches: physical optics, PO, (also known as wave optics), and geometrical optics, GO.

The PO methods are based on scalar theory, ignoring the vector aspect of the wave, and they can cover phenomena such as diffraction, interference and polarisation, [190]. PO accounts for specific methods such as the physical theory of diffraction, PTD, developed by Ufimtsev P.Y. [191], and are an analogy for the LF methods that exploit the integral format [192]. The PO are more common for small to medium problem modelling, their accuracy being comparable with their LF counterparts, and for these reasons the present study has not focused further on them.

The GO methods, on the other hand, are using light rays to describe the reflection, refraction and transmission phenomena. The technique is based on the Snell's refraction formula and Fresnel's equations for the reflection and transmission of light. GO encompasses techniques such as ray tracing, RT, geometrical theory of diffraction, GTD, introduced by Keller B. J. [193], and the uniform theory of diffraction, UTD (a generalisation-extension of GTD). The GO methods are exploiting the light discrete expression, similarly to the LF differential methods [192]. These methods are widely used when the traditional LF techniques are unable to provide a solution due to the large size of the problem.

The GO method accuracy, more precisely the accuracy of the ray tracing method, which is the base technique for all GO methods, depends on the number of rays used to model the RF propagation, the domain geometrical shape handling being similar in approach with FEM and MoM. Consequently, high attention needs to be paid to RF source ray modelling. A great advantage of RT is that it represents a geometrical technique and is no longer dependent on the electrical size of the geometrical target, the $\lambda/10$ boundaries for the minimum mesh geometry being no longer required [194-196]. For GO, the ray, kinetic or eikonal formulations are based on the scalar wave equation, where the plane wave provides a solution [197], as:

$$u(t,x) = A(t,x)e^{-j\omega\varphi(t,x)} \tag{1.6}$$

where u is a plane wave function variable in time and space, A is the amplitude of the wave, ω is the angular frequency and φ is a phase function. To summarise, GO based on RT makes a good candidate for the scenario investigated in this study, as it is

suitable for CAD geometry without imposing restrictions, the extractions of parameters such as distances from the source to the target and incidence angles, are explicit, and a large variety of examples involving large scenarios recommend it.

The meshless methods (also known as the mesh free methods) were developed as an alternative to the classical meshed methods, in order to compensate for their inability to represent mesh discontinuities resulted from the evolution of the problem, such as cracks and large particle displacements related to astrophysics or particle hydrodynamics [198, 199]. Their beginnings are marked by the development of smooth particle hydrodynamics, SPH, technique introduced by Lucy [200], and Monaghan [201], designed for applications in solid mechanics impact [202]. Another meshless method is the element-free Galerkin, EF- Galerkin or EFG. The method may be applied to arbitrary shapes and is considered consistent and stable (the consistency and stability problems are specific for the meshless methods), its calculations being based on the moving least-squares interpolants [203]. The radial basis functions, RBF, is worth to be mentioned as a method similar to EFG, its hybrid usage with collocation and Galerkin methods being acknowledged for the resulted dimensional mesh free independence and spatial higher dimension extendibility [204]. Although meshless techniques were developed for large sized problems, such as particle dynamics, seismic, or astronomy, considering that the domain and vehicle spatial geometry have a well-defined shape (i.e., the mesh geometry does not vary), specified by the vertex relationships inside the edges, faces, volumes, etc., meshless methods are not suitable for this type of electromagnetic simulation as the information contained in the mesh will be duplicated by the method specific techniques.

The variation between time and frequency domain is mediated by the Fourier transform [205], therefore, if necessary to be applied in the electromagnetic simulation, the Fourier analysis needs to be considered [206].

Figure 1.8 summarises the problem domain analysis from the perspective of the mathematical method that are applicable. As the GO based on RT numerical method is chosen, the problem will be solved on time domain.

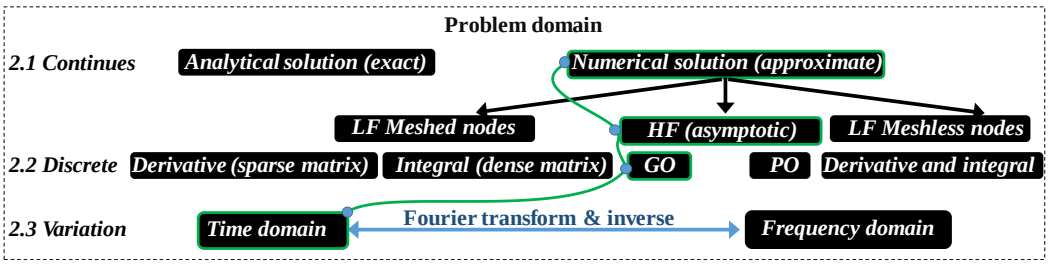

Figure 1.8 Summary diagram of the CEM problem domain outlining this work's selected approach (green)

1.7.2.3 Problem complexity

The problem complexity relates to the requirements dictated by the scenario's geometry dimensionality and the numerical solver algorithm that can be applied to it.

The 3D geometrical space can accommodate any sequential behaviour studied in 1D or parallel functionalities deployed in 2D. Consequently, a problem involving 3D geometry such as the vehicle scenario is more complex than the ones which can emulate the low dimension spaces. The same reasoning is found in the multidimensional data domain, requiring complexity reduction for handling, analysis, or storage, and reducing dimensionality with a minimal error [207, 208]. Another exemplification of the differences that may appear due to the problem's space dimensionality can be illustrated by using the analogy with the three-dimensional photonic crystal simplification analysis [209, 210], where the 3D aperiodicity of crystal lattices is reflected in the type of simplification that can be applicable in that case. For the simulation case relevant to the present study, lower dimensional simplifications are not applicable as the 3D vehicle geometry is aperiodic on all xyz-axes, the complexity being therefore high.

The solver algorithms themselves attempt to find solutions based upon either a differential, or integral format that results in the generation of a sparse or dense matrix result [211-215]. Further to this, solvers may be considered as either iterative or non-iterative (i.e., direct). The non-iterative direct solvers are applicable to both sparse and dense matrix representations, however, they are efficient only on small problems. The

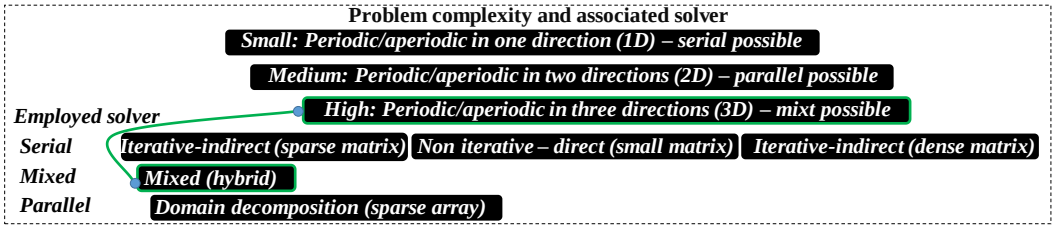

Figure 1.9 Summary diagram of the CEM problem complexity and associated solver outlining this work's selected path (green)

actual solver design falls outside the scope of this project, as the solvers' peculiarities, properties and differences are studied and tested by mathematicians and computer scientists, (please refer to Submission 2 for more information related to the most commonly used solvers employed by numerical methods). For this case study, as the focus is more on the ray tracing method, it can be assumed (and demonstrated later by 3D MATLAB spatial discretisation used in source modelling and vehicle interior discrimination) that multigrid techniques are more suitable solvers for the 3D vehicle scenario, the other solvers being more relevant for parallelisation, optimisation and acceleration.

Figure 1.9 outlines the problem complexity analysis. Provided that the difficulty of the 3D scenario geometry is high, the multigrid techniques are considered as a possible solution suitable for the present study since they provide interleaving alternatives such working simultaneously with various spatial metrics convenient when techniques involving 3D point digitising, area and volume comparison are to be employed.

Figure 1.10 summarises the findings from the literature investigation related to CEM methods applicable to this work. Example methods considered include: finite differences time domain (FDTD), transmission line method (TLM), finite element method (FEM), method of moments (MoM), finite integration technique (FIT), finite volume method (FVT), partial element equivalent circuit method (PEEC), geometrical optics (GO), physical optics (PO), ray tracing (RT), geometrical theory of diffraction (GTD), uniform theory of diffraction (UTD), physical theory of diffraction (PTD), smoothed-particle hydrodynamics (SPH), element-free Galerkin (EF-Galerkin), radial basis functions (RBF), conjugate gradient (CG), generalized minimal residual (GMRES), conjugate gradient-fast Fourier transform (CGFFT), Runge-Kutta (RK), alternating direction implicit (ADI), fast Fourier transform (FFT), adaptive integral

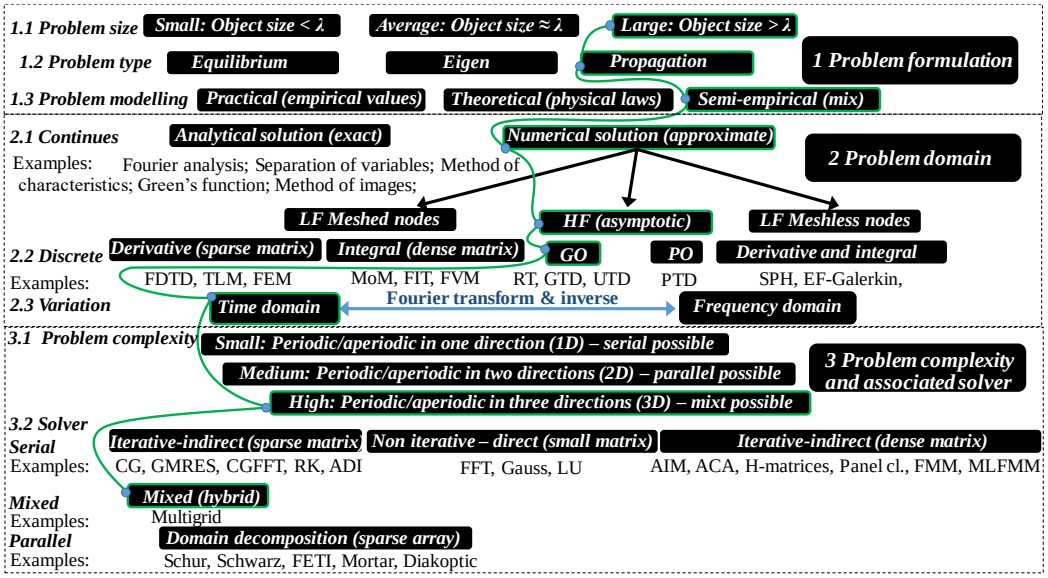

Figure 1.10 CEM classification and synthesis diagram outlining this work's selected solving path

method (AIM), adaptive cross approximation (ACA), fast multipole method (FMM), multilevel fast multipole algorithm (MLFMA), and finite element tearing and interconnecting (FETI).

1.7.3 RF propagation models

The RF theoretical models, commonly known as propagation models, may explain and predict experimental measurement data based on mathematical equations. In literature, they are categorised by the method employed for data modelling: deterministic, empirical, and stochastic [216, 217]. Some of the well-known empirical models are USI, Cost-231 Hata, Okumura, Ericsson 9999. For the deterministic models, Friis free space propagation, two-ray, and Ikegami [217] are most widely recognised. Stochastic models rely on distributions to derive their formulas, Rayleigh Rice, Hoyt, Weibull and Nakagami-m being most popular in this category [218].

Since the measured data can be emulated by mathematical series, polynomial expansions, interpolations and regressions, various research works have built their theoretical models purely mathematical. The terms present in their equations do not relate directly to physical propagation parameters. Examples of RSSI based data models representative for this mathematical abstract category include Taylor series [219], Fourier series [220], curve fitting [221], spline interpolation [222], Kriging interpolation [223], and least square and regression [224].

Since all theoretical models apply smoothing to the RSSI nonlinear measurement data and adjust the variations around the fitted curve, they act as filters. Two widely adopted filters in this area are Gauss and Kalman, both deriving their origin from the well-known least-squares method [225]. In the last decade, the Kalman filter was the method of choice for smoothing ranging distances for radars [226, 227], however since the location problem in this work does not involve trajectory tracking by using time dependent RSSI measurements, the use of a Kalman filter is not imperative.

Two of the most common propagation models used in literature are the log-distance path loss (1.7) and the log-normal path loss model (1.8):

$$PL(avg) = PL(d_0) + 10n \log\left(\frac{d}{d_0}\right) \tag{1.7}$$

$$PL(avg) = PL(d_0) + 10n \log\left(\frac{d}{d_0}\right) + X_\sigma \tag{1.8}$$

where n is the path loss exponent, $PL(d_0)$ is the path loss at the reference distance d_0, and X_σ is a zero-mean Gaussian-distributed random variable with standard deviation σ [228]. Researchers have adopted both models because of their straightforwardness. Knowing that the electromagnetic wave intensity and implicitly the transmitted propagating power follows the inverse square law of attenuation due to spatial dispersion [229], it can be considered that n equals 2. Moreover, the equation clearly shows that the power attenuation is due to the spatial distance and noise rather than being frequency or wavelength dependent. The frequency relation in the propagation models is due to the fact that the formulas are mainly derived from the deterministic model of Friis' free space propagation formula [230, 231] (1.9), where the antenna gain is introduced as the frequency dependent term [232]:

$$P_{Rx} = P_{Tx} + G_{Tx} + G_{Rx} - 20 \log\left(\frac{4\pi d}{\lambda}\right) \tag{1.9}$$

where P_{Rx} is the received power, P_{Tx} is the transmitted power, G_{Tx} is the transmitting antenna gain, G_{Rx} is the receiving antenna gain, d is the measured distance between Tx and Rx, and λ is the signal wavelength.

To summarise, since this work's RF measurements will account for a transmitter-receiver short distance link, and the RSSI data collection will be built on an outdoor environment benefiting from line-of-sight (LOS) and reduced interferences, the deterministic model of Friis' free space propagation equation (1.9) will be adopted and

used for modelling the signal's path loss, as well as used as a reference against the empirical data model.

1.8 Design restriction and research questions valued by the industrial partner

One important design requirement imposed on this study by the automotive partner Jaguar Land Rover, was that the RF location system needs to be completely contained inside the cabin, with no exterior fittings or additional openings such as drilled holes, being allowed. By following this constraint, the possible positional advantage offered by a receiving system positioned on the car body exterior, separate from the one inside, is made unavailable, increasing the overall challenge by reducing the number of potential options.

Moreover, when considering the overall RF location problem from the industrial perspective, three interrelated research questions required to be answered by the proof-of-concept detection system were identified:

1. When the complete receiving system is placed inside the vehicle, is it possible to discriminate the target's location between inside and outside the vehicle?
2. What are the minimum configuration requirements to enable such discrimination?
3. What is the detection accuracy for inside and outside detection?

It can be observed that the main challenge to be addressed relates to the possibility of discrimination of the RF target position between inside and outside a vehicle, and to establish the minimum configuration of a possible system fit to support the above. The accuracy of the location comes as a secondary aspect after establishing the RF system's ability to produce the discrimination. This is due to the fact that a large uncertainty in locating the target inside or outside the vehicle will render an exact ranging mechanism impractical as it will be susceptible of both positions.

1.9 Self-imposed design restrictions

Before describing the problem statement and proposing the solution based on the implications and knowledge gathered from a comprehensive literature survey,

acknowledging the multiple challenges and expectations, a number of initial empirical setup conditions were selected so as to provide the most disadvantageous case scenario. Through this measure flexibility is allowed by setting the lowest budget margin, similar with the case when one starts tuning an instrument from its coarse mode towards the fine one. Moreover, if the setup will produce good results for the most disadvantageous case scenario, then will produce better or at least equal performance on improved conditions. In other words, this measure provides robustness if the system performs well under less optimal settings.

Channel 11 2405 MHz will be set for all RF experiments, to not favour the work by choosing a channel that is recommended for not interfering with European Wi-Fi band such as channels 15, 16, 21, 22 [233]. Moreover, since a high data rate is decreasing the range by increasing the errors therefore reducing the Rx sensitivity, the high data rate of 250 kbps is adopted as default RF testing setting. Since the outside environment is the selected setup for RSSI fingerprinting and for the mobile target location outside the vehicle, the ground plane was selected as covered with 20 – 30 mm gravel. It was considered that this will provide a scattering environment similar to tarmac or concrete pavements due to its non-compact distribution, same random break stones layers but without the additive, allowing water to accumulate and get to the soil, clay or sand underneath. A final consideration is set for the omnidirectional RF sensor to emulate the mobile source elevated at 0.9 m: since it mimics the smartphone on the user it may get any random position reported to the ground plane, therefore EM coupling or ground reflections may occur. If the RF sensor is located on a phone, these possible scenarios are mitigated through careful RF PCB layout, routing and shielding design, however the present study focuses on implementing a basic design for a basic functionality, guided by the principles of the Minimum Viable Product (MVP), i.e. a product with a basic set of features to validate a product idea.

Nonetheless, the minimalistic approach that was adopted to address the RF location challenge may be defined as selecting the minimum number of components allowing the designed system to perform its basics functions. The RF sensor should be able to transmit and receive correctly while powered via USB cable and battery, at the same time providing a programming and debugging interface and a serial port or USB connection to a computer. The RF detection system will be designed to include the lowest number of sensors necessary for radio location inside-outside the vehicle. The

reasoning is on the same note as for the above considerations: if a system works well in a restrictive minimalistic approach, then it will work better or at least similar on higher specifications.

1.10 Problem summary

A critical review of the research body has been conducted, and an assessment has been performed over the viability, challenges and possible merits of a 2.4 GHz localisation solution inside-outside a static parked vehicle with possible applications for PKE or PEPS, and as a result this study's specific problem formulation may be defined as follows.

Since current state-of-the-art techniques addressing the localisation of smart devices using the license free 2.4 GHz frequency achieve an individual location accuracy of within ±1 to 3 m, given the average size of modern vehicle cabins of approximately 1.6-1.8 m [234], and the typically close relative location of neighbouring vehicles outside the car, this level of accuracy is thus not sufficient for future OEM class leading applications. Motivated by this shortcoming, the present study proposes a 2.4 GHz LBS solution, which relies on the IEEE 802.15.4 protocol as a future smartphone integratable solution. The aim of this work is to propose a solution capable of determining with a low associated error or with a high confidence:

- If the smart device is inside or outside the vehicle.
- If inside the vehicle, the location of the device needs to be established with an accuracy of less than ±1 m.
- If outside the vehicle, the ranging distance towards the smart device needs to be identified adequately. The term adequately relates to the outside monitoring sensor number and range, for instance a low number of sensors and low RF area coverage will result in a low resolution distance estimation as compared with the opposite high end solution. Moreover, considering that the car's external environment characteristics such as size, shape and structure are not constant while the study's approach favourites the minimalistic low end design, the outside location accuracy is expected to not exceed the current

state-of-the-art interval of ±1 to 3 m as illustrated in Section 1.4.1. **Figure 1.11A** summarises the proposed problem format for this study, with the RF target detection and location system fully enclosed in the car's cabin, including similar nodes that deliver comparable measurements, data and data links to detect and locate an RF target inside-outside the static vehicle.

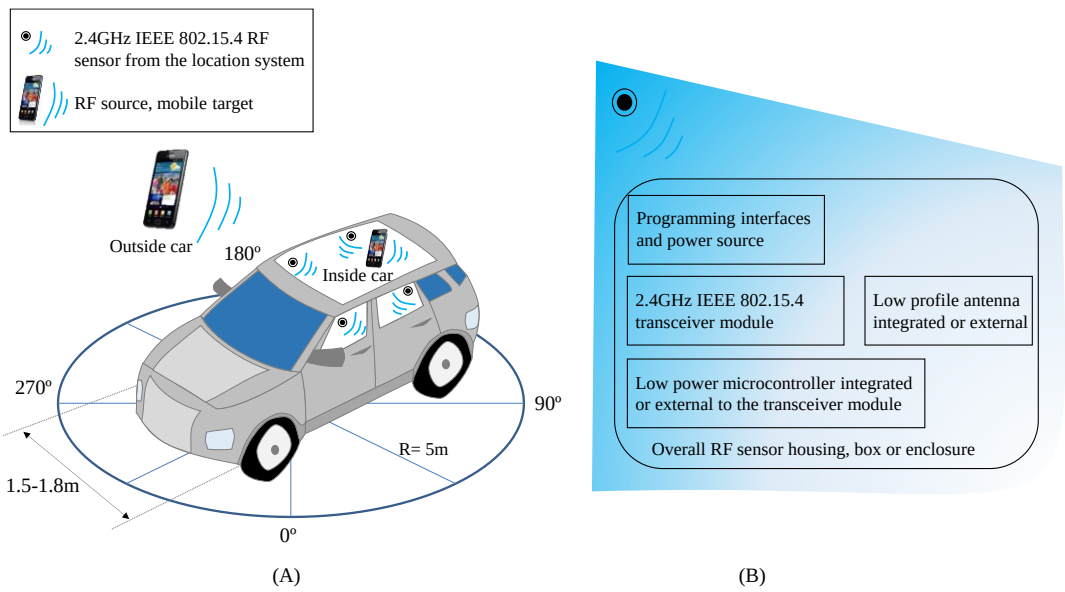

Figure 1.11 RF inside-outside target location system for a static car based on 2.4 GHz IEEE 802.15.4 standard The RF detection system is fully enclosed inside the car (A), while all possible sensors are similar, capable of delivering comparable measurements, data and data links with a proposed general minimalistic design (B)

Down to the RF sensor node level, this work proposes a minimalistic approach capable to satisfy the requirement of no additional hardware, data links and data types apart from the sensor's system default configuration. Moreover, at this level, RSSI and AoA based location techniques may apply, whereas a parallel MATLAB simulation based on GO and RF empirical and theoretical modelling will support the sensor design and data analysis. Since the final sensor may require a protecting box, enclosure, or housing this will be considered as a default configuration since it does not count as additional hardware. **Figure 1.11B** illustrates the general RF sensor design proposed by this work, in alignment with the literature investigation findings presented previously.

The RF location system measurements will benefit from a 3D map delivering the precise spatial positions for the sensors and for the mobile source on the testing points, to overcome the possible errors resulted from short range 2D to 3D mismatch.

1.11 EngD: aim and objectives

This aim of this work is to provide the necessary knowledge and information describing the viability and implementation through a proof-of-concept approach of a 2.4 GHz low power location system completely confined inside a vehicle's cabin, suitable for automotive applications such as for instance PKE or PEPS.

1.11.1 Objectives

1. Critically review the body of literature referring to 2.4 GHz location systems.
2. Designate the best 2.4 GHz location technology candidate based on a meticulous documented investigation suggesting near future changes in the smartphone secondary RF services, such as the IEEE 802.15.4 implementation.
3. Outline the current state-of-the art location accuracies associated to the 2.4 GHz location systems.
4. Identify the suitable signal parameters for performing RF location techniques employing a minimalistic approach.
5. Determine the appropriate EM methods and RF techniques applicable to the low-profile RF sensor system and outline the benefits and shortcomings of such approach.
6. Select a suitable platform such as MATLAB, for the simulation deployment by critically balancing the work's requirements versus potential benefits derived from modelling.
7. Apply the MATLAB simulation to the CAD schematised vehicle body to determine the interrelationship between the receiving areas in the context of the variable RF source position around and inside the model.

8. Validate the simulation results through RF empirical tests.
9. Design and prototype the RF location system.
10. Perform empirical measurements employing the RF system prototype to acquire the necessary data through RSSI-fingerprinting for constructing an RF empirical model.
11. Formulate given the scenario of this study an RF theoretical model and compare its properties with the empirical one.
12. Perform empirical tests for target location inside-outside vehicle, generating the RF sensors' ranging estimations based on the previous RF empirical and theoretical models.
13. Based on recorded results implement a straightforward algorithm able to discriminate the RF mobile target position as inside-outside the static vehicle.
14. Calculate and analyse the location accuracy data based on computed 3D distances and estimate ranging accuracy using root mean square error (RMSE).
15. Assess if the competitive location technique of multi-lateration, when applicable, reduces the location error.
16. Answer based on the study's results the three research questions raised initially by this project's industrial partner.
17. Discuss the findings, limitations and potential benefits of this work based on the final results from the perspective of the automotive partner and other potential users.

1.12 Statement of innovation

I. Defined a 2.4 GHz based RF location system by considering the anticipated inclusion on the next smartphone generation of the IEEE 802.15.4 standard, capable of delivering the initial work objectives and answer the industrial project partner's research questions (Chapter 1).

II. Applied the results of the critical investigation of state-of-the-art literature to determine the essential characteristics to be considered for a 2.4 GHz based location system that can benefit the industrial automotive sector (Chapter 1).

III. Proposed a method to derive directional RF sensors by exploiting their potential housing enclosure based on a quantitative MATLAB 3D ray tracing (RT) assessment of the RF location problem (Chapter 2).

IV. Identified during the MATLAB 3D RT simulation the optimal RF source model applicable to a large scenario including small geometrical features by combining backward ray casting and domain digitalisation via super-sampling methods (Chapter 2).

V. Developed lightweight decisional algorithms with potential integration on a minimalistic RF low power system, used to compute the ranging distances from RSSI empirical data and provide inside-outside vehicle target position discrimination, method which achieved 100% success (Chapter 3).

VI. Developed the 2.4 GHz based RF location system by delivering a prototyped proof-of-concept toolkit, and demonstrated its performance (Chapter 3).

VII. Proposed based on transmitter-receiver communication data result analysis, the future use of smartphone's embedded gyro sensor data to enhance the data broadcasted by the positional signal beacon, opening the opportunity of selecting the optimal polarisation for location detection (Chapter 4).

1.13 Organisation of the portfolio

An integral part of the EngD degree is the student requirement to produce a research project portfolio consisting of multiple submissions approved and recorded over the enrolment period.

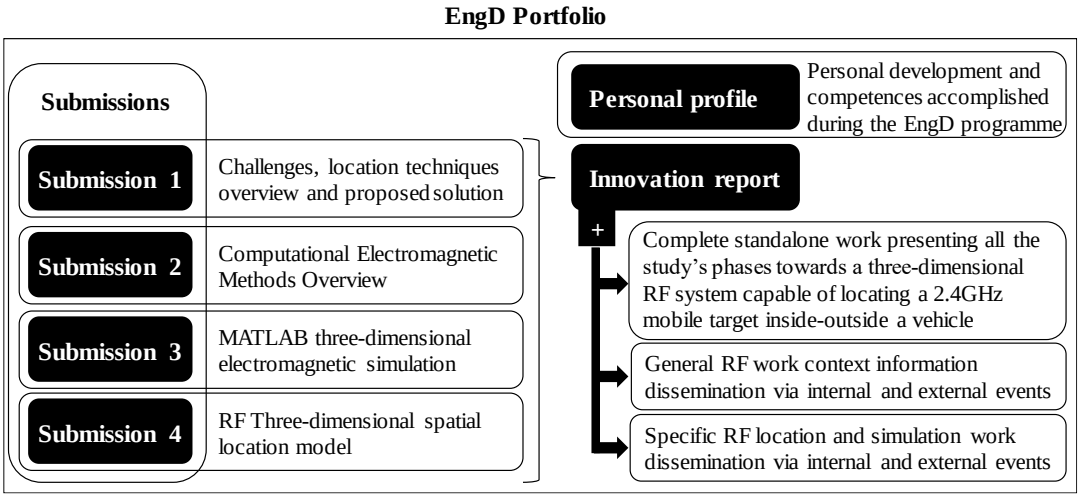

Figure 1.12 Structure diagram of the EngD research portfolio for this study

In the case of this EngD project, the portfolio consists of four technical submissions, a personal profile, and this current Innovation Report, as outlined in **Figure 1.12.**

Submission 1 describes the innovation challenges introduced by the RF location problem to solve. It synthetises the methods used in RF location, formulates the initial problem, proposes a solution based on 3D RT simulation support and RF modelling, and proposes a methodology and a timeline for its execution.

Submission 2 presents an in-depth review of the current state-of-the-art CEM, while considering the optimal and most suitable methods for this study.

Submission 3 describes the steps followed to implement the RT quantitative analysis based on the MATLAB 3D RT simulation, as well as the decisional chain involved at the low-level computational implementation.

Submission 4 focuses on the solution implemented for solving the RF location problem by describing the development and testing of the RF sensors, combined with the RF empirical and theoretical modelling of the location identification problem.

The overall work answers the original research questions and delivers the inside-outside vehicle target location discrimination and ranging accuracies desired by the industrial partner.

The personal profile document explains how the required EngD competences are fulfilled by the author by illustrating the ones which were improved or gained during the completion of this project.

1.14 Academic Publications

The specific EngD work thematic was internally disseminated on regular quarterly RACeD reviews, presenting and evaluating the research progress and challenges in front of a wide audience comprising both academic and industrial partners. In addition, the RF location system design, implementation and its inside-outside discrimination results' analysis are captured in two peer-reviewed publications:

- Marsic, Vlad, Kampert, Erik and Higgins, Matthew D. (2021) *Position discrimination of a 2.4 GHz IEEE 802.15.4 RF mobile source inside-outside a vehicle.* In: 2021 International Conference on Smart Applications, Communications and Networking (SmartNets), Glasgow, 22-24 Sept 2021. Published in: 2021 International Conference on Smart Applications, Communications and Networking (SmartNets) ISBN 9781665435451. doi:10.1109/SmartNets50376.2021.9555414.
- Marsic Vlad, Kampert Erik and Higgins Matthew D. (2021) *Ray tracing 3D source modelling for optical reflectance sensing with wireless ranging application.* In: 2021 IEEE International Symposium on Robotic and Sensors Environments (ROSE), Virtual, 28-29 Oct 2021. Published in: 2021 IEEE International Symposium on Robotic and Sensors Environments (ROSE) pp. 1-8. ISBN 9781665440622. doi:10.1109/ROSE52750.2021.9611767.

Since this work involved an extensive review of existing literature body, fragments of the preliminary review in the context of RF location services from a user perspective rather than system design have been included in peer-reviewed publications such as the ones listed below:

- Vlad Marsic, Harita Joshi, Gunwant Dhadyalla, Paul Jennings, *"Connected Car and Communications Infrastructure – Impact on User perception of QoS"*, ETSI Summit on 5G: From Myth to Reality, Sophia Antipolis, France, 2016.
- Gunwant Dhadyalla, Vlad Marsic, Harita Joshi, Siddartha Khastgir, Stewart Birrell, Paul Jennings, "*Towards Smart, Connected and Autonomous Vehicles: A User-in-the-Loop Test Methodology for the Connected Car*", In Proceedings of Driving Simulation Conference (DSC), pg.151-154, Paris, 2016.

Moreover, the same general RF LBSs context from a user perspective have been presented in local organised poster conferences to stimulate academic debates and demonstrate the ability to summarise the overall work results in a reduced space:

- Vlad Marsic, Harita Joshi, Gunwant Dhadyalla, Tom Mizutani, Paul Jennings, *"A User-in-the-Loop Test Methodology for Wireless Network Services in Vehicles"*, WMG Internal Poster Conference, Coventry, UK, 2016.
- Vlad Marsic, Matthew D. Higgins, Harita Joshi, Tom Mizutani, *"A User-in-the-Loop Test Methodology for Wireless Network Services In-Vehicles"*, Jaguar Land Rover Internal Poster Conference, Gaydon, UK, 2016.
- Vlad Marsic, Matthew D. Higgins, Harita Joshi, Gunwant Dhadyalla, Tom Mizutani, David Oxtoby, Alex Mouzakitis, Paul Jennings, "*A User-in-the-Loop Test Methodology for Wireless Network Services in Vehicles*", WMG Internal Poster Conference, Coventry, UK, 2017.

1.15 Structure of the Innovation Report

This Innovation Report is structured into four chapters organised as follows.

The introductory chapter delivers the EngD project's aim and objectives in the context set by the industrial partner reported and linked to a vast literature investigation. Additionally, the work's statement of innovation and impact are outlined. The general research methodology employed by this work, summarising briefly the stages of the study and their interconnection, are also included at the end of this chapter.

Chapter two describes the 3D simulation implemented via MATLAB, by employing the ray tracing method to quantitatively investigate the advantages that may be derived from transforming the RF sensor's enclosure into a metal housing inducing RF directivity. Moreover, insights related to RF source modelling using the implemented ray tracing method are described, since they unveil practical approaches addressing possible simulation challenges.

Chapter three focuses on the RF tests and modelling. The RF link polarisation is analysed prior to RF testing for different setup settings and the less stable case is selected together with a disadvantageous transmission channel prone to Wi-Fi

interferences, to test and ensure the study's robust approach for the location scenario. Furthermore, the two empirical test setups used for RSSI fingerprinting and target location inside-outside the vehicle are presented, followed by the result analysis based on empirical and theoretical propagation models.

Chapter four draws the conclusions for the overall work, outlines alternatives of possible industrial applications based on the research output, discusses the study's immediate limitations, and suggests potential directions for further work.

1.16 General research methodology

The general research methodology employed by this work is based on a hybrid scientific method framework. Since the scientific method is empirical by nature, whereas this study combines empirical knowledge acquisition with reinforcing findings through theory and validating theoretical performance through empirical measurements, the resulted hybrid methodology accounts for the classical approach adapted to modern times to account for resource availability.

The EngD project methodology can be seen as consisting of the main stages described below:

1. Critical review of the literature body to set a solid background of the research subject identifying individual advantages and limitations for different test setup characteristics.
2. Formulating the RF location problem and hypothesising its solution based on previous findings.
3. Predicting a higher RF accuracy for the vehicle's inside based solely on a minimalistic RF hardware approach, without additional hardware, data links or data processing than the one supported by default, and without any smart infrastructure assistance from inside or outside the vehicle.
4. Testing the prediction through RF empirical measurements reinforced by theoretical comparison validation. The tools developed for the RF empirical tests such as the RF sensor metal enclosure, have been supported through computational simulation adding their own merits to the overall value of the study.

5. Analysing the results outlining the expected values such as the success of the position discrimination inside-outside vehicle and under ±1 m location accuracy inside car's cabin, without disregarding the experimental limitation and possible improvements based on data investigation.

Since the resources used in this study involve computational simulation and RF modelling, they are presented below in separate chapters, each including its specific experimental methodology, test setup and results, whereas a summary of the experiments is provided in the chapter introductions.

2. MATLAB 3D ray tracing simulation

The simulation implemented in MATLAB is based on RT methods and employs classical programming functions and algorithmic toolsets. The diversity of software interconnections and tests involved towards producing the software instrument able to process this study's 3D scenario are explained in detail in technical Submission 3. However, since the purpose of the programming platform was to assist the overall RF investigation and not to develop new algorithms or simulation enhancements, this work adopts the MATLAB 3D RT algorithm in this work's RF context. The RT method is employed on its quantitative layer, therefore the ray-area intersection, visually represented by a dot, after reflections and variable source positioning is accounted as a total sum of hits, for ray reception, or miss for ray not being intercepted by the plane. The quantitative results of the simulation applied in the definition process of the RF sensor enclosure are validated with an empirical RF test on a similar geometrical structure by transforming the RSSI measurements for a 2.4 GHz IEEE 802.15.4 signal via an indicator function to sets of binary values. Nevertheless, one aspect of the MATLAB simulation is outlined as of possible importance for the RT 3D ray source modelling. Six different implementations for an omnidirectional ray casting are exemplified by employing the classical two slits experiment translating it in a large-scale 3D virtual environment and discussing the different results produced on the same receiving screen. The ray source modelling shows the importance of the initial ray casting consideration for a scenario employing the RT method, since different methods aiming for spatial ray homogeneity distribution such as for omnidirectional transmissions, may deliver different results impacting the overall analysis.

Figure 2.1 schematically summarises the workflow for employing the MATLAB 3D electromagnetic simulation, the comparison and empirical validation of its results, how the resulted information guides the RF sensor definition, and the outlined potential importance of the ray source modelling for RT implementations as an omnidirectional transmission emulation. Moreover, the ray source modelling approach is presented and illustrated towards the end of this chapter, since it is considered an important aspect of the simulation implementation stage.

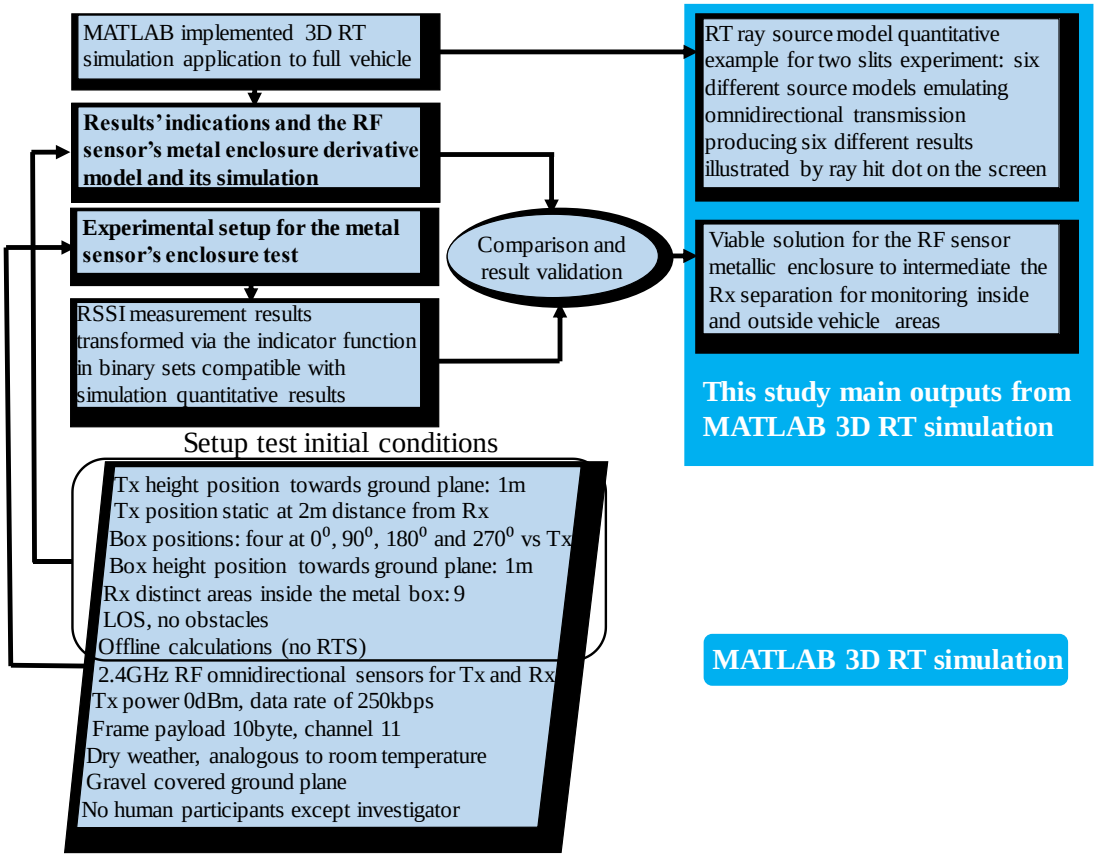

Figure 2.1 The schematised workflow diagram for MATLAB 3D electromagnetic simulation using Ray Tracing

2.1 MATLAB 3D quantitative RT on vehicle evidencing RF sensor premises

The initial simulation intention was to deliver insightful information regarding the EM processes surrounding a large geometrical volume such as the vehicle's body. Apart from achieving its initial goal, it has also uncovered information that guided the design of the RF sensor structure and positioning definitions.

Based on the initial assumption, a 3D RT algorithm has been developed and implemented in MATLAB. It relies on ray-triangle intersection hit-miss method computed through the Möller–Trumbore intersection algorithm [235] and follows the reflections rules derived from Snell's law. Moreover, the partial 3D CAD geometry of the test vehicle as provided by the industrial partner was imported in STL format, pre-processed and adapted for the RT procedure. It was supplemented with direct measurements of the test vehicle. After the simulation processing phase the data was gathered and analysed in a post-processing stage.

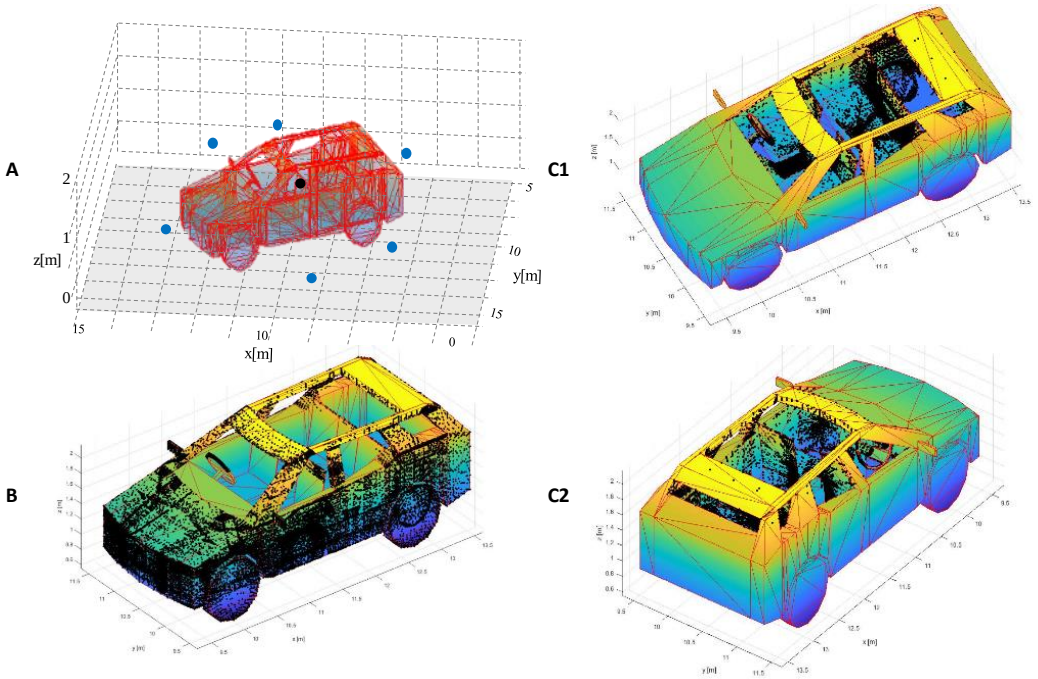

Figure 2.2 3D CAD vehicle model inside MATLAB 3D EM simulation: (A) Vehicle on the ground plane surrounded by the external RF sources (six blue dots); (B) Intersections of the rays with the vehicle's exterior walls indicating "1", for the six RF sources placed outside (black dots show the ray-face intersection); (C1)-(C2) The exterior vehicle walls show "0" if an RF source is placed inside the vehicle.

The preliminary tests, involving a full body vehicle based on direct measurements and partial CAD schematics, composed from convex volumes to facilitate a smooth RT run-time suggested that the RF sensor's structure and position needs to be assessed at sensor level since the simulation showed that splitting the Rx in one for outside and one for inside detection may be the beneficial. **Figure 2.2A-C** illustrate the quantitative RT simulation results, the black dots on the geometrical surface illustrating the ray hits. The test vehicle body, surrounded by six ray sources for external locations and one for inside is presented in A, while the cumulative ray intersection result for all six outside cases is displayed in B, while the case of the ray source being completely inside is captured in C1-C2.

The observation of the black dots showing the ray reception suggests that the Rx may need to be split in two independent units: when the ray source is outside, the interior and exterior of the car body show interception B, however when the ray source is inside the cabin the sidewalls from the doors are clear of any reception. This information would prove useful in this format if this work would not be restricted in

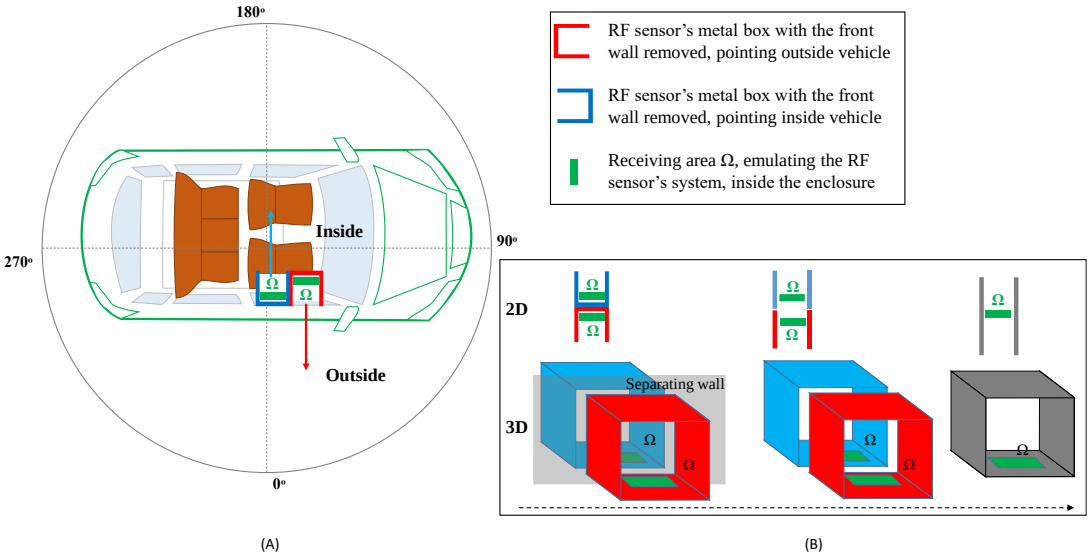

Figure 2.3 The proposed solution for the RF sensor metal enclosure positioned on the cabin window's extreme edges to avoid inside reception for the sensor designated for outside monitoring (A), and the box with two opposite walls missing simplified for the RF test (B)

terms of any installation or hole-drilling in the external car walls. However, since this is an important requirement from the industrial partner, the attention was directed towards enhancing the configuration of the individual RF sensor, as well as its positioning inside the vehicle.

The RF sensor individual configuration, as defined in the introductory section focusing on the problem formulation, includes a system enclosing box. If the box could be modified to some extent to allow reciprocation of the car sidewall's reception while separating the sensor from the cabin volume, this approach may generate the solution for the reception system. Following the above observation, the logical action is to make the enclosing box metallic, remove the front sidewall while housing the whole RF sensor inside and position the box pointing towards outside, while a similar sensor setup may point in the opposite direction achieving the inside detection. To directly test the possible enclosure design alternatives, an initial experiment needs to establish if the RF sensor metal encasing box walls can block the 2.4 GHz IEEE 802.15.4 signal as they stop the simulation rays. Therefore, a large metal box encasing a receiving sensor representative for this study is required to be created. **Figure 2.3** presents the potential alternatives of positioning the enclosed RF sensors pointing inside and outside the car: either the two sensors are located in two distinct enclosure boxes with separating walls (A), while a potentially simpler setup for testing may result by

positioning the two sensors in a single rectangular enclosure with two opposite walls missing (B).

The test box with two opposite walls missing will be tested to observe if when a 2.4 GHz signal transmitted perpendicular to the walls may attenuate the received signal inside the enclosure to the level that when compared with the signal received when the box openings are orientated towards the RF source may be considered as equivalent with a simulation ray miss. The two missing walls solution instead of just one is preferred for testing as it doubles the chances that the signal reaches inside the box, transforming the scenario in an unfavourable one. Since the RSSI levels will determine a set of values when the signal points to the walls and another set when is directed to the openings, in order to differentiate between the two sets, an arbitrary threshold will be required. Moreover, since the box size chosen for the RF test size may enclose more than one RF sensor, it will be recommended that the area inside the box to be divided in smaller areas and the sensor's receiving antenna to be positioned sequentially in all positions.

2.2 RF sensor metal enclosure test setup

Following the considerations outlined in the previous section, the setup for the empirical test of the metal box enclosing the RF sensors in multiple positions is built as follows. The metal enclosure is a rectangular metal box missing two opposite sides, placed on top of a rotating shaft. The shaft is fitted on a metal tube one meter above the ground and fixed using a wooden frame. At the opposite end of the wooden frame, two metres away, a PVC tube has been used to support a 2.4 GHz transceiver module (i.e., the RF source) orientated towards the box with its PCB dipole antenna. A rectangular cardboard sheet divided in nine equal areas is placed inside the metal box to guide the positioning of the RF sensor. The dipole antenna of the 2.4 GHz receiver is progressively moved on each marked cardboard area and secured with adhesive tape, while the receiver module is attached underneath the box on the metal tube. The RF source is set to continually transmit a fixed length bit frame via the IEEE 802.15.4 communication protocol with 0dBm power on channel 11 (2.405 GHz). The RF receiver is set to count 100 received frames and to display the average RSSI value. As

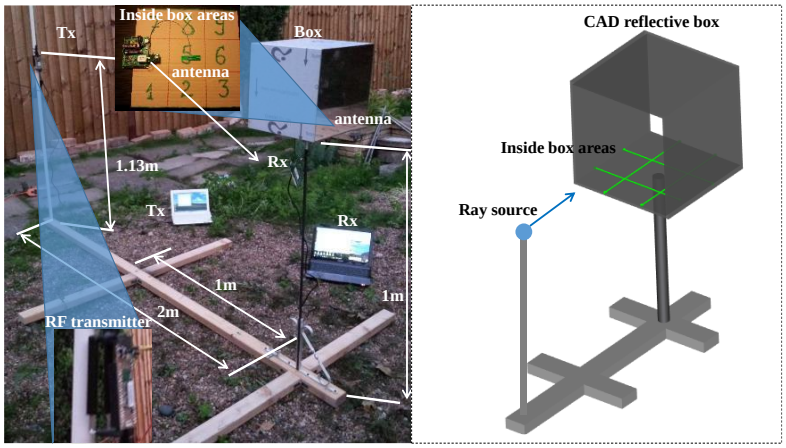

Figure 2.4 MATLAB 3D electromagnetic simulation: empirical simulation setup (A); CAD design of the empirical scenario setup (B)

the frame is set to be short, it takes between 3 and 5 seconds to record 100 values. In the 2 m testing setup's range there were no packages lost (0% PER), but only occasional frame errors (variable% BER) and since the RSSI is related to the received frame's preamble bits and not to the error susceptible payload, the account for the erroneous received frames was not necessary. The receiver antenna is then moved successively to all cardboard areas for each box rotation. The box is rotated using four angles of rotation, starting at 0º and facing the RF source with its openings, and then to 90º, 180º and 270º. As the rotation step is 90º and the box is rectangular, the 0º and 180º degree, and 90º and 270º degree positions are equivalent, and only the positions from the cardboard numbered areas indicate a spatial difference. The 36 results recorded from this experiment are saved in a .csv file. The experimental setup used a 2.4 GHz PCB antenna (Pulse electronics) W3525B100 – UFL [236], in combination with a Jennic NXP wireless microcontroller JN5168 delivering an Rx sensitivity down to -95 dBm [237]. **Figure 2.4** illustrates the experimental setup A, and the CAD design of the scenario B used for RT simulation. To be noted that the outside temperature was between 22-24º C, dry, with no obstacles between Tx and Rx.

2.3 Results and discussion for the RF sensor enclosure test

The 3D measurement setup was replicated in FreeCAD by using real component sizes. The CAD data was exported in STL format and subsequently imported in MATLAB.

Two ray reflections were simulated, to replicate the quantitative simulation previously applied to the car, since ray tracing scenarios involving only two reflections are performed in several studies [238, 140], demonstrating their sufficiency in characterising the EM field inside a large cavity like a vehicle.

When validating the results between measurements and simulation, it is desirable that the simulation results conserve their ideal scenario profile without bringing new errors due to transformation, therefore the conversion of the empirical RF measurements to quantitative data, such as hit-miss intersection points will be employed. To perform this transformation, the RSSI measurements are organised in receiver-related sensitivity sets mapped to a binary value. This binary mapping of intervals is known as the indicator or characteristic function, and is used in various forms in areas such as signal processing [239], mathematics [240], computer vision [241].

The general form of an indicator function is:

$$F(x) = \begin{cases} 1, x = 1 \\ 0, x \neq 1 \end{cases} <=> \begin{cases} 1, x = 1 \\ 0, x \in (-\infty, 1) \cup (1, \infty) \end{cases} \quad (2.1)$$

For the case presented in this study the following form will be adopted:

$$F(x) = \begin{cases} 1, x \in [Rx_{low}, Threshold] \\ 0, x \in [Threshold, Rx_{high}] \end{cases} \quad (2.2)$$

where the interval [Rx_{low}, Rx_{high}] is the receiver sensitivity interval in dBm and *Threshold* is an arbitrary value belonging to it.

The simulation results are consistent with the RF measurements and are presented in **Table 2.1**. Whereas the simulation shows the quantitative ray-area intersection in absolute values as "1" for presence and "0" for absence, due to environmental reflections, box edge diffraction and interferences, the measurement setup shows as expected a maximum set of values for presence and an attenuated set of values for absence. The measurements present a "-" outlier for the box rotation at 90º on area 3, generated by the absence of the receiving signal. It can be noted that to distinguish the same binary behaviour delivered by the simulation, the RSSI values need to be grouped in sets, where each individual area corresponds to its own set, in relation with "1" and "0". Overall, due to the spatial position differences between the areas, small area sizes (each area measures 9 x 8cm), multipath environment inside the metal box,

Table 2.1 The RSSI measurements, in dBm units, recorded from the rotating metal box experiment, (top table) for the nine receiving square areas, at 0º, 90º, 180º and 270º. Each column threshold is also shown for the indicator function F(x), transforming the dBm values in binary values. The bottom table presents the MATLAB 3D electromagnetic simulation binary results for the hit/miss of the receiving square areas inside the box. The red values show the result errors evidenced when the theoretical values were compared with practical ones. The errors are due environmental reflection and measurement conditions.

Degrees	**Metal box measurements, one to nine square areas RSSI reception [dBm]**								
	1	**2**	**3**	**4**	**5**	**6**	**7**	**8**	**9**
0	-78.3	-82.7	-85.6	-87.5	-90.3	-81.8	-84.2	-91.1	-76
90	-94.7	-91.2	-	-91.1	-86.1	-89.7	-92.2	-95	-93
180	-82.2	-89.2	-82.8	-85.4	-87.1	-86.6	-86.5	-79.2	-78
270	-95	-91.1	-94.3	-88.1	-94.6	-95	-95	-91.4	-93
Minimum threshold per column	-83	-90	-86	-88	-91	-87	-87	-91.2	-79

Degrees	**Experimental results transformed via indicator function *F(x)* to binary outputs [hit/miss]**								
0	1	1	1	1	1	1	1	1	1
90	0	0	0	0	1	0	0	0	0
180	1	1	1	1	1	1	1	1	1
270	0	0	0	0	0	0	0	0	0

Degrees	**Reflective box RT simulation, square areas hit/miss reception**								
0	1	1	1	1	1	1	1	1	1
90	0	0	0	0	0	0	0	0	0
180	1	1	1	1	1	1	1	1	1
270	0	0	0	0	0	0	0	0	0

and imperfect omnidirectional antenna, a general distinct subset delivering for all test areas specific transformation values of "1" or "0" is not feasible.

When the measurement values are transformed from dBm to binary, based on individual thresholds for each receiving area and compared against simulation values, two more errors are observed for areas 5 and 8:

- In area 5, despite fully receiving the packages, the recorded signal at 90° is stronger than the one received at 180° probably due to secondary environmental reflections. Therefore, finding a local threshold to display the expected binary behaviour is not possible.

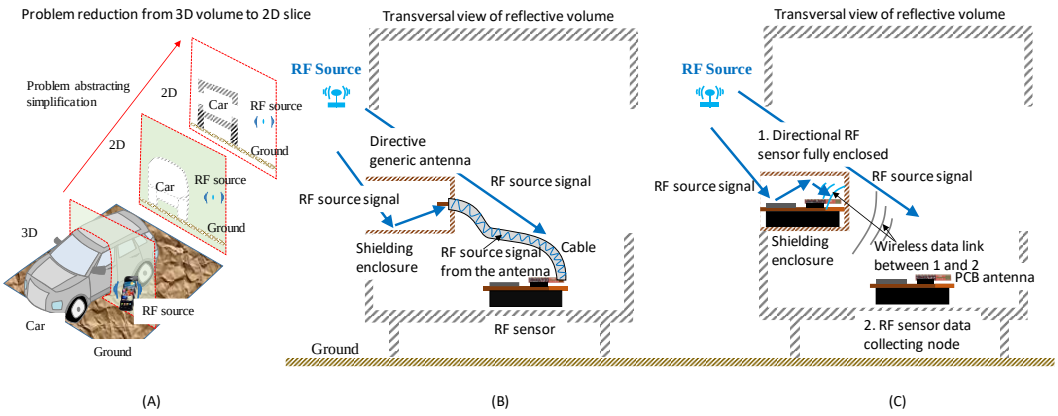

Figure 2.5 Two possible RF sensor synthesis explained on a 2D slice of the car (A) based on the shielding enclosing result: a central RF sensor connected through cable to a network of directional antennas (B); a central RF sensor equipped with a local omnidirectional PCB antenna wirelessly connected to a similar RF sensor fully encased (C)

- In area 8, the received values for 0º and 270º are very close, the threshold being separated only by a subunit interval. This is due to the receiver imperfections and surrounding reflections.

By accounting the three errors from a total of thirty-six possible resulted from nine receiving areas measured at four different angles, the confidence interval is over 91.7%. In fairness, it should be 94.5% by considering the "ray miss" case labelled as "–" as an acknowledgement of signal absence for area 3.

Moreover, relying on the observations from the simulation and empirical results, it is recommended that the enclosed RF sensors transmit to a central node the processed data instead of collecting through an antenna network the raw signals, in order to avoid cable coupling and therefore false detection inside the car's cabin. If the raw signal is transmitted through long cables (length is relative to the ~12.5cm RF wavelength for 2.4GHz) the cables may act as antenna extensions and the sensor's directionality advantage will be lost. The RF sensor's transceiver therefore needs to be inside the shielding enclosure, together with its primary antenna and should not use the enclosure as a potential antenna. The two scenarios are schematically depicted in **Figure 2.5**, outlining the directivity benefit of the recommendation for complete RF sensor housing. In scenario B, the raw RF signal traveling the cable may interfere with the RF source signal whereas, the wireless data link between the two RF sensors illustrated in scenario C, despite enclosure back attenuation, given the short distance constrained by the size of the vehicle in the case of this work, can produce a robust data link.

To summarise, the 2.4 GHz based empirical tests through transformation via indicator function supported the expected binary behaviour predicted by RT quantitative simulation. Therefore, by exploiting the observation that the metal enclosing box with a missing wall may deliver a valid RF separation between two opposite pointing sensors, we may proceed and use the information for the RF sensor design. Moreover, the sensor will be completely encased in the metal enclosure along with its primary PCB antenna while detecting the RF mobile source presence and then transmitting wirelessly the data to a central node. For this work, the central node could be placed outside the cabin since it is wirelessly connected to the RF sensors, however as it emulates a potential vehicle's on-board connection, it will be placed on a central console inside the cabin, realising relative homogenous link distances with the network's detecting sensors.

2.4 MATLAB simulation of 3D RT ray source modelling

The MATLAB RT simulation overall implementation provided the basic means supporting the RF sensor design. However, since the software coding of its functions and algorithms required careful adjusting and tailoring of the available toolkit's resources, it would be considered important to mention possible background information representative for the 3D RT simulation such as ray source modelling.

The 3D simulation via RT of the RF source as an omnidirectional point source, after implementing the vector ray-face intersecting algorithm may seem to be a trivial programming task. The classical physics books provide examples based on RF sources modelled as spherical and plane waves [242], however, the RT as a discrete simulation may produce various implementations each yielding different results. From the algorithmic ray forming perspective, we can distinguish three methods: forward, when the ray is constructed from the source towards the geometrical target; backwards, when the ray is constructed from the geometrical target towards the source; and hybrid when a mixture of the previous two methods is employed [243].

Figure 2.6 sketches the main differences between RT method usage in digitisation (A), and in 3D simulations (B). The digitisation method transforms an analogue shape in discrete samples commonly represented as pixels, while the 3D simulation benefits

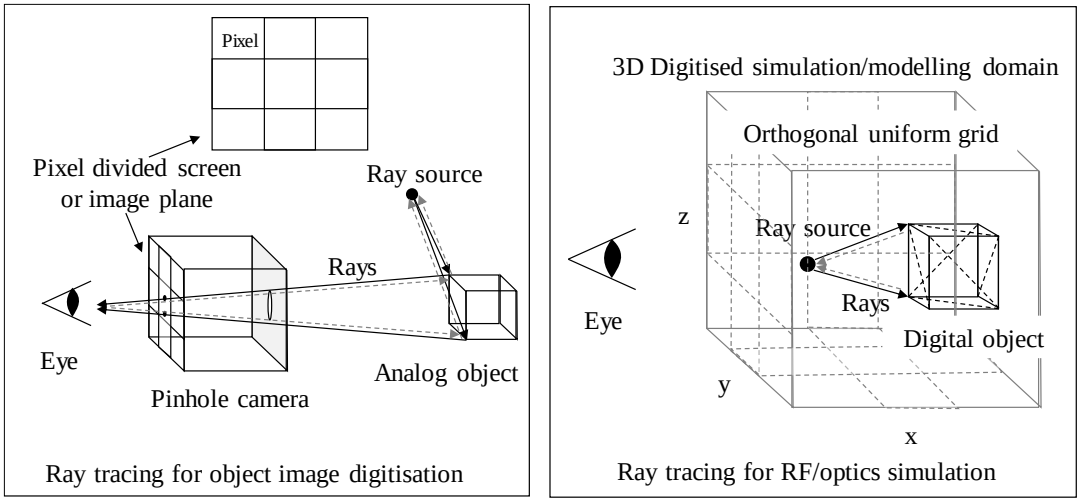

Figure 2.6 Illustration of the distinction between ray tracing methods used in analogue object digitisation (A), and the ray tracing used in 3D optics and RF simulations (B). The grey dotted rays show the backwards casting technique,

from a default digital environment. The geometry point transformation of the simulation object follows straightforward rules, such as point-by-point generation of a line with a pre-set step. Since the forward method may be inefficient by wasting resources and not covering the whole scenario, the last two methods, by discretising the scenario geometry at point level and employing one point from the digitised target geometry as the ray origin and the RF point source as the destination, are commonly used in light propagation simulations [244].

The terms sampling and super sampling adopted from analogue to digital conversion are used for a simulation area to define the same principles, however since the geometry is by default in digital format the well-defined faces and volumes may be reduced to point representation without ray sampling as mentioned before. Therefore, depending on how many points are generated to represent a geometrical area, the sampling term defines one point allocation per digitised shape, commonly a central one, whereas the super sampling assigns more than one point per shape [245, 246].

Considering the RT source model in the general case of omnidirectional propagation and acknowledging that the ray's destination points may be generated in various ways, a selection of ray source modelling examples, such as those illustrated in **Figure 2.7,** is provided to outline the different results that may occur for the same problem:

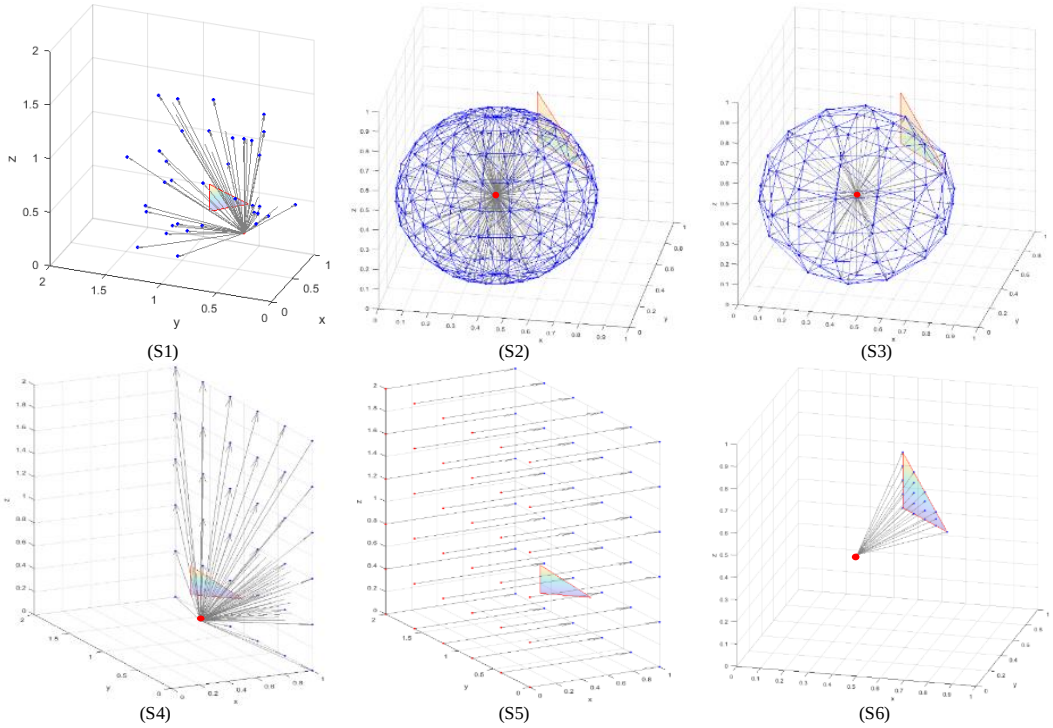

Figure 2.7 3D ray source models direction points generated by (S1) 3D random function; (S2) sphere resulting from azimuth and elevation angle; (S3) sphere resulting from octahedral edge split; (S4) enclosure box set on orthogonal grid – one wall; (S5) enclosure box set on orthogonal grid – two opposite walls; (S6) digitised target triangle – backwards super sampling. The ray source origin is illustrated as a red dot, the rays as grey arrows and the direction points as blue dots.

Source one (S1) is modelled with all its ray destinations being 3D random point coordinates associated with the Cartesian grid of the scenario's six enclosing box walls. The source origin is unique and fixed in a predefined position, in front of the reflective plane containing the two slits. The random point distribution is a common technique employed by spatial sampling methods [247] to deliver an unbiased overall homogeneity.

Source two (S2) is generated as its complete set of ray destination points are producing a spherical surface with its centre on the source's origin. Spherical wave propagation simulation is based on the principle that all surface points are equal-distant distributed. In practice, the principle raises great modelling challenges as the discrete points on a spherical surface may be constructed separately by approximate equal angles or sharing roughly equal edges. To generate an angle-based distribution, the azimuth and elevation angles are generated from the origin and then transformed from spherical coordinates to Cartesian points. By producing the same number of points for all the sphere's elevation planes, the method shows a higher point density to the sphere's top

and bottom, hence equal-distanced angles produce a nonhomogeneous point distribution. S2 follows this generation method. These types of source models are characteristic for scanning obtained by a rotating sensor or array, and if a full circle is completed, systematically increasing its elevation angle.

Source three (S3) is based on a different rule for the spherical surface generation. To construct an equal edge based spherical distribution, a method of iterative splitting of the edges from a regular polyhedron is suggested [248]. In this study case, an octahedral triangular mesh is used. The method produces uniformly distributed points on a spherical surface, with their amount controlled by the number of iterative edge splitting steps. The angles are difficult to collect and interrogate in an orderly manner, and the number of total points, respectively ray directions, is not prone to arbitrary values, since it depends on the iterative splitting process.

Source four (S4) is emulated with the destination points on a virtual uniformly spaced grid attached to the six walls of the enclosing test box. The resulting points are separated by an adaptable resolution step allowing arbitrary values for the total associated ray number. In **Figure 2.7**, S4 illustrates the method for only one of the six enclosing walls for greater clarity. The spatial homogeneity for the ray direction points is reached at the orthogonal grid level, emulating the grid projection on a spherical surface. However, to obtain the relative equal distributed point mesh through this method, the common rays' origin needs to be positioned in the middle of a cubic grid, for this example case in the middle of a cubic enclosing test box.

Source five (S5) is modelled with the destination points attached to one face of the test box's virtual grid and pointing backwards from the ray source origin mirrored on the opposite test box wall. This technique produces a ray fascicle parallel to the ground, propagating in planes of equal phase, and is often called plane wave simulation as it is used to model the EM far-field. This method does not generate the rays from the source's common origin, but from a plane perpendicular to the ground and containing the common origin. The direction points' spatial homogeneity is reached at rectangular grid level similarly to S4, however not similar to that obtained in an array point representation of space.

Source six (S6) is constructed by backwards casting, the ray starts from the geometrical target towards the source [249], and the mesh's triangular geometry is

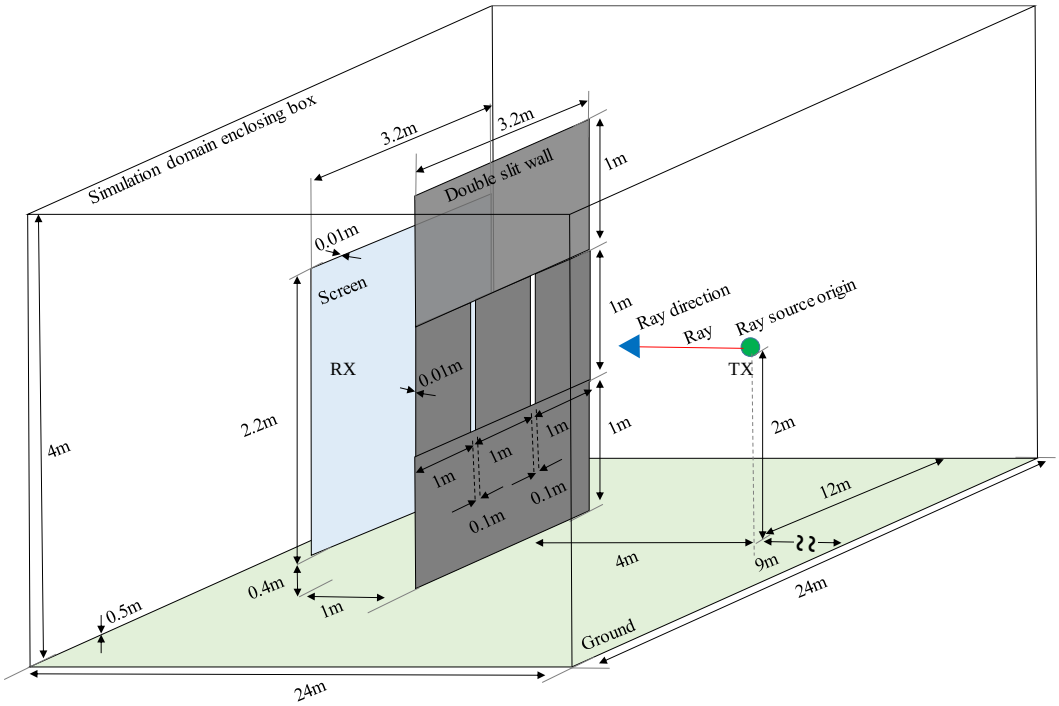

Figure 2.8 MATLAB 3D electromagnetic simulation. Two slit scenario 3D geometry. The implementation takes in account a real scenario including a ground plane

super-sampled by generating more than one ray for every geometrical simplex. To generate the beam's direction points from the scenario geometry, each shape requires a digitisation or rasterisation that transforms the 2D or 3D meshed geometry in a point cloud. The number of points generated per area or volume unit may be delivered in the RT simulation by following various rules. For this study, each mesh's triangle generates a constant number of points, independent from spatial sizes, as demonstrated in [250]. By implementing this procedure, any minor geometrical feature in the scenario, such as a thin sheet's thickness, is accounted for and is given the same status as a large detail.

One of the best ways to illustrate the effects of different source modelling for the same scenario would be to consider the simulation example of the classical double-slit experiment: a source is placed in front of a screen, separated by a straight wall with two slits in it, as in **Figure 2.8**. The RT source origin is placed inside a virtual 3D test environment represented by a large rectangular box with dimensions 24 × 24 × 4 m. The reflective plane accommodating the two narrow slits and the one behind it representing the receiving screen, are positioned parallel to each other and both perpendicular to the ground surface. Whereas the slit wall rests its base on the ground,

the back screen is 0.4 m raised above the floor and centred relative to the front wall. This illustrates a scenario where multiple reflected rays may escape due to consecutive reflections under the screen and not contribute to the overall reception. The quantitative reception principle is based on the ray's emulation as a straight-line segment and its possible intersection with a geometrical shape in the simulation environment: a successful intersection is considered a hit and marked as a dot or X on the surface of incidence, whereas a miss is left unmarked. The total number of dots or hits on a predefined receiver geometry, such as the back screen in this study, represents the quantitative signal reception, and the percentage of hits with respect to the initial ray shot number provides a scale of comparison between different ray source models sharing the same origin. It is straightforward to notice that some methods that optimise the ray cast towards a predefined target will take a toll on the total simulation time, numerous algorithms move this action from the processing or on-line phase to a separate pre-processing or off-line stage.

Figure 2.9 illustrates a 25,000-ray source modelling example, each ray being able to reflect up to ten times. It can be observed that each source's specific distribution rule may be accounted for by the back screen's pattern of dots. For S1 it displays a random arrangement with a very low point density in the middle, indicating a predominance of rays passing the openings under different angles than a slit reflection; for S2 and S3 it delivers a fringed pattern with a higher density on the left and right sides, accordingly to progressive spatial dispersion of their spherical radii, however the rays delivered by S3 present a better spatial homogeneity represented by presence of points in the screen middle region; S4 shows point fringes on the upper screen's triangular mesh as the grid associated with the enclosing box is rectangular rather than cubic, and the source origin is not central to the scenario; S5 produces two projection bands of the slits' openings on the screen as a result of its perpendicular incidence on the double-slit wall's geometry, displaying only the passing rays non-interactive with the 3D scenario; S6 delivers a fringe distribution similar to a diffraction pattern, however this is due to the multiple reflections generated by the slit openings wall thickness and the reflective space between the slit wall and the screen. The percentage of successful ray hits of the screen from the total launched, as well as the specific source simulation times for the above scenarios are presented and discussed below.

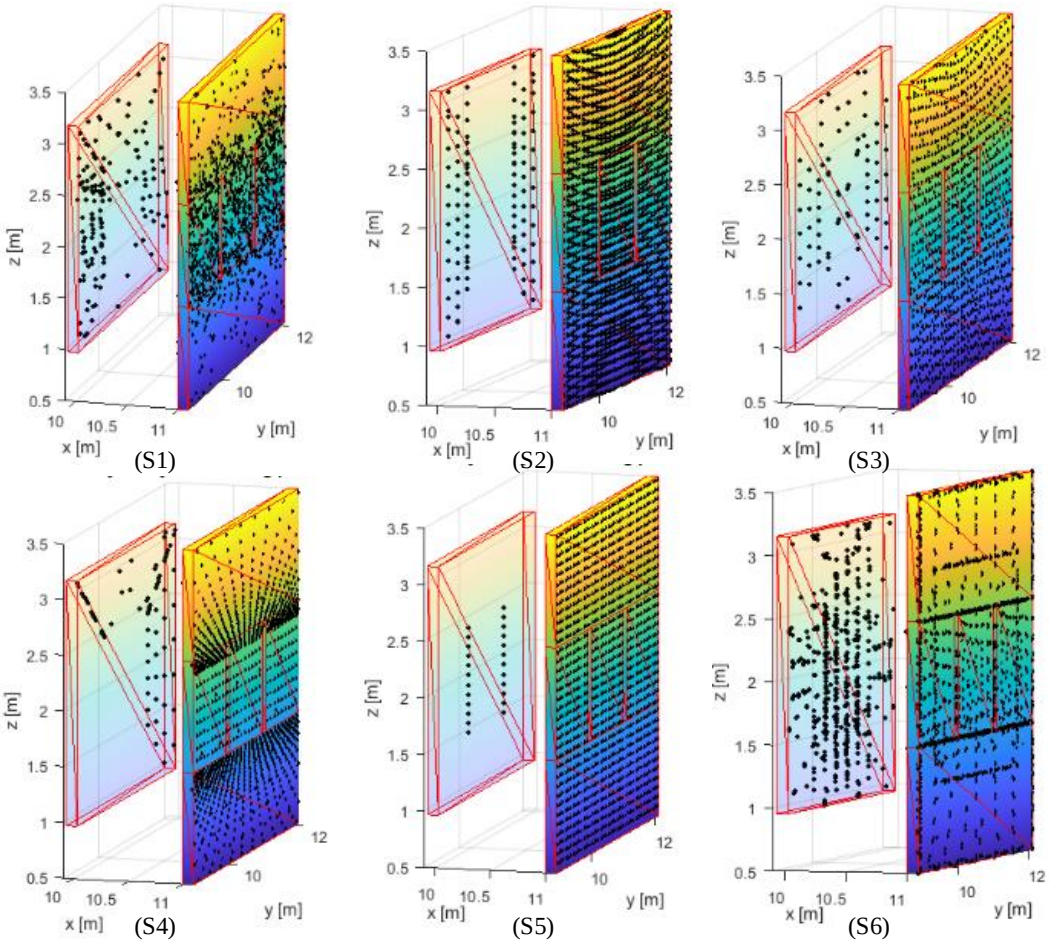

Figure 2.9 3D double-slit experiment "target “hit” visualization (black dots) for 25,000 rays using the source model: (S1) 3D random function; (S2) sphere resulting from azimuth and elevation angles; (S3) sphere resulting from octahedral edge split; (S4) enclosure box set on orthogonal grid – one wall; (S5) enclosure box set on orthogonal grid – two opposite walls; (S6) digitised target triangle – backwards super sampling.

The first result set displays the percentage of ray intersections with the Rx back screen resulting from an initial variable number of rays modelling the Tx source. Since the screen is considered during the simulation as a reflective surface, some rays will bounce between the slit wall and Rx plane producing multiple hits, others will intersect only once if their incident angle to the surface’s normal is 90º, and the rest will not pass through the two-slit wall and will be absorbed by the enclosure box’s boundary walls. **Table 2.2** shows the quantitative results as a percentage metric. It can be observed, that despite using the same number of initial shooting rays when increasing the beam density, the methods using S1, S5 and S6 tend to deliver a constant result,

Table 2.2 3D double-slit experiment ray screen-hit percentage for six different ray source (S) models and various ray densities of 2000; 10,000; 25,000 and 100,000 rays

Ray No	S1	S2	S3	S4	S5	S6
100,000	1.62	0.19	0.32	0.96	0.30	9.00
25,000	1.58	0.21	0.33	0.79	0.22	9.38
10,000	1.49	0.00	0.58	0.72	0.23	10.54
2000	1.81	0.00	0.13	0.60	0.20	10.46

whereas S2 and S4 gradually improve their hit rate, and S3 displays a local optimum. The sources S2 and S6 deliver the minimum and respectively maximum successful receptions, S2 exhibits a poor directionality due to its parallel stacked circular planes of equal angle, whereas S6 is constructed from the scenario's geometry backwards to the source, and therefore displays a high efficiency. The 3D random direction generation of S1 accounts for the second-best hit performance after S6. And despite of S1's performance being approximatively nine time lower when compared to S6, S1 still delivers a much higher percentage when compared to the remaining four sources. Contrary to expectations, the source S2 misses the two slits entrance completely for an initial number of up to 10,000 rays, whereas the parallel beams generated by S5, deliver a better performance for all ray densities, although out of focus, perpendicular to the screen's surface, and producing no more than one hit per ray. Comparing S3 and S4, which both follow a homogenous spatial distribution for their direction points, S3 on a spherical uniform grid and S4 on a rectangular orthogonal spacing, S4 delivers an almost double hit count on the Rx plane.

Table 2.3 displays the comparison of the on-line RT simulation durations for the results recorded in **Table 2.2.** The durations show that despite of S6 producing the best Rx hit results, it is the slowest performer because it requires additional time to digitise the 3D scenario. The random ray direction generation of S1 displays similarly low simulation times as for the sources S2, S3 and S4, whereas the fastest execution is delivered by the parallel ray fronts modelling source S5. It should be noted that for small experimental scenarios, such as those used in this study, with a total number of faces smaller than 1,000 and only up to ten reflections, the implementation of RT accelerating methods may not be necessary based on these results.

Table 2.3 3D double-slit experiment running simulation times in seconds without graphics for six different ray source (S) models and ray densities of 2000; 10,000; 25,000 and 100,000 rays

Ray No	S1	S2	S3	S4	S5	S6
100,000	7.01	8.58	8.53	10.41	4.98	15.62
25,000	1.90	1.90	1.99	2.08	1.52	2.98
10,000	1.24	1.17	1.15	1.44	1.19	1.58
2000	1.11	0.98	0.95	1.07	0.99	1.18

It can be observed that the RT method and sampling strategy is very important in the context of the simulation's aims and objectives, as each one can provide a different solution for the same problem. For this project, the RT backward super sampling method (S6) was used, since this method accounts for the thickness of the metal box's walls or the car's windows frames which present small geometrical details when compared with the total scenario.

3. RF modelling

The RF modelling is a composite sequential process. The first step of the process relies on previous results from the 3D RT simulation implemented in MATLAB with the aim of developing the RF sensors necessary for the empirical data acquisition setup.

After presenting the RF sensor manufacturing, schematics and characteristics, they are employed in two different experimental setups: RSSI fingerprinting data base and inside-outside vehicle detection and location of a mobile RF target. The importance of different transmission-reception setups is evidenced by the RSSI fingerprinting results for three different polarisation combinations, however only the horizontal polarisation is used for the rest of the study since it represents a disadvantageous case versus mix polarisation, while vertical polarisation is not a practical solution for the vehicle scenario.

Two propagation models are created, one based on the RSSI fingerprinting empirical data and one resulted from Friis' path loss formula. The models are compared and used in parallel to deliver ranging estimations for the second experimental setup, the mobile source location inside-outside vehicle. A straightforward detection algorithm able to discriminate between inside-outside RF target position with a success of 100% is presented. Moreover, for the location accuracy analysis, the multi-lateration method is discussed in parallel with the sensor ranging, to determine if any error reduction is possible through this technique. The overall accuracy for inside-the-vehicle localisation achieves a maximum RMSE of ±0.4 m, meeting the initial aim of achieving an accuracy of under ±1 m. For the outside location, the RMSE accuracy is found to vary between ±0.02 and ±1.44 m, which is acceptable when considering the low density of RF sensors covering the outside perimeter. The actions involved during the RF modelling and testing workflow are summarised in **Figure 3.1**.

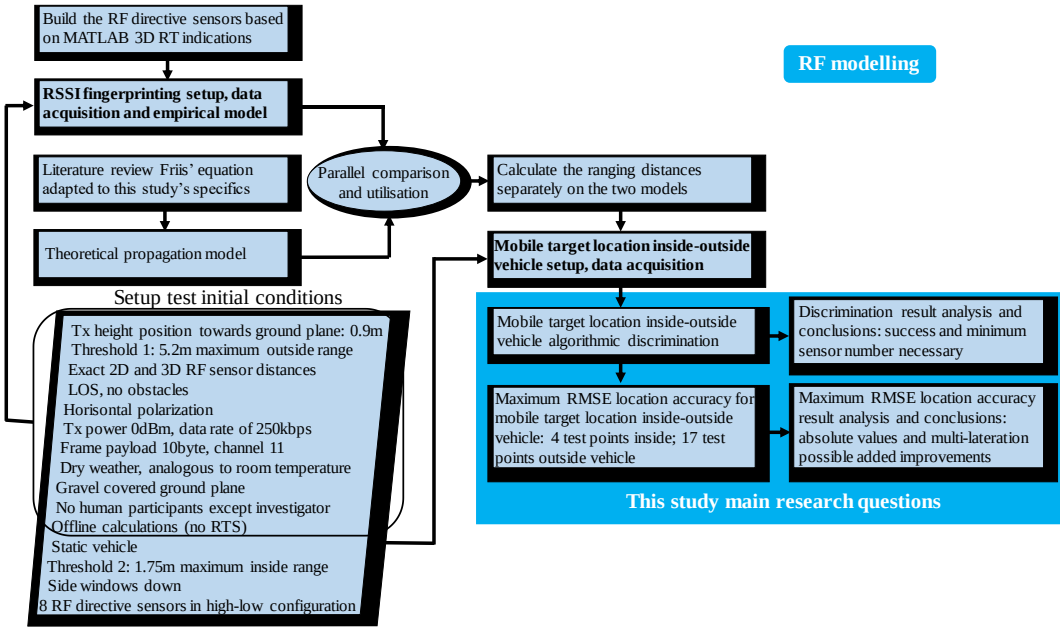

Figure 3.1 Workflow diagram for RF modelling and testing

3.1 Construction of the directional RF sensors

Following the findings highlighted in the previous 3D RT simulation section, the next steps of this study towards the overall goal involve prototyping and placing the RF sensor inside a metal enclosure, as well as separating the Rx in two detecting units, one for inside and the other for outside detection. Since no Automotive Electronics Council (AEC) qualified alternatives were found for JN5168 transceiver chip used previously in the RT simulation validation, the component was replaced with Microchip's 2.4 GHz transceiver MRF24J40MA [251] in combination with PIC24F16KA102 using eXtreme Low Power (XLP) technology [252]. Microchip's variants MRF24J40-I/MLVAO and MRF24J40T-I/MLVAO are automotive qualified transceivers, therefore after passing the proof-of-concept testing stage the RF sensor design involving car integration may continue its development path according to current standards. To reduce ordering and manufacturing time, the RF sensor boards were manufactured internally via CNC machining, the process presenting advantages for immediate error corrections and design improvements, but drawbacks in miniaturisation opportunities, challenges when combining multiple copper layers, and overall aesthetics, **Figure 3.2.**

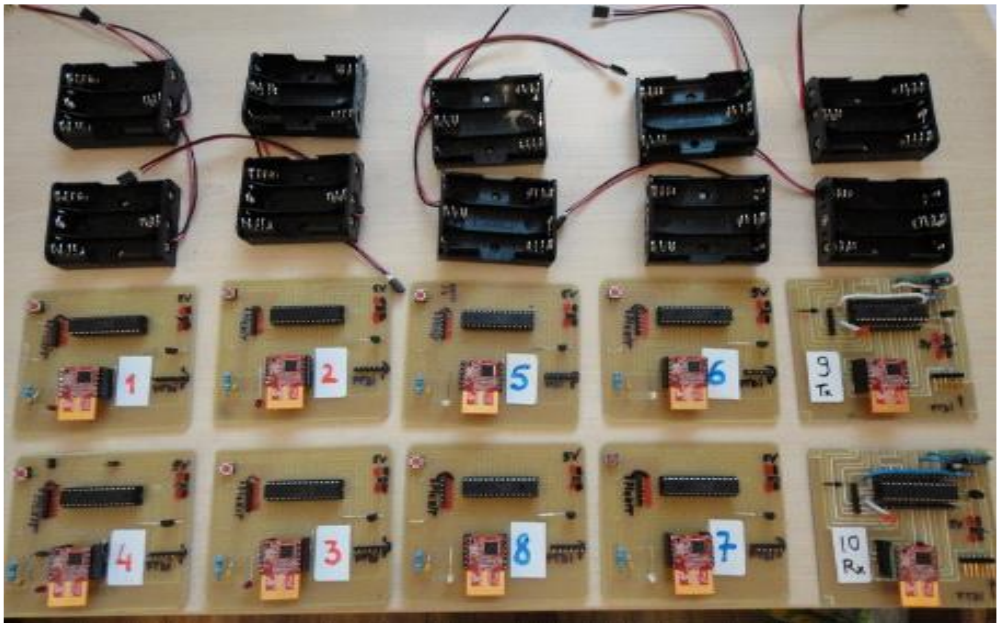

Figure 3.2 Ten single board RF sensors, CNC-manufactured on single-layer FR4 copper (bottom) clad and their associated battery supports (top)

The electronic schematic for the RF sensor is presented in **Figure 3.3**.

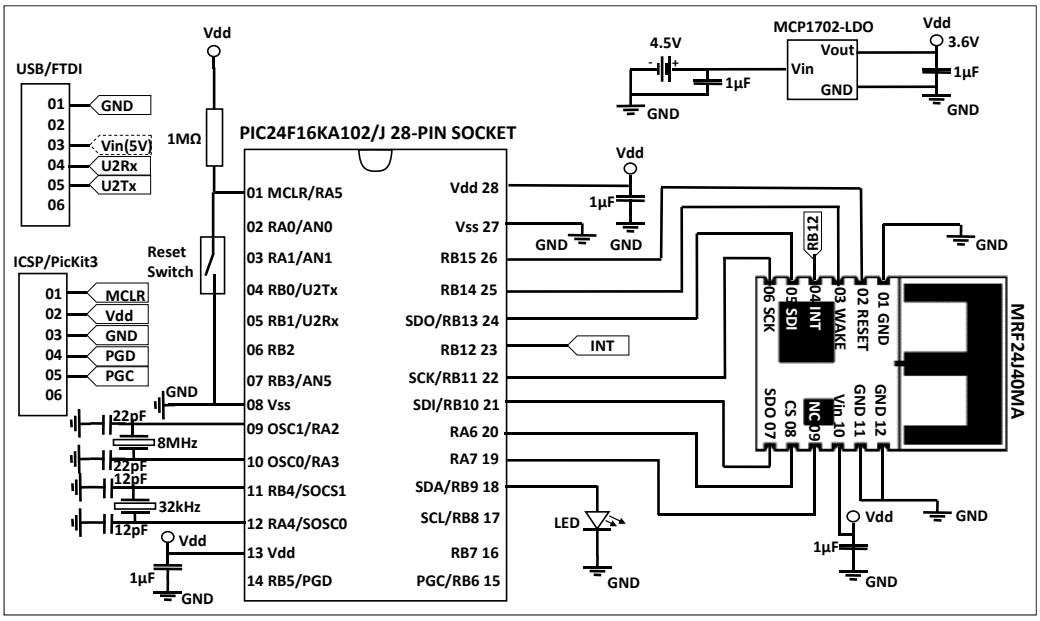

Figure 3.3 Electronic schematics of the RF sensor based on 2.4GHz MRF24J40MA transceiver and PIC24F16KA102 16-bit microcontroller

The sensor offers a direct-programming interface through its In-Circuit Serial Programming (ICSP) connection, whereas the serial port, mediated by a Future Technology Devices International (FTDI) TTL-232x [253] cable, is based on the PIC's second Universal Asynchronous Receiver/Transmitter (UART) interface. To increase the sensor lifespan, a larger power source composed from three-1.5V AA batteries was used in conjunction with the external MCP1702 low dropout (LDO) voltage regulator.

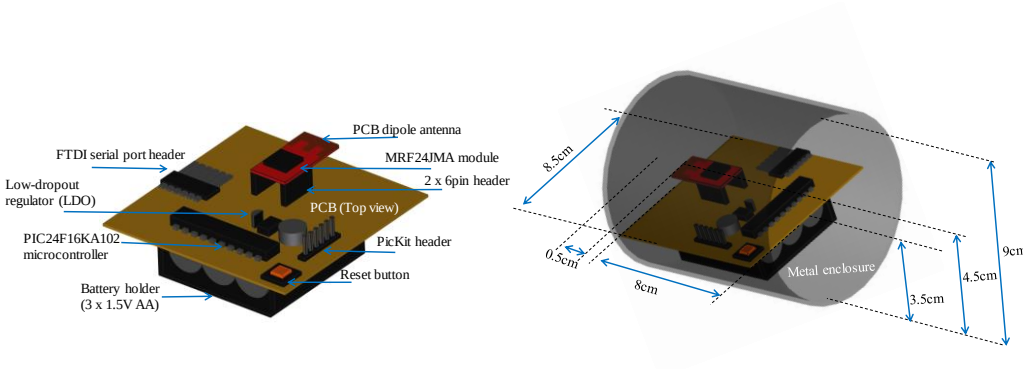

Figure 3.4 Dimension and three-dimensional (3D) schematics of the proposed RF sensor based on a MRF24J40 transceiver, outside and inside a cylindrical metal enclosure

The 3D overall wireless sensor schematics, its enclosure, position and dimensions are shown in **Figure 3.4**. Since the sensor circuitry is completely confined within the cylindrical shielding, the wireless transceiver's embedded PCB antenna is placed in close proximity of the enclosure's back wall to reduce side-receiving sensitivity towards delivering an increased directivity.

The radiation pattern of the RF module in the xy-plane was measured with and without the enclosure. **Figure 3.5** illustrates the empirical results of the measurements carried out to test the efficiency of the metal enclosure at 0dBm transmitting power in a horizontal polarisation configuration. At the same time, the MRF24J40MA transceiver datasheet [251] states that -35 dBm is the RSSI starting value, thus indicating a good reception. Since the RF sensor was placed inside the enclosure with the transceiver antenna pointing towards the cylinder's obstructed end, the maximum RSSI of -35dBm is received at 0º.

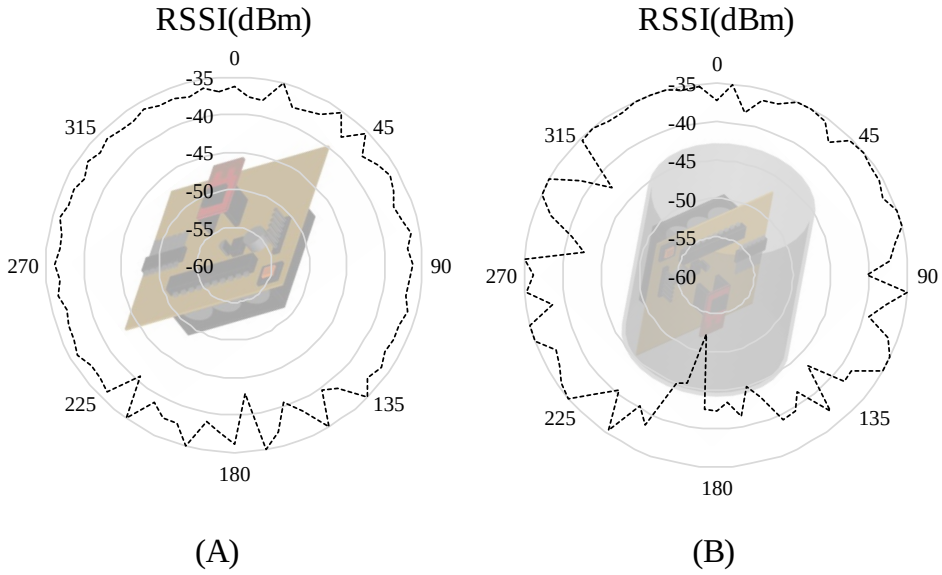

(A) (B)

Figure 3.5 Radiation pattern for the RF module for horizontal polarisation measurements without enclosure (A), and inside enclosure in the xy-plane (B)

Measuring the 2.4 GHz sensor RSSI polar pattern for custom RF sensors accepts angle steps of 15º [254] down to 30º [255], and previous research measuring the directionality of the MRF24J40MA custom sensor reports recording angles down to 10º per step [78, 256]. The polar measurements conducted in this work employed a 5º step measurement.

Since the sensor circuitry is completely confined within the cylindrical shielding its design may resemble a coffee-can antenna [257-259], a circular waveguide [260], a cylindrical [261] or tubular antenna [262]. However, since the wireless transceiver's embedded PCB antenna is placed in close proximity of the cavity's back wall to reduce side-receiving sensitivity towards delivering an increased overall directivity, the complete sensor resemblance is with an antenna operating inside an imperfect cylindrical shield [263].

3.2 RSSI fingerprinting measurement setup

For the RSSI ranging-fingerprinting setup used in this study, the transmitter node (Tx) was set to transmit on channel 11, 2405 MHz based on IEEE 802.15.4 standard protocol with 0dBm power, a short frame of ten bytes payload. The Tx and Rx are both placed on aluminium tripods at 0.9 m height above the ground.

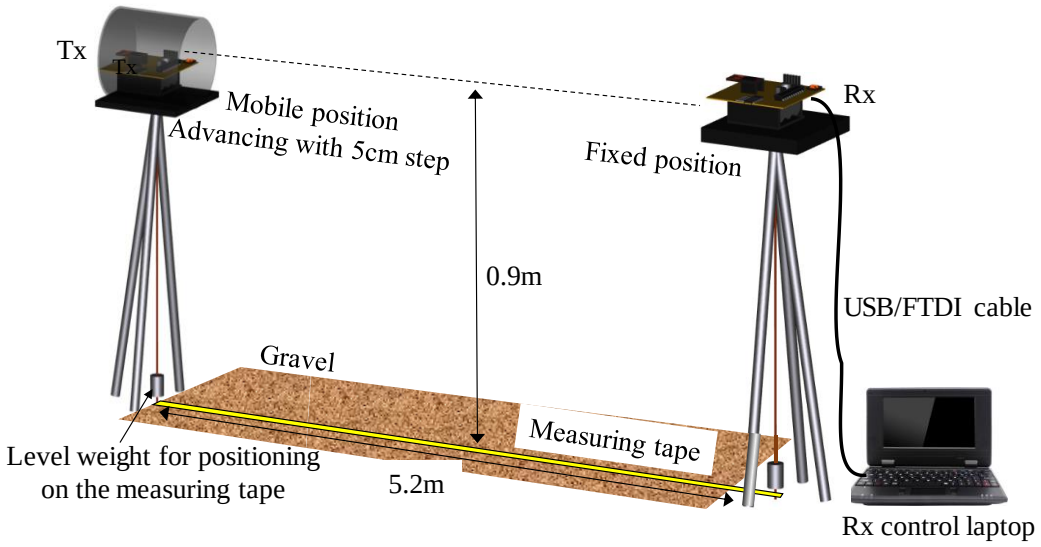

Figure 3.6 RSSI ranging-fingerprinting setup for horizontal polarisation

While the Rx's location was fixed, and it was connected to a laptop running MATLAB recording data in a text file after receiving 100 packages with zero package error rate (PER), the Tx was moved progressively with 5cm steps along a 5 m long straight line, **Figure 3.6**. A measuring tape was used on the ground to mark the straight line between Tx and Rx, the line starting at 0.2 m and ending at 5.2 m.

3.3 RSSI fingerprinting results and RF link polarisation combinations discussion

The RSSI is sensitive to the polarisation between the transmitter and the receiver, a difference of 90º producing theoretically a complete signal loss. However, as in practice different reflective surfaces are not aligned in parallel to the Tx-Rx system, due to polarisation shifts, communication is still possible [264]. The RSSI sensitivity to different combinations of polarisation between Tx and Rx have been outlined by other studies as well [104, 105], however since in this work the integrated MRF24J40MA module's PCB monopole antenna [78] is used for Tx, and a similar module housed by a cylindrical metal enclosure will deliver the Rx, the polarisation investigation will differ as the two systems Tx and Rx are not identical.

Nevertheless both Tx and Rx RF sensors have their radiation pattern slightly modified when compared with the original transceiver module, due to the PCB mountings, enclosure, etc., their polarisation towards the ground plane may be referred to as the module's original when communication systems are arranged in specific test combinations [78, 265]. For the purposes of this study, three main polarisation configurations will be investigated based on the same setup as the one presented previously for the RSSI fingerprinting. **Figure 3.7** illustrates the three Tx-Rx combinations in the vehicle context. Since the omnidirectional RF sensor emulates the mobile source whereas the directional shielded RF senor represents the in-cabin detection system, it is obvious that only the scenarios presented in the cases A and C, corresponding to horizontal and mixed polarisation, respectively, may add value in this work context. Mounting the directional sensors on one of the configurations for

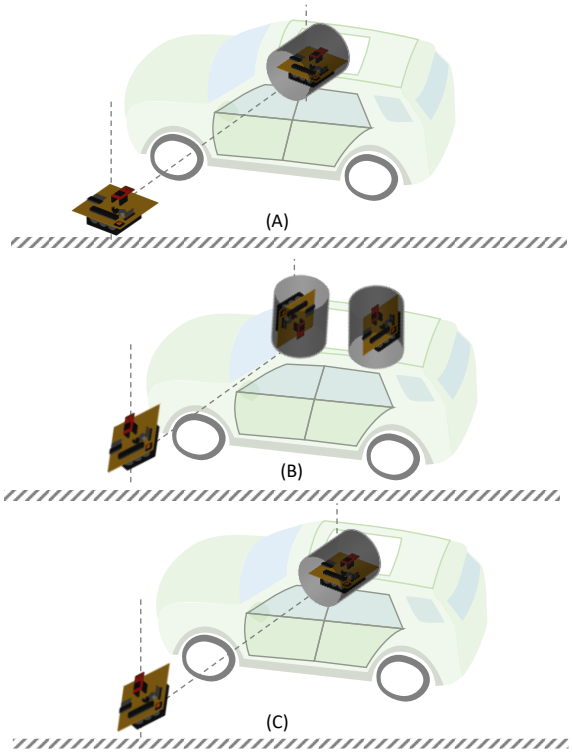

Figure 3.7 RSSI ranging-fingerprinting Tx-Rx RF sensors polarisations: horizontal (A), vertical (B) and mixed polarisation (C). For vertical polarisation, two position settings may be accounted for the shielded RF sensor, one facing the ground plane and the other one facing the sky, none of them presenting practicality for the presented RF location scenario.

vertical polarisation as illustrated in **Figure 3.7C** may be presented only for comparison or scientific curiosity reasons.

Figure 3.8 illustrates the three measured polarisations plotted over a 5 m distance with a measurement point at every 5cm. It was observed, as expected, that the vertical Tx-Rx setup provides the most inconsistent RSSI, however communication was perfectly

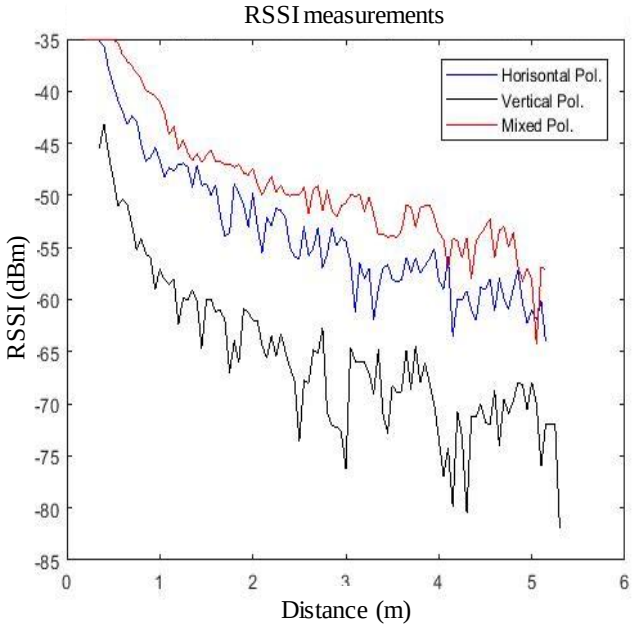

Figure 3.8 RSSI ranging-fingerprinting data for horizontal, vertical and mixed polarisations

possible. Mixed polarisation achieved the highest RSSI, because the vertically polarised signal suffered less attenuation due to earth coupling when the receiver sensor's enclosure direction is directed towards the transmitter. Although used only for comparison reasons, the vertical setup supports the suggestion of using the directional RF sensors as a wireless network system communicating the RSSI received data to a central node, despite RSSI being unreliable the communication link is still above the default transceiver's highest Rx sensitivity of -94dBm [251]. As the sensor orientation is similar to that of vertical polarisation while the source position is that of mixed polarisation, horizontal polarisation provides a compromise between the two in terms of RSSI attenuation.

Following the same path as for the RF communication channel selection, we will take forward the horizontal polarisation for the ranging-fingerprinting data modelling as the worst-case scenario, since the vertical polarisation does not represent a possible

deployment scenario and was added only for comparison reasons, while the mixed configuration provides the best Tx-Rx link. By excluding the vertical setup as not physically viable and the mixed one as providing the best results therefore favouring subjective aspects of the concept to be demonstrated in this work, this study will focus to demonstrate proof-of-functioning only for horizontal polarisation.

3.3.1 Theoretical propagation model

For this study's location problem, the Friis free space propagation formula (1.9) was adopted in the below format:

$$P_{Rx} = P_{Rx0} + P_{Tx} + G_{Tx} + G_{Rx} - 20\log\left(\frac{4\pi d}{\lambda}\right) \quad (3.1)$$

where P_{Rx0} is the received power at the reference distance d_0, in this case 20cm. Based on the initial setup and settings, the received power at 20cm is -35dBm, therefore:

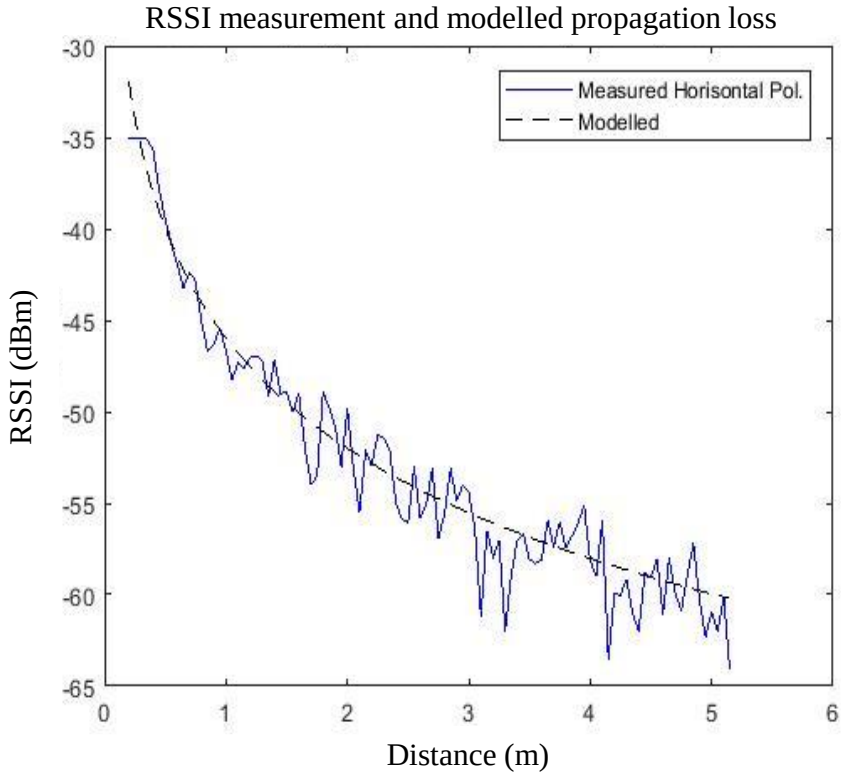

Figure 3.9 RSSI ranging-fingerprinting data for horizontal polarisation and the theoretical model plotted over the empirical data

$$P_{Rx0} = -35 - P_{Rx}(d_0) \quad (3.2)$$

Acknowledging the presence of a generic 3 dB ambient noise in the equation (3.1) and introducing the initial conditions described by (3.2), the resulting theoretical model is compared against the empirical data in MATLAB, resulting a high correlation of 0.97 (i.e., Pearson's correlation coefficient) and a minimum RMSE of 1.72dBm between the two models:

$$P_{Rx\_model} = P_{Rx} + N = P_{Rx} + 3 \quad (3.3)$$

The theoretical model's curve plotted over the RSSI empirical measurements for horizontal polarisation is displayed in **Figure 3.9.** From this point onwards, the focus will be on the two models described above, one derived empirically from ranging-fingerprinting and the second one based on Friis' free space propagation formula.

3.3.2 Generating ranging distances from data models

Whereas generating the ranging distances is a straightforward process when using the theoretical model without including in it the effects of multipath or shadowing [85, 86], in the case of the empirical model, which implicitly includes location specific induced interferences, the distance estimation based solely on the RSSI data is

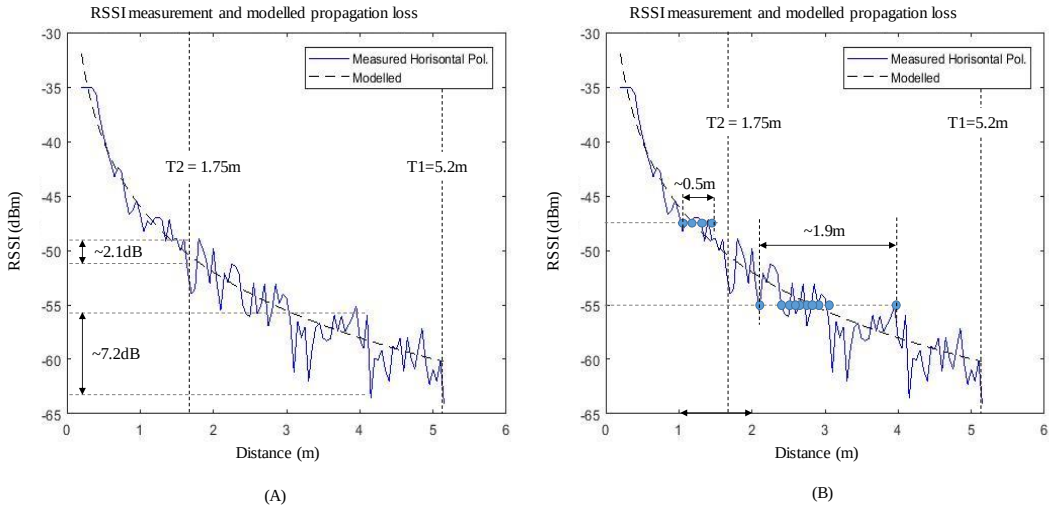

Figure 3.10 RSSI ranging-fingerprinting data for horizontal polarisation and the theoretical model plotted over the empirical data together with spatial Threshold 1 (T1) indicating the maximum outside coverage and Threshold 2 (T2) marking the cabin's width: maximum RSSI variation for T1 and T2 based on empirical data (A); maximum spatial error (location accuracy) for each of the T1 and T2 based on empirical data (B)

challenging. **Figure 3.10** illustrates the maximum RSSI variation (A), and the maximum spatial errors (B), produced by the noisy empirical data versus the smooth path loss data generated by the theoretical model. Two main representative spatial thresholds (Ts) are represented on the path loss graph: *T1* at 5.2 m indicating the maximum RF range covered inside-outside, and *T2* at 1.75 m marking the vehicle's cabin width and reflecting the inside domain limit. It is straightforward to acknowledge based on the graphical results that by varying the RF coverage interval, both RSSI and ranging errors will change accordingly: diminishing for small distances and increasing for wider extents.

Another observation regarding the RSSI and spatial errors represented in **Figure 3.10**, relates to the fact that compared with other studies' similar data, such as the ones presented in the literature review section, the maximum errors presented here show an optimistic RF location example. This is due to the high-resolution step of 5 cm used when constructing the RSSI fingerprinting data outdoor, good weather, low ambient noise and absence of close obstacles such as constructions, plants or humans. Since the observed spatial error of 0.5 m associated for cabin environment fits this study's aim of achieving an inside accuracy lower than 1 m, ideally in the range of 0.5 m representing the common width of a seat, it is reasonable to agree the model usage for both inside-outside location environments. In the case that a data model would have been produced for the inside vehicle environment, switching between the inside and outside fingerprinting databases when one does not know if the mobile source is outside or inside will require extra help from additional hardware to implement supplementary methods such as ToF or the use of infrastructure sensors.

Following the above analysis, since the empirical model may generate for certain RSSI values various ranging equivalent points, and by relying on the good resolution of the fingerprinting database, a straightforward algorithm for generating the ranging distances is proposed:

- Measure the RSSI value and by interrogating the fingerprinting data base find how many possible associated positional points exist.
- If only one is retrieved, then adopt the estimated distance value.
- If more than one is found, then adopt the smallest distance value.

Estimating the smallest distance from the set is equivalent with the assumption that we are choosing the strongest RSSI value implying less instability, therefore less error. However, the method's worst result is recorded when the correct location value is for the weakest RSSI, therefore, a potential future improvement may be to consider the mid-range value instead of the minimum. **Figure 3.11** illustrates the adopted algorithm diagram (A), and the potential proposed alternative (B).

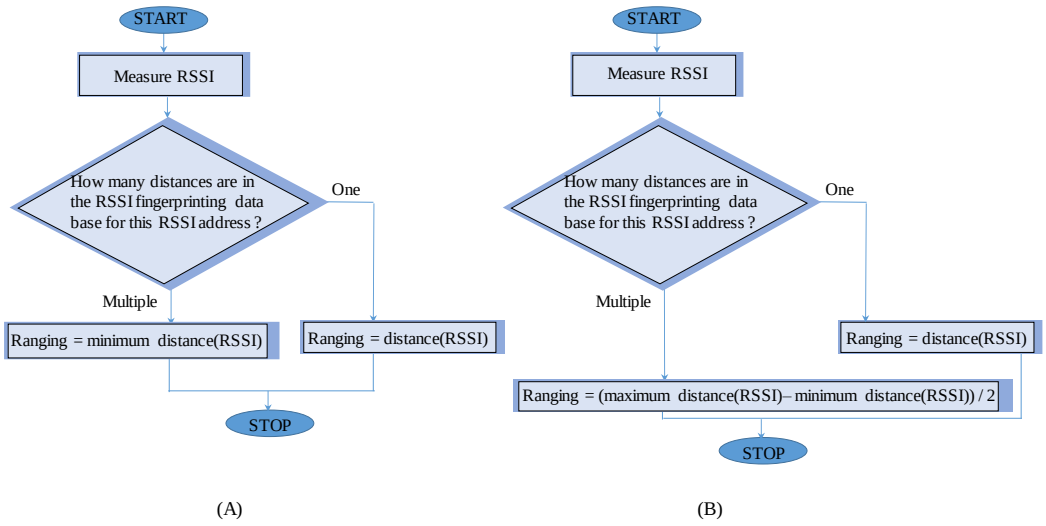

Figure 3.11 The straightforward algorithm used in this work to calculate the ranging values from the RSSI fingerprinting data model (A), and the proposed alternative of selecting the mid-range value (B)

The algorithm has been implemented in MATLAB and tested for more than 100 runs on a generated path loss model including a simulated noise from shadowing and from multipath and adjusted via correlation to this work's empirical model. It was found that for 96.1% of the runs, on a threshold situated at 1.75 m the maximum RMSE was under ±0.5 m. The advantages of the above proposed method result from its straightforwardness allowing a direct implementation on a low power system without requiring additional signal processing resources. Its limitation is related with the RSSI fingerprinting database resolution, and future RF sensor's ability to deliver consistent measurements, such as in this study's case relying on its achieved directionality.

3.4 Mobile RF source localisation inside-outside vehicle test setup

The initial plan was to generate an approximatively homogeneous distribution of the testing points around the vehicle, however the parking area's spatial constraints adding to the vehicle's irregular shape produced three different separations on the measurement axes, independent from the signal's wavelength. The four RF target test points inside the car are symmetrically situated on the front and rear seats. Since the proof-of-functioning detection system assesses the setup's viability in solving the inside-outside position discrimination problem, the online or real-time feature is not implemented: one hundred RSSI readings from each of the eight directive sensors are averaged, delivering one value for each of the RF mobile source test point evaluations. Then, each resulting RSSI value is transformed in a ranging distance estimation based on the RSSI fingerprinting database and sent immediately to the Rx node by means of a wireless time division multiple access (TDMA) protocol designed for this experiment.

The eight RF directive sensors were placed first at the extreme points of the vehicle windows down, then high. In this way, sixteen locations were covered, such as eight pointing inside and eight pointing outside for both high-low setups together. Since this study adopted a minimalistic configuration for each RF sensor, the same approach was extended to the overall reception system: four sensors for outside and four for inside monitoring. A total of four sensors has been selected as the minimum necessary suggested for 3D spatial detection [266].

Figure 3.12 shows the spatial location setup for the RF sensors high-low configuration, whereas **Figure 3.13** outlines the measuring points around the vehicle following a schematic representation. The RF mobile source Tx was emulated through an unshielded omnidirectional sensor on a tripod situated at 0.9 m above the ground, equivalent to the possible position for a smartphone carried by an average sized person, as described in Section 1.6 expanding the reasoning for the Tx height choice. The Tx power was set to 0dBm, while a ten-byte payload was continuously broadcasted, simulating a common BLE location beacon.

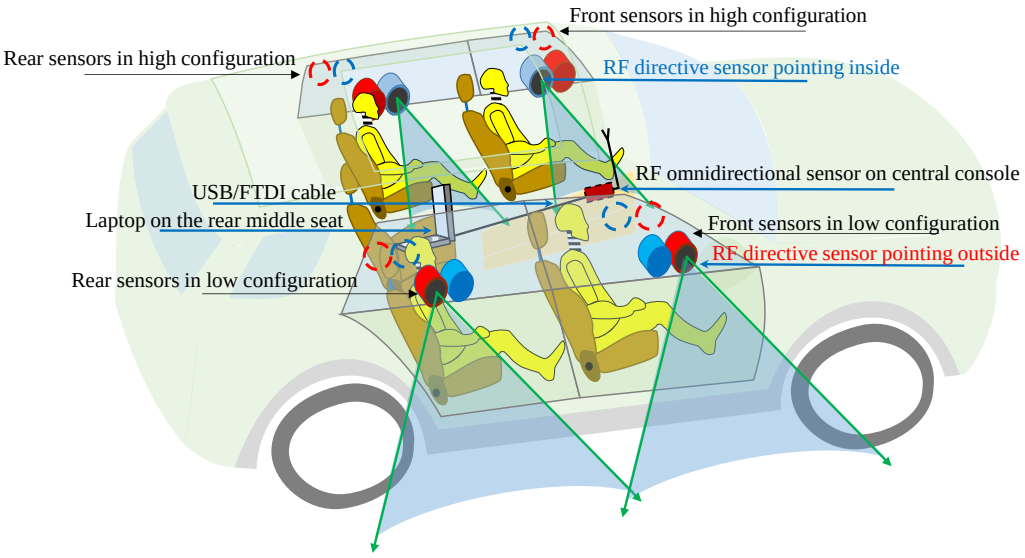

Figure 3.12 RF mobile target location measurement setup: 1+8 RF sensors in low configuration, the high configuration placing the sensors on window's top frame is showed with dotted lines to not compromise schematic's clarity. The laptop is operated during the measurements from the central rear seat and connected to the RF sensor node placed on the central console. The node from the central console receives the data from all eight sensors wirelessly based on a time division multiple access (TDMA) protocol developed for the tests; The RF sensors orientation is shown with blue for inside and red for outside pointing, with their approximate detection domain sketched for the forward-facing ones.

In the experimental setup, the RF directive sensors were grouped together in complementary pointing pairs (i.e., one pointing inside, and the second pointing outside) and positioned at the extreme ends of the side windows to cover a wider perimeter with a minimum of RF nodes so as to enhance the outside detection. The rear RF sensors were positioned at the rear window's lower and higher extremes instead of close to the central pillar pointing towards the empty space in front of the seats, **Figure 3.14A**. This setup deviation does not significantly influence the overall algorithmic inside-outside discrimination decision, however it will contribute to outliers in location accuracy data analysis for the rear seats, once more supporting the initial sensor organisation plan: the position of the inside sensors should ensure they are pointing towards the empty space in front of the seats.

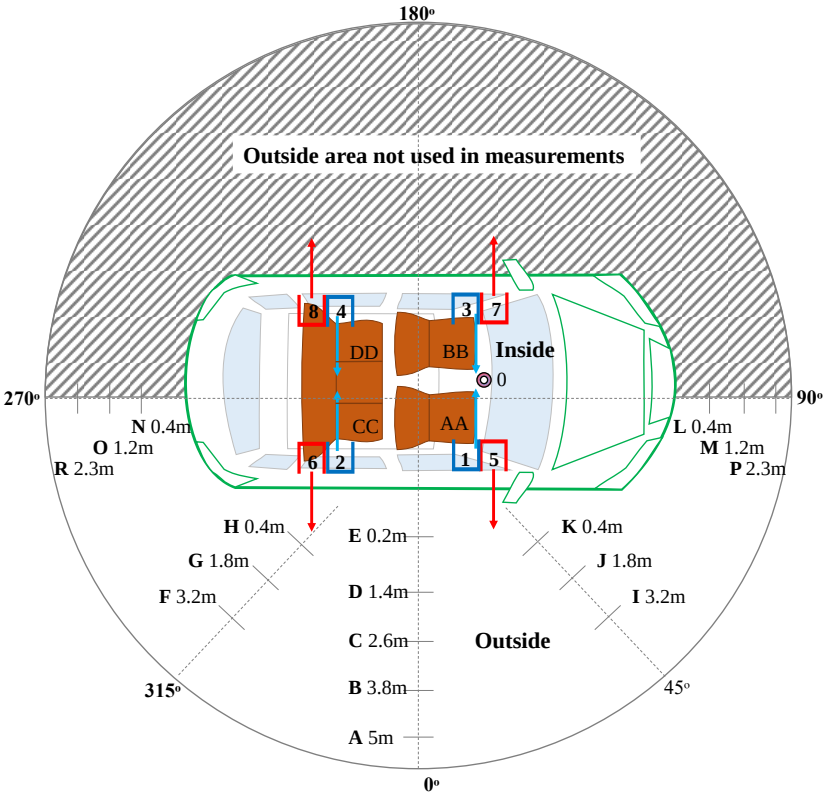

Figure 3.13 RF target location measurement setup: sensors 1-8 target position A-R (outside) and AA, BB, CC, DD (inside) the car's cabin. As the scenario is symmetrical, only the presented side will be considered in location tests. The RF source on the tripod is sequentially moved, and the RF sensors placed in the car receive the signal and send their RSSI readings via a TDMA protocol to the node placed on the central console. The results from all sensors are recorded and stored on a laptop for analysis.

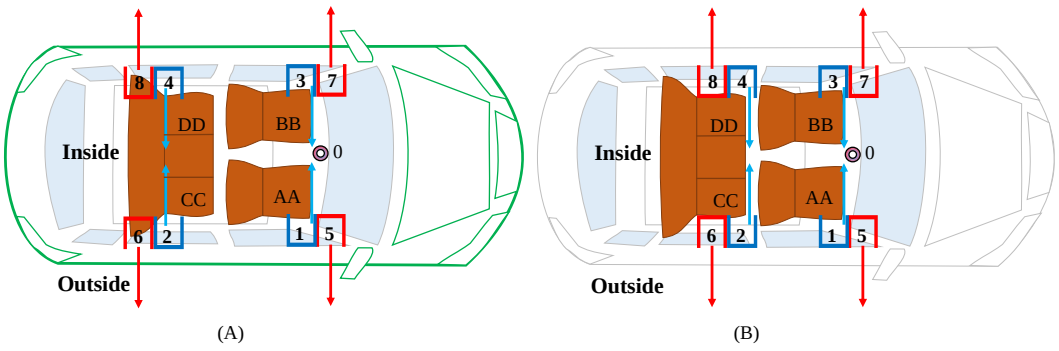

Figure 3.14 RF target location measurement setup: the back RF sensor pair position at the rear window's during the empirical location measurements (A), and the advised RF directional sensor orientation inside car's cabin to avoid human interference and focus on the possible mobile target area (B)

3.5 Inside-outside position discrimination results and discussion

As described in Section 1.8, the first research question addressed by this work relates to the ability to discriminate a vehicle's inside from the outside area as a first step of the RF spatial localisation problem. **Figure 3.15** illustrates the 3D sensor and target location test point positioning modelled in MATLAB based on precise measurements and vehicle's CAD schematics. This model delivers the real distances between each sensor and the RF target positioned in one of the test points, accounting for height differences and 3D spatial angles. For each RF individual sensor the differences between 2D and 3D distances are not large, however when the inside-outside discrimination algorithm makes location decisions based on fixed threshold values, any relevant inequality can make a difference.

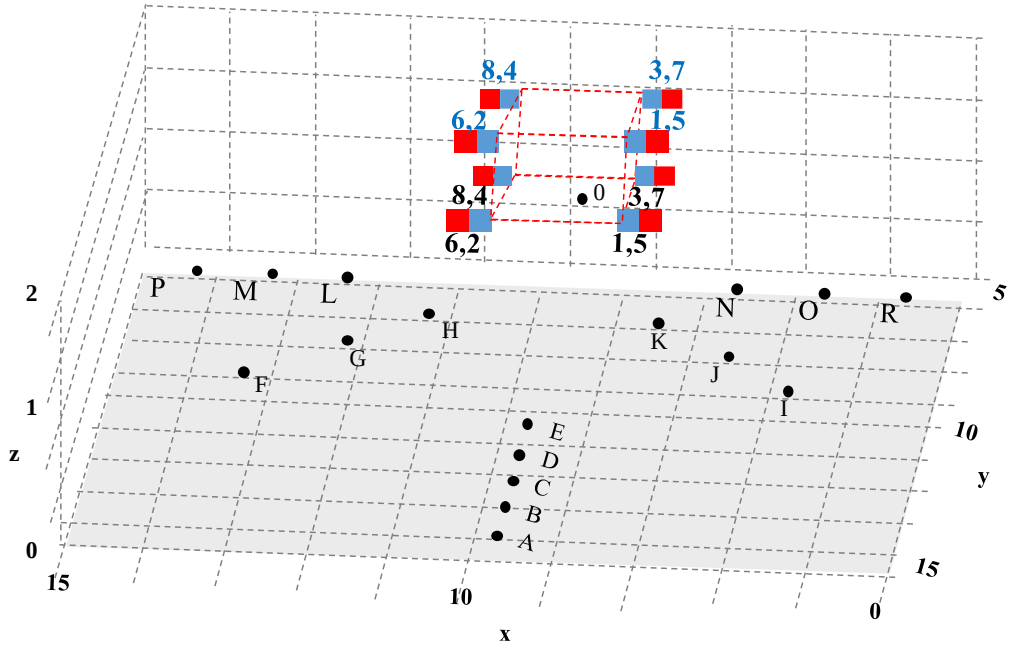

Figure 3.15 3D sensor and test point location. The red squares represent the sensors pointing outside, the blue squares the sensors pointing inside, the round black dots the mobile RF source test points and the point labelled 0 placed on the car's central console is the coordinator sensor node. The blue labelled sensor nodes are in high configuration position while the black labelled sensors are in the low configuration position.

The algorithmic system employed by this study to discriminate the inside-outside RF mobile source position is presented as follows:

- The directional sensors are divided into two numbered groups: 1 to 4 are oriented inside and 5 to 8 point outside, whereas the omnidirectional central sensor is labelled as 0 since its ranging results are not used.
- The maximum outside detection threshold *T1* is set to 5.2 m. Therefore, any sensor indicating a value equal to *T1* estimates the mobile source position as outside and will generate a "0", equivalent to a "miss" of the car's cabin.
- The RF source is considered inside the vehicle if at least three of the four inside-oriented sensors indicate a predicted distance value smaller than *T1*, **and** at least one sensor estimates a ranging measurement smaller than the maximum vehicle's width of 1.75 m, labelled as *T2*. If this occurs, the algorithm will generate a "1", equivalent to a "hit" of the vehicle's interior.
- The Boolean decision system based on the external threshold *T1* and the internal threshold *T2* applies a logical OR-relationship between the sensor groups oriented towards the inside and the outside.

Figure 3.16 illustrates the inside-outside position discrimination algorithm for the RF sensors in the low configuration (black colour font), since its utilisation is identical for the high configuration (blue colour font). The figure's schematics highlights the importance of the inside pointing RF sensors' for position discrimination, while the outside pointing RF sensor group contribution is important for the next stage in the study involving absolute accuracy calculation, when the multi-lateration technique comes also to attention.

Following the transformation of the RSSI data in spatial ranging estimations for both low and high sensor setups, and by applying the decision steps described in the previous section, the RF source position discrimination results were recorded as shown in **Table 3.1** for the empirical model (top), and for the theoretical model (bottom). The light blue ranging values in **Table 3.1** capture those distances estimated by the inside sensors' smaller than *T2*, based on which the algorithm's decision generates a "1", as the target is detected within the cabin's interior. When the target is detected inside, the

Inside-outside position discrimination diagram for RF sensors' low configuration

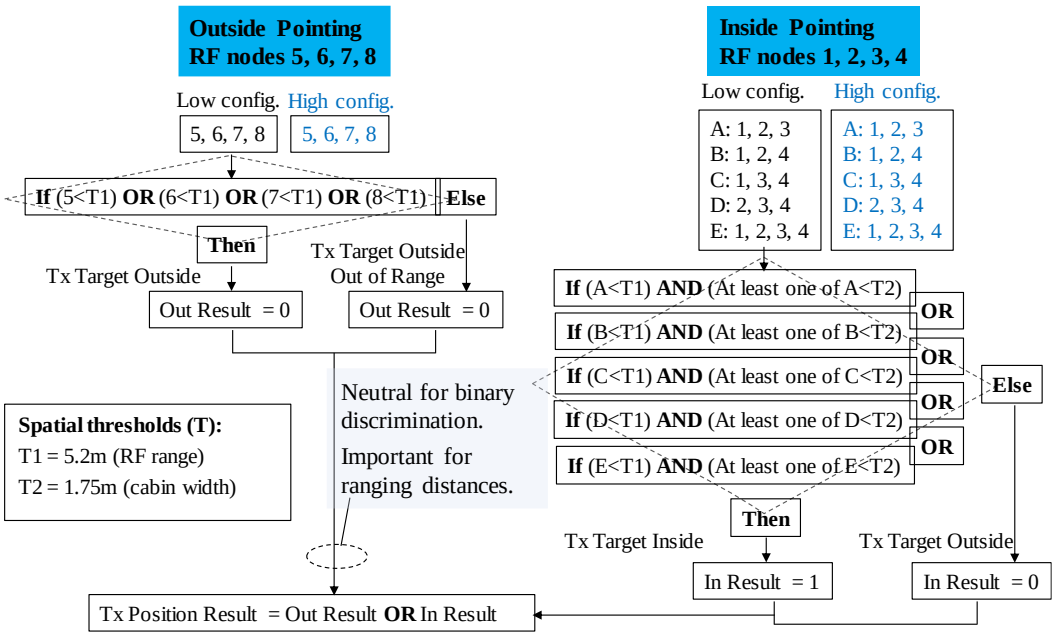

Figure 3.16 Logical schematic diagram illustrating for the RF sensors in low configuration (black font) the inside-outside vehicle position discrimination algorithm used in this work. Same algorithm has been applied for the sensors in high configuration (blue font). The inside pointing RF sensor configuration is divided in groups labelled from A to E and it is outlined that their decision for position discrimination is essential while the outside pointing sensors are important when absolute location accuracy is calculated in the next study's step (section "RF location accuracy")

outside pointing sensors display ranging measurements smaller than or equal to *T1* due to RF reflections and parasitic back reception. Nevertheless, the inside sensors consistently detect the mobile target inside the cabin, and applying a logical OR function between the decisions of the sensor groups yields a correct inside position outcome.

The same results are displayed for both empirical and theoretical models, demonstrating that a short distance ranging system based on RSSI and sensor directivity produces consistent results. The human presence is known to influence RSSI measurements; however, it is recommended that the internal oriented sensors point towards the empty space in front of the seats, avoiding interference with human occupants of the car. Therefore, the effects can be minimised by the short-distance sensing and sensor directivity.

Table 3.1 Results for applying the Inside/Outside discrimination decision for the empirical and theoretical ranging model

Sensor setup	Sensor Direction	Sens. no	Ranging with the empirical model																			
			Outside test points																Inside test points			
			A	B	C	D	E	F	G	H	I	J	K	L	M	N	O	P	R	AA	BB	CC	DD
Low	Sensors In decision		0	0	0	0	0	0	0	0	0	0	0	0	0	0	0	0	0	1	1	1	1
	In	1	5.2	5.2	5.2	5.2	5.2	5.2	5.2	5.2	5.2	5.2	5.2	5.2	5.2	5.2	5.2	5.2	5.2	0.85	1.2	2	0.9
	In	2	5.2	5.2	5.2	5.2	4.35	5.2	5.2	5.2	5.2	5.2	5.2	5.2	5.2	5.2	5.2	5.2	5.2	2.35	2.15	0.6	1.7
	In	3	5.2	5.2	5.2	4.8	3.2	5.2	5.2	5.2	5.2	4.2	5.2	5.2	5.2	5.2	5.2	5.2	5.2	5.2	**0.7**	4.2	4.45
	In	4	5.2	5.2	5.2	4.2	5.2	5.2	5.2	5.2	5.2	5.2	5.2	5.2	5.2	5.2	5.2	5.2	5.2	1.9	1.7	0.65	2.25
	Sensors Out decision		0	0	0	0	0	0	0	0	0	0	0	0	0	0	0	0	0	0	0	0	0
	Out	5	4.35	5	3.3	1.2	4.1	4.2	5.2	1.6	3.35	3.8	4.95	5.2	5.2	5.2	5.2	5.2	5.2	1.75	5.2	4.5	3.15
	Out	6	3.9	4.7	3.1	2.2	3.9	5.2	5.2	5.2	3.3	2.3	3	5.2	5.2	5.2	5.2	5.2	5.2	5.2	3.25	2.95	0.7
	Out	7	5.2	5.2	5.2	5.2	5.2	5.2	5.2	5.2	5.2	5.2	5.2	5.2	5.2	5.2	5.2	5.2	5.2	3.6	4.1	5.2	5.2
	Out	8	5.2	5.2	5.2	5.2	5.2	5.2	5.2	5.2	5.2	5.2	5.2	5.2	5.2	5.2	5.2	5.2	5.2	5.2	5.2	3.2	5.2
	Total In-Out Decision		Out	Out	Out	Out	Out	Out	Out	Out	Out	Out	Out	Out	Out	Out	Out	Out	Out	In	In	In	In
High	Sensors In decision		0	0	0	0	0	0	0	0	0	0	0	0	0	0	0	0	0	1	1	1	1
	In	1	5.2	5.2	5.2	4.5	3.4	5.2	5.2	5.2	5.2	5.2	5.2	5.2	5.2	5.2	5.2	5.2	5.2	1.95	1.3	3	2.95
	In	2	5.2	5.2	5.2	5.2	4	5.2	5.2	5.2	5.2	5.2	3.25	5.2	5.2	5.2	5.2	5.2	5.2	1.1	1.8	2.4	1.1
	In	3	5.2	5.2	5.2	5.2	4.1	5.2	5.2	5.2	5.2	5.2	5.2	5.2	5.2	5.2	5.2	5.2	5.2	1.25	5.2	3.05	2.95
	In	4	5.2	5.2	5.2	4.35	5.2	5.2	5.2	5.2	5.2	5.2	5.2	5.2	5.2	5.2	5.2	5.2	5.2	2.7	2.25	1.45	1.8
	Sensors Out decision		0	0	0	0	0	0	0	0	0	0	0	0	0	0	0	0	0	0	0	0	0
	Out	5	5.2	5.2	2.8	2.9	1.35	5.2	5.2	5.2	4.25	3.6	5.2	5.2	5.2	5.2	5.2	5.2	5.2	1.4	5.2	2.8	2.25
	Out	6	1.75	3.05	1.6	1.4	1.6	4.4	4.9	5.2	2.55	2.4	0.7	5.2	5.2	5.2	5.2	5.2	5.2	3.4	5.2	1.25	4.8
	Out	7	5.2	5.2	5.2	5.2	5.2	5.2	5.2	5.2	5.2	5.2	5.2	5.2	5.2	5.2	5.2	5.2	5.2	5.2	3	5.2	4.2
	Out	8	5.2	5.2	5.2	5.2	5.2	5.2	5.2	5.2	5.2	5.2	5.2	5.2	5.2	5.2	5.2	5.2	5.2	5.2	5.2	3.35	1.7
	Total In-Out Decision		Out	Out	Out	Out	Out	Out	Out	Out	Out	Out	Out	Out	Out	Out	Out	Out	Out	In	In	In	In

Sensor setup	Sensor Direction	Sens. no	Ranging with the theoretical model																			
			Outside test points																Inside test points			
			A	B	C	D	E	F	G	H	I	J	K	L	M	N	O	P	R	AA	BB	CC	DD
Low	Sensors In decision		0	0	0	0	0	0	0	0	0	0	0	0	0	0	0	0	0	1	1	1	1
	In	1	5.2	5.2	5.2	5.2	5.2	5.2	5.2	5.2	5.2	5.2	5.2	5.2	5.2	5.2	5.2	5.2	5.2	0.95	1.3	2.3	1.15
	In	2	5.2	5.2	5.2	5.2	4.8	5.2	5.2	5.2	5.2	5.2	5.2	5.2	5.2	5.2	5.2	5.2	5.2	1.95	3	0.6	2.05
	In	3	5.2	5.2	5.2	5.2	3.45	5.2	5.2	5.2	5.2	5.2	5.2	5.2	5.2	5.2	5.2	5.2	5.2	5.2	0.8	5.2	5.2
	In	4	5.2	5.2	5.2	5.2	5.2	5.2	5.2	5.2	5.2	5.2	5.2	5.2	5.2	5.2	5.2	5.2	5.2	1.6	2.05	0.7	2.3
	Sensors Out decision		0	0	0	0	0	0	0	0	0	0	0	0	0	0	0	0	0	0	0	0	0
	Out	5	4.6	5.2	3.6	1.25	4.55	5.2	5.2	1.65	5.2	3.2	5.2	5.2	5.2	5.2	5.2	5.2	5.2	2.5	5.2	4.3	5.2
	Out	6	3.5	4.05	3.35	2.05	3.5	5.2	5.2	5.2	3.65	1.9	2.55	5.2	5.2	5.2	5.2	5.2	5.2	5.2	4	2.8	0.8
	Out	7	5.2	5.2	5.2	5.2	5.2	5.2	5.2	5.2	5.2	5.2	5.2	5.2	5.2	5.2	5.2	5.2	5.2	4.25	4.55	5.2	5.2
	Out	8	5.2	5.2	5.2	5.2	5.2	5.2	5.2	5.2	5.2	5.2	5.2	5.2	5.2	5.2	5.2	5.2	5.2	5.2	5.2	3.4	5.2
	Total In-Out Decision		Out	Out	Out	Out	Out	Out	Out	Out	Out	Out	Out	Out	Out	Out	Out	Out	Out	In	In	In	In
High	Sensors In decision		0	0	0	0	0	0	0	0	0	0	0	0	0	0	0	0	0	1	1	1	1
	In	1	5.2	5.2	5.2	4.4	4.45	5.2	5.2	5.2	5.2	5.2	5.2	5.2	5.2	5.2	5.2	5.2	5.2	1.85	1.15	2.6	2.8
	In	2	5.2	5.2	5.2	5.2	2.9	5.2	5.2	5.2	5.2	5.2	3.95	5.2	5.2	5.2	5.2	5.2	5.2	1.35	2.45	2.15	1.3
	In	3	5.2	5.2	5.2	5.2	4.55	5.2	5.2	5.2	5.2	5.2	5.2	5.2	5.2	5.2	5.2	5.2	5.2	1.2	5.2	2.75	2.75
	In	4	5.2	5.2	5.2	4.6	5.2	5.2	5.2	5.2	5.2	5.2	5.2	5.2	5.2	5.2	5.2	5.2	5.2	2.9	2.25	1.2	2.45
	Sensors Out decision		0	0	0	0	0	0	0	0	0	0	0	0	0	0	0	0	0	0	0	0	0
	Out	5	5.2	5.2	3.6	2.35	1.2	5.2	5.2	5.2	5.05	4.2	5.2	5.2	5.2	5.2	5.2	5.2	5.2	1.5	5.2	3.6	2.25
	Out	6	2.55	2.7	1.65	1.5	1.65	5.2	3.7	5.2	3.25	2.1	0.85	5.2	5.2	5.2	5.2	5.2	5.2	4.45	5.2	1.2	5.2
	Out	7	5.2	5.2	5.2	5.2	5.2	5.2	5.2	5.2	5.2	5.2	5.2	5.2	5.2	5.2	5.2	5.2	5.2	5.2	2.55	5.2	5.2
	Out	8	5.2	5.2	5.2	5.2	5.2	5.2	5.2	5.2	5.2	5.2	5.2	5.2	5.2	5.2	5.2	5.2	5.2	5.2	5.2	5.2	2
	Total In-Out Decision		Out	Out	Out	Out	Out	Out	Out	Out	Out	Out	Out	Out	Out	Out	Out	Out	Out	In	In	In	In

When examining the decision hierarchy, it can be noted that the inside detection group can generate 1 whereas the outside oriented sensors can only produce 0. Therefore, the decision balance for inside-outside RF target discrimination is dependent only on the inside pointing sensors. With the next envisaged research step being the estimation of the RF mobile source's spatial position, the role of the outside oriented sensor group will become equally important.

Another important observation relates to the sensors' high directivity, when the mobile RF source was on the outside test points L, M, N, O, P, R (i.e., in the front and rear of

the vehicle), all sensors provided estimations equal to *T1*, meaning in this context that the target was out of range.

3.6 RF location accuracy

The absolute location accuracy is the accuracy related to the measurement unit, here in metres. When the unit is a 2D area or a 3D voxel, then the accuracy becomes more relaxed, and obtaining the right area or voxel is represented by a "hit" or a "miss".

At the start of this localisation project, it was proposed to assess the location accuracy for outside in quadrants (i.e., 2D area units), and for the vehicle's interior in voxels (i.e., 3D volume units). As the work progressed through procedures such as spatial division and octree partitioning, etc. in the context of the 3D RT simulation, it was acknowledged that the 2D and 3D units could prove misleading by showing high accuracy when well fitted to the data. Also, to report the results in simple terms, without complicated formulations, and to be able to compare the results with other works, it was decided to use absolute accuracy to present the results of the experiments aimed at inside-outside localisation.

In order to derive the RF target spatial location accuracy in a 3D space, several preliminary steps need to be addressed as described in the following. First, the position points and all RF sensors need to be placed in a 3D coordinate system and the exact geometrical distances between them, *d*, need to be calculated. Second, ranging distances, Rd, between each test point and each sensor position are already calculated, however, as the ranging distances resulted via ranging-fingerprinting are 2D, a 3D translation via multi-lateration is necessary. The multi-lateration technique can be applied if, for the same point, at least three readings from the outside pointing sensors indicate distance values smaller than *T1*, 5.2 m, and, similarly for the inside pointing sensors, if the values are smaller than *T2*, 1.75 m. Multi-lateration distances, Md, may have different values for the same sensor due to its different group combinations. Then, based on precise geometrical distances, a comparison in terms of RMSE of the absolute difference between two points will be made between d and Rd and d and Md to identify the absolute location accuracy.

3.6.1 RF target localisation inside a multi-node network

Geometrically, the localisation of a precise point in a 2D space requires a minimum of three sensors simultaneously detecting the target and providing a valid ranging distance. The ranging distance is the radius of a circle with the centre coordinates placed exactly where the sensor is located. By writing the circle's equation for each sensor, the resulting equation system could be solved via classical addition/subtraction or by Cramer's rule. The system has a unique solution if, and only if, the three circles intersect in a single point. This means that for each ranging distance, a very precise value is needed and, if a ranging error occurs even at decimal point, the system will have no solution. The same logic is applied in 3D for circular or spherical intersections. In practice, ranging distances without errors or tolerances are impossible to obtain for a certain precision, therefore target geometrical trilateration and triangulation is an option suitable for the theoretical domain.

Finding a target involves location approximation, like placing it inside a bounding box, common centroid, intersecting area, etc., instead of a single point. In addition, in practical situations, more parameters are used rather than RSSI alone. These parameters include signal phase, time, 2D-3D terrain fingerprinting, intersecting common overlapping areas in AoA, etc. [267-269].

Circular and hyperbolic positioning algorithms are two promising methods that treat spatial target localisation as an optimisation problem, and approximate the geometrical location by means of a minimum of three detecting sensors as the optimal point between them in terms of RMSE. They require only the RSSI ranged distances as the spheres' radii, and the geometrical sensor coordinates as the spheres' centres. Previous work demonstrates that the circular method performs better than the hyperbolic one in certain conditions [270]. Therefore, the circular algorithm will be employed to solve the multi-lateration problem, which relies on its MATLAB implementation involving the Nelder-Mead simplex method [271].

3.6.2 AoA detection zones inside a multi-node RF network

Depending on the hardware structure and orientation used in AoA, to exploit the advantage of cooperative location with more sensor points detecting the same target, and the subsequent usage of multi-lateration to predict the position, a certain level of redundancy is necessary.

Figure 3.17 illustrates the AoA redundancy point of view for three sectorial RF base stations each composed from directional sectorial antennas.

If, from a minimalistic point of view, one node covering an area is considered as 100% sufficient, then, a 200% redundancy needs to be employed to be able to cover the same area by three nodes. Although from a security perspective, this kind of redundancy over costs might be justified, in practice it is sometimes encountered because the nodes designed for communication are used for a secondary service like location. Looking at the example in **Figure 3.17**, nodes 2 and 6 may have been designed to provide direct

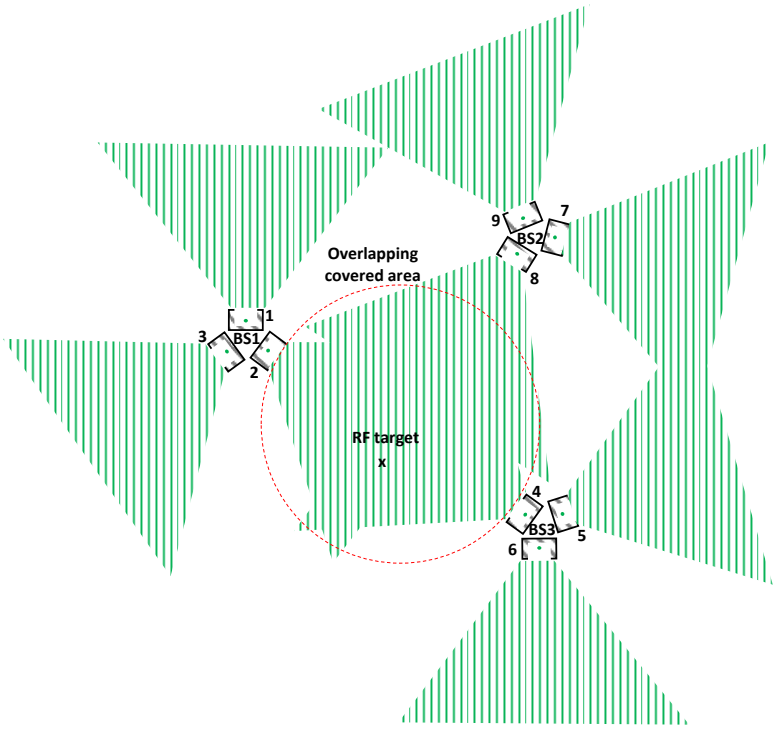

Figure 3.17 Three base stations (BS) equipped with sectorial directive antennas (nodes) can locate a RF target employing AoA techniques. However, only RF nodes 2, 4, and 8 can improve ranging distances via tri-lateration. This is because nodes 2, 4 and 8 are covering/surveying the same spatial area, however from different positions.

communication links between base stations (BS) 1 and 2, while node 8 may be linking other BSs or covering an area with potential obstacles unsolved by BS 1 and 2.

In the context of this work, the AoA sensor configuration is schematically described in **Figure 3.18**. As may be observed, true redundancy for overlapping zones is found only for the vehicle cabin, by considering the nodes in the 1, 3 and 2, 4 groups from the low (black sensor numbers) and high setup (blue sensor numbers). For outside, a maximum of two true sensor overlapping zones can be identified for nodes 5 and 6 in the high-low configurations. However, by extrapolating and considering the sensors 5 and 6 as surveying the same zone, it can be considered for the purposes of the analysis that for outside, sensors 5 and 6 can be grouped together in a low-high scenario.

Therefore, grouping up to four sensors together by their overlapping area (two sensors in low-high setup) and then employing multi-lateration, this may improve the ranging distances from a theoretical point of view. In practical terms, the improvement needs to consider the previously established logic for inside-outside discrimination. By analysing **Table 3.1**, and after excluding the ranging distances equal with *T1* for the outside pointing sensors, and the ranging distances larger than *T2* for the inside pointing sensors, we can observe that the theoretical grouping possibilities are reduced

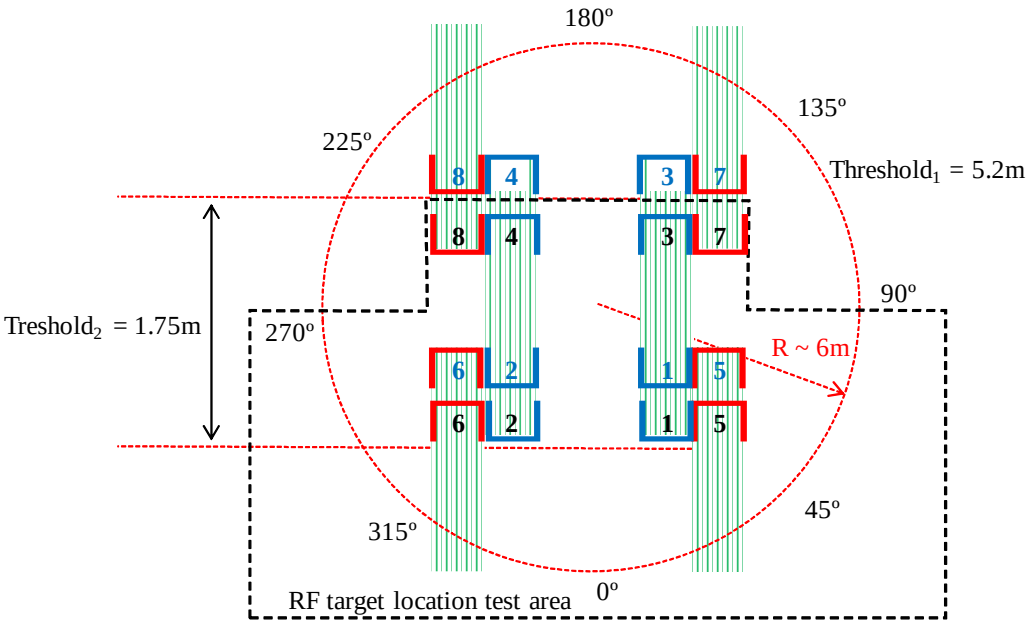

Figure 3.18 Overlapping coverage zones for the RF sensor nodes (black numbers for "low setup", blue numbers for "high setup"). The RF target test points were covering only the outside area between 270º, 0º, 90º due to scenario symmetry, therefore sensors 7 and 8 in high and low configuration are not contributing with ranging distances to the scenario, but they reinforce the directivity and scenario logic by detecting the target being Outside by indicating *T1*

to just a few cases. For the inside case it is necessary to extend the overlapping zone to all four sensors in low-high configurations to be able to apply multi-lateration.

3.6.3 RF location accuracy results and discussion

Introducing the analysis for the outside area RF positioning scenario, **Table 3.2** illustrates the possible sensor combinations qualified for multi-lateration technique in both empirical and theoretical propagation models. The models share some similar configurations for the test points C and D for example, and present some differences on the A and B test points, nevertheless it can be noted that the maximum size of sensor groups valid for multi-lateration does not exceed four. The number of the qualified outside test points is reduced since the detecting sensors for the external

Table 3.2 Multi-lateration sensor grouping for outside pointing sensors in low (black sensor numbers) and high (blue sensor numbers) setup for the empirical and theoretical model. The uncoloured row shows where a combination is applicable and the grey row where it is not due to threshold logic

Empirical ranging results for Outside Location (Rd)					Absolute 3D distances (d)				RMSE(d, Rd)			
Low setup	**A(2D: 5.2m)**	**B(2D: 3.8m)**	**C(2D: 2.6m)**	**D(2D: 1.4m)**	**A**	**B**	**C**	**D**	**A**	**B**	**C**	**D**
5	4.35	5.00	3.30	1.20	5.22	4.04	2.88	1.78	0.87	0.96	0.42	0.58
6	3.90	4.70	3.10	2.20	5.20	4.02	2.85	1.72	1.30	0.68	0.25	0.48
High setup												
5	5.20	5.20	2.80	2.90	5.32	4.14	2.97	1.85	0.12	1.06	0.17	1.05
6	1.75	3.05	1.60	1.40	5.32	4.14	2.98	1.86	3.57	1.09	1.38	0.46
Combinations for multi-lateration ranging												
5, 6, 6												
5, 6, 5												
5, 5, 6												
6, 5, 6												
5, 6, 5, 6												
Theoretical ranging results for Outside Location (Rd)					**Absolute 3D distances (d)**				**RMSE(d, Rd)**			
Low setup	**A(2D: 5.2m)**	**B(2D: 3.8m)**	**C(2D: 2.6m)**	**D(2D: 1.4m)**	**A**	**B**	**C**	**D**	**A**	**B**	**C**	**D**
5	4.60	5.20	3.60	1.25	5.22	4.04	2.88	1.78	0.62	1.16	0.72	0.53
6	3.50	4.05	3.35	2.05	5.20	4.02	2.85	1.72	1.70	0.03	0.50	0.33
High setup												
5	5.20	5.20	3.60	2.35	5.32	4.14	2.97	1.85	0.12	1.06	0.63	0.50
6	2.55	2.70	1.65	1.50	5.32	4.14	2.98	1.86	2.77	1.44	1.33	0.36
Combinations for multi-lateration ranging												
5, 6, 6												
5, 6, 5												
5, 5, 6												
6, 5, 6												
5, 6, 5, 6												

perimeter is low and due to their directivity and parallel alignment the coverage areas do not overlap it their proximity, as is the case of the central test point E. The remaining detected points situated towards the vehicle's front and rear are adhering to the same principle outlined above, and since their ranging value cannot be confirmed by more than two different sensors, they are also excluded from multi-lateration. The remaining test points A, B, C and D are situated on the central car axis therefore shared by sensors 5 and 6 in both low and high configurations.

A similar reasoning applies for the inside location results presented in **Table 3.3,** however the benefit of a theoretical high sensor density delivered by a combined eight sensor high and low setup is reduced by the algorithmic filtering employed in the inside-outside discrimination phase. This consequence is reflected on the maximum number of inside RF sensors qualified for multi-lateration, again the limit of four is not exceeded. Moreover, the non-optimal orientation of the rear inside pointing RF

Table 3.3 Multi-lateration resulted sensor grouping for inside pointing sensors in low (black sensor numbers) and high (blue sensor numbers) setup for the empirical and theoretical model. The uncoloured row shows where the combination is applicable and the grey row where it is not due to threshold logic

Empirical ranging results for Inside Location (Rd)					Absolute 3D distances (d)				RMSE(d, Rd)			
Low Setup	AA(Right Front)	BB(Left Front)	CC(Right Rear)	DD(Left Rear)	AA	BB	CC	DD	AA	BB	CC	DD
1	0.85	1.20	2.00	0.90	0.57	1.28	1.68	1.28	0.28	0.08	0.32	0.38
2	2.35	2.15	0.60	1.70	1.46	1.85	1.35	1.85	0.89	0.30	0.75	0.15
3	5.20	0.70	4.20	4.45	1.28	0.58	1.24	0.58	3.92	0.12	2.96	3.87
4	1.90	1.70	0.65	2.25	1.86	1.46	0.72	1.46	0.04	0.24	0.07	0.79
High Setup												
1	1.95	1.30	3.00	2.95	0.77	1.31	1.54	1.31	1.18	0.01	1.46	1.64
2	1.10	1.80	2.40	1.10	1.50	1.84	1.38	1.84	0.40	0.04	1.02	0.74
3	1.25	5.20	3.05	2.95	1.31	0.77	1.12	0.77	0.06	4.43	1.93	2.18
4	2.70	2.25	1.45	1.80	1.84	1.50	0.88	1.50	0.86	0.75	0.57	0.30
Combinations for multi-lateration ranging												
1, 2, 3												
2, 4, 4												
1, 2, 2												
1, 3, 4												
1, 3, 1												
1, 4, 1												
3, 4, 1												
1, 3, 4, 1												
Theoretical ranging results for Inside Location (Rd)					Absolute 3D distances (d)				RMSE(d, Rd)			
Low setup	AA(Right Front)	BB(Left Front)	CC(Right Rear)	DD(Left Rear)	AA	BB	CC	DD	AA	BB	CC	DD
1	0.95	1.30	2.30	1.15	0.57	1.28	1.68	1.28	0.38	0.02	0.62	0.13
2	1.95	3.00	0.60	2.05	1.46	1.85	1.35	1.85	0.49	1.15	0.75	0.20
3	5.20	0.80	5.20	5.20	1.28	0.58	1.24	0.58	3.92	0.22	3.96	4.62
4	1.60	2.05	0.70	2.30	1.86	1.46	0.72	1.46	0.26	0.59	0.02	0.84
High setup												
1	1.85	1.15	2.60	2.80	0.77	1.31	1.54	1.31	1.08	0.16	1.06	1.49
2	1.35	2.45	2.15	1.30	1.50	1.84	1.38	1.84	0.15	0.61	0.77	0.54
3	1.20	5.20	2.75	2.75	1.31	0.77	1.12	0.77	0.11	4.43	1.63	1.98
4	2.90	2.25	1.20	2.45	1.84	1.50	0.88	1.50	1.06	0.75	0.32	0.95
Combinations for multi-lateration ranging												
1, 3, 1												
2, 4, 4												
1, 4, 2												
1, 4, 3												
1, 2, 3												
4, 2, 3												
1, 4, 2, 3												

sensors results in elimination from multi-lateration of the test point DD on the theoretical model result set, due to having only two valid ranged distances.

An important observation may be noted by further analysing the data from **Tables 3.2 and 3.3**: although the ranging distance estimation presents a similar variation for the low and high setups, the low configuration provides more valid results for the outside and inside localisation. This may be a consequence of the fact that the sensors in the low configuration when detecting the mobile RF source were reproducing more closely the ranging-fingerprinting measurement conditions. Therefore, since the sensors in both low and high configurations were orientated parallel to the ground plane, the high configuration may require further positional tweaking to improve readings and reduce unwanted reflections, for instance tweaks such as tilting on the z axis and rotating in the xy-plane.

The **Annex Tables A1-A4** include extended experimental data based on which the **Tables 3.2 and 3.3** have been synthetised, storing the values for calculated real geometrical 3D distances *d*, the multi-lateration method resulted distances *Md*, sensor combinations and their associated ranging distances *Rd*, the RMSE between each

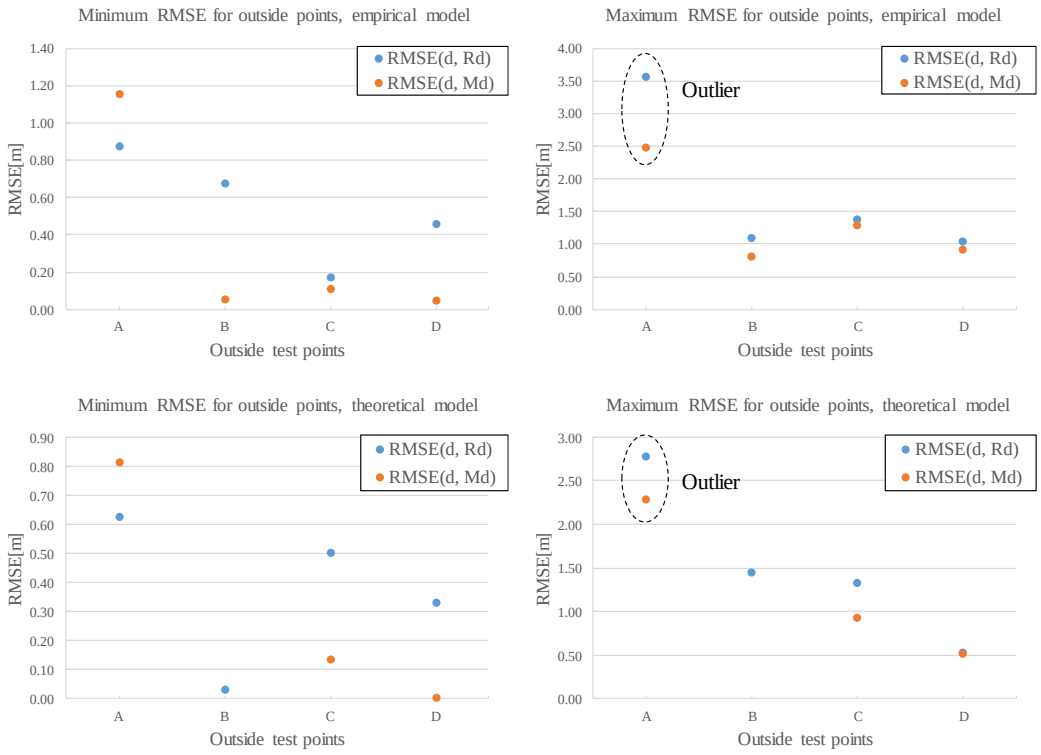

Figure 3.19 Maximum and minimum RMSE between 3D real distances d, ranging distances Rd and, between real distances d and multi-lateration distances Md for empirical and theoretical data model, in outside test scenario

distance pair (*d*, *Rd*) and (*d*, *Md*), finalising with maximum and minimum RMSE for the RF sensor combinations.

Figure 3.19 presents the RMSE comparison between the 3D real distances against ranging estimations *Rd*, and the multi-lateration results *Md*, calculated for the outside testing points, A, B, C and D. When inspecting the theoretical model, one may notice the missing *Md* values for the outside point B since it did not qualify for multi-lateration with at least three valid *Rd*'s. Moreover, it may be accounted that the error values presented by the theoretical model are lower than the ones induced by the empirical set. The highest error for both models is encountered on point A, which is normal since the RF sensor height on the low configuration is similar with the RF source although at angle reported to test point's axis, whereas in the case of the high setup, the RF sensor height is above RF source on test point A and at angle, therefore the real 3D geometrical distance exceeding the 2D 5.2 m.

One may note that, if point A is excluded since it represents an outlier value, the absolute worst accuracy for outside localisation becomes ±1.44 m, whereas the best

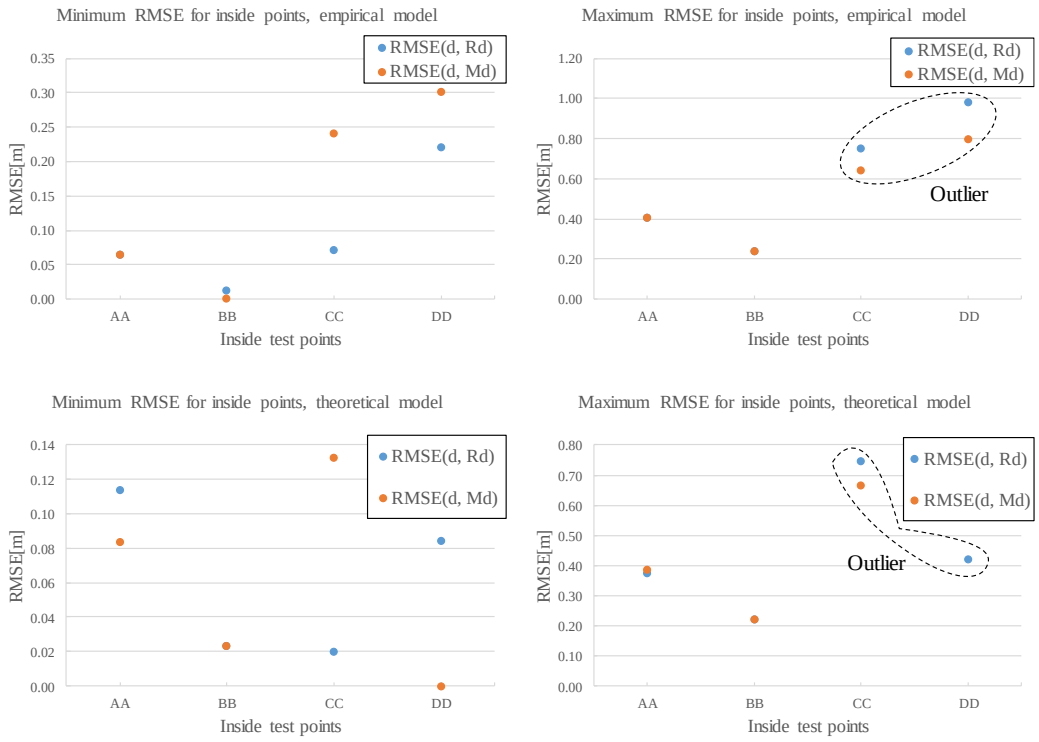

Figure 3.20 Maximum and minimum RMSE between 3D real distances, d, ranging distances, Rd and, between real distances d, and multi-lateration distances, Md for empirical and theoretical data model, in RF target inside scenario

accuracy would remain constant at ±0.02 m. The multi-lateration process shows a ranging error reduction in both empirical and theoretical models after outlier removal, suggesting that techniques valid in cooperative RF location, when applicable, contribute to position uncertainty reduction.

The location values determined for the inside test points AA, BB, CC and DD are illustrated in **Figure 3.20**. When investigating the theoretical model results, one may note that the *Md* marker is missing for the inside point DD since it did not qualify for multi-lateration with at least three valid *Rd* values. Moreover, the location accuracy is lower for the rear passenger seat positions situated at CC and DD when compared to the front seats AA and BB. A possible explanation relies on two influencing factors:

- In both low and high setups, the positions of the inside pointing rear sensors are at the rear window's extreme sides, orientated close to the backseat supports and not as recommended towards the space in front of the seats.
- Although attempting to avoid human interference during measurements, the human operator was present on the rear middle seat between CC and DD managing the data acquisition laptop during experiments.

Therefore, acknowledging that the results for the inside points CC and DD deliver anomalous values in the context of the inside localisation test setup, they may be excluded and the same reasoning as for the outside measurements can be followed.

Since the cabin area is smaller when compared with the outside localisation range, and the density of the RF detection sensors covering the inside perimeter is higher than for the outside case, the maximum localisation error result is ±0.4 m.

4. Conclusion, limitations and future work

4.1 Summarised conclusions

The presented work delivers the initial objectives through RF modelling based on empirical investigation supported by propagation theory. Moreover, for the RF sensor synthesis, a custom MATLAB 3D RT simulation have been implemented and exploited at quantitative level, producing insightful indication regarding overall sensor's metal enclosure. The initial RF location problem proposed formulation and hypnotised solution have been tested and analysed during this work, the overall results aligning with the initial premises.

The main study's achievements may be summarised as the answers to the preliminary research questions recommended by the project's industrial partner:

1. *When all receivers are placed inside the vehicle, is it possible to discriminate between a target location inside-outside the vehicle?*

   Yes, by employing RF directive sensors, such as the ones presented in this study, and separating the inside detection from outside. The inside-outside discrimination success of 100% (Section 3.5) achieved through the proof-of-concept RF location system supporting the above statement, however limitations such as the static vehicle's windows and passenger omission may need to be considered in a further step towards an online detection development.

2. *What are the minimum configuration requirements to enable such discrimination?*

   If a location system is required only to indicate the mobile RF target position based on inside-outside binary decision, then the minimum system configuration consists of four inwards pointing RF directional sensors, one of the four sensors acting as the Rx network data collecting node linked to a laptop or to the vehicle's telematics module. If a distance estimation for both inside-outside environments is considered, the minimum number of RF directional sensors is eight (Section 3.5). The multi-lateration technique may not be applicable for a minimalistic detection system, therefore planning is necessary for building a complex configuration capable to deliver advanced enhancing positioning functions.

3. *What is the expected detection accuracy for inside and outside localisation?*

   Employing this work's proof-of-concept RF sensor configuration and algorithms for delivering 100% inside-outside discrimination success (Section 3.5), the following performance may be inferred:

   - For inside RF target detection, the RMSE localisation accuracy takes values inside the closed interval ± [0 to 0.4] metres (section 3.6.3).
   - For outside RF target detection, the RMSE localisation accuracy takes values inside the closed interval ± [0.02 to 1.44] metres. The outside accuracy can be improved by increasing the density of the outward pointing RF sensors (Section 3.6.3).

It should be noted that to improve the RF detection and location system to address the limitations for the outside ranging accuracy, an increase of the overall system redundancy would be required by adding more RF sensors pointing outside. Moreover, sensor positioning optimisation trough tilting may need to be considered, since this study adopted a default parallel orientation with the ground plane, transversal orthogonal on the vehicle's body.

This study provides an important contribution to the academic research field by demonstrating a systematic framework for investigating both theoretical and practical aspects of the initial radio location problem. The intricate and complex nature of the subject is meticulously explored through both empirical RF testing and theoretical electromagnetic experiments. The theoretical investigations led to a 3D raytracing simulation code implemented in MATLAB demonstrating the underlying aspects of wireless source modelling and circuit designing based on quantitative analysis. Experimental setups focussed on various data aspects associated with RF polarisation and fingerprinting, whereas the demonstrator displayed the performance of the innovative prototypes both independently and in networks. Based on the theoretical and empirical results, a unique perspective was demonstrated for solving the location problem in an extrapolated context of smartphone platform implementation.

The two papers disseminating this study's results presented at IEEE events from SmartNets and ROSE, support this work's academic high impact by both being rated among the best papers at the conferences and the latter winning the award for best student paper on the MATLAB ray tracing simulation topic (https://rose2021.ieee-ims.org/rose-2021-awards).

Through this project, industrial partner Jaguar Land Rover has been offered an innovative solution to the problem of discriminating an RF source position inside and outside of a vehicle, using a detection system that is completely integrated within the vehicle. By following a minimalistic approach in terms of sensor number and conducting tests in the most challenging scenarios, the solution provides a location accuracy below ±0.5 m inside the vehicle and close to ±1.5 m outside the vehicle. This performance, however, was only possible after successfully addressing all of the transdisciplinary steps outlined in this work's statement of innovation (Section 1.12). With this approach, and by following the pre-set design restrictions, the automotive partners can continue to exploit the developed technology in a manner that will eventually lead to optimal smartphone-based car key systems.

4.2 Study limitations

In possible further developments of the principles demonstrated in this work, some important limitations may need to be considered. One relates to the RSSI variance between devices produced by different manufacturers, already outlined for Wi-Fi [272] and BLE [273] technologies. The variation may be addressed at manufacturer level through a new standard release or at user level by performing initial calibrations. A second limitation results from the RF sensor miniaturisation process that will need to be pursued further for the technology to be considered for vehicle manufacturing industry. For instance, if certain electronics manufacturers may deliver the RF sensors confined in enclosures significantly reduced in size, or the vehicle manufacturer includes pressed cavities to house the sensors considering that each vehicle chassis is different, the sensor positions suggested in this study may not be available. To solve the problem, the new available RF positions will need to be reassessed. Another limitation of the study to be addressed is the scenario of mounting the outside pointing RF sensors behind an electrically conductive coated window, property that may affect signal reception. However, this scenario depends directly on the vehicle manufacturer, since the outside detecting RF sensors may be placed on the cabin's metal pillars in suitably devised positions.

A last possible challenge to be solved in future implementations when considering that the human passenger's interference has been addressed by recommending for the

inside detection RF sensors to point on the space in front of the seats, involves real time detection. Since this work demonstrated the proof-of-concept design based on an averaged RSSI value, when considering an online scenario, less values will be assessed by the system to reduce the detection time, thus potentially leading to a decrease in the location accuracy. This may also be solved in the future implementations at the communication protocol level, the interfacing LBS smartphone running app allowing different transmission speeds for the exchanged location frames: a slow retransmission when the user is out of vehicle's detection range to save energy and a rapid broadcasting when the user's estimated trajectory indicates approaching to the static car. The proof-of-concept work presented in this study aligns on a technology readiness level (TRL) no further than level four from the total of ten [274], therefore some other omitted refinements may be required on the path to the market and implementation.

4.3 Future work and potential applications

The study's novel approach presenting the directive sensors synthesis based on 3D RT and logical reasoning may be used with or without computational aid, delivering a powerful visual solution for a new RF layout when a cross-disciplinary audience participates, before employing any classical resource demanding electromagnetic simulations used on complex CAD models. A direct improvement for the RF detection system will be the changing of the communication channel with one less susceptible to Wi-Fi or BLE interferences as recommended by this study when discussing the reason behind the selection of channel 11 to pursue an unbiased reception scenario. The RF modelling illustrates furthermore the importance of the signal polarisation combination between the RF source and the detection system. Therefore, since low power wireless technologies used in LBS such as BLE start including in their broadcasted positional beacons additional data, for instance the RF source ID and its instantaneous transmitting power [275, 276], to compensate for the technological mismatch, it is proposed that a value encoding the smartphone's default antenna position and its variation due to the user's instant posture is added to the location beacon to mitigate the signal polarisation ranging error. Since the recent game industry

and virtual reality (VR) technology are requiring a 3D gyro sensor to be embedded in the smartphone providing the necessary hardware to account for device orientation, adding the data to the location beacon and mapping it to a certain RSSI polarisation fingerprinting database becomes a feasible operation.

Other potential application examples for the RF detection system may include:

- Perimeter security alerts against airborne threats such as drones intruding in high security areas like airports or prisons.
- Person identification by recognising a previously paired mobile device associated with an access area, by delivering the functionality of an active RFID interrogator.
- Parking occupancy detection via surface flushed RF sensors detecting the static vehicle's PEPS or PKE wireless beacons.

Overall, the results and procedures described in this work, if adapted specifically to a cross-disciplinary use case requiring a solution for a similar RF location problem, may assist and provide the means to further progress in their investigatory studies.

References

[1] JaguarLandRover, “The future starts here,” Jaguar Land Rover, 2016.

[2] C. Paukert, “Jaguar Land Rover Activity Key wearable sales are hot,” CNet, 18 2 2018. [Online]. Available: https://www.cnet.com/roadshow/news/jaguar-land-rover-activity-key-sales-f-pace-velar-e-pace-hot/. [Accessed 6 6 2020].

[3] J. Groves, “Jaguar Land Rover's Activity Key: does it work?,” Car magazine, 15 3 2019. [Online]. Available: https://www.carmagazine.co.uk/car-news/tech/jaguar-land-rover-activity-key-what-is-it-how-does-it-work/. [Accessed 6 6 2020].

[4] MercedesBenz, “Digital vehicle key,” Mercedes Benz, 2019. [Online]. Available: https://www.diplomaticsales.mercedes-benz.com/passengercars/mercedes-benz-cars/models/glb/glb-suv/comfort.pi.html/mercedes-benz-cars/models/glb/glb-suv/comfort/connectivity/digitalkey. [Accessed 6 6 2020].

[5] BMW, “BMW: iPhone can be used as digital car key,” BMW, 24 6 2020. [Online]. Available: https://www.fleetnews.co.uk/news/manufacturer-news/2020/06/24/bmw-iphone-to-become-digital-car-key. [Accessed 6 6 2020].

[6] Audi, “Audi connect key,” Audi, 17 2 2017. [Online]. Available: https://www.audi-mediacenter.com/en/technology-lexicon-7180/infotainment-7183. [Accessed 6 6 2020].

[7] Volkswagen, “Mobile key,” Volkswagen, 2020. [Online]. Available: https://www.portal.volkswagen-we.com/portal/en_GB/web/gb/content/-/content/info-center/we-connect/mobile-key#1. [Accessed 6 6 2020].

[8] Ford, “How to use remote features with FordPass Connect,” Ford, [Online]. Available: https://www.ford.co.uk/owner/resources-and-support/how-to-videos/owner-services/fordpass-remote-lock. [Accessed 6 6 2020].

[9] F. Lambert, “Tesla Model 3: how the keyless and phone entry works and user manual,” 22 9 2017. [Online]. Available: https://electrek.co/2017/09/22/tesla-model-3-how-keyless-and-phone-entry-works/. [Accessed 6 6 2020].

[10] Volvo, “Volvo Digital Key Makes Service Simple,” Volvo, 2020. [Online]. Available: https://www.volvooflouisville.com/volvo-digital-key-makes-service-simple.htm. [Accessed 6 6 2020].

[11] Tesla, “MODEL 3 Owner's manual,” Tesla, 2020.

[12] J. McCann, “Volvo's keyless car makes your smartphone the master,” Techradar, 25 2 2016. [Online]. Available: https://www.techradar.com/uk/news/car-tech/volvo-s-keyless-car-makes-your-smartphone-the-master-1315817. [Accessed 6 6 2020].

[13] Volvo, “Car sharing with the Volvo On Call app,” Volvo, 25 11 2019. [Online]. Available: https://www.volvocars.com/en-ca/support/topics/volvo-on-call/app/car-sharing-with-the-volvo-on-call-app. [Accessed 6 6 2020].

[14] A. Alarifi, A. Al-Salman, M. Alsaleh, A. Alnafessah, S. Al-Hadhrami, M. A. Al-Ammar, Al-Khalifa and H. S., “Ultra wideband indoor positioning technologies: Analysis and recent advances,” *Sensors*, vol. 16, no. 5, p. 707, 2016.

[15] D. Dardari, P. Closas and P. M. Djurić, “Indoor tracking: Theory, methods, and technologies,” *IEEE Transactions on Vehicular Technology*, vol. 64, no. 4, pp. 1263-1278, 2015.

[16] D. Stojanović and N. Stojanović, “Indoor localization and tracking: Methods, technologies and research challenges,” *Facta Universitatis, Series: Automatic Control and Robotics*, vol. 13, no. 1, pp. 57-72, 2014.

[17] R. Mautz, “Indoor Positioning Technologies,” Institute of Geodesy and Photogrammetry, ETH Zurich, 2012.

[18] S. R. Mallipeddy and R. S. Kshetrimayum, “Impact of UWB interference on IEEE 802.11 a WLAN system.,” in *National Conference On Communications (NCC)*, 2010.

[19] D. Landi and C. Fischer, “The effects of UWB interference on GSM systems,” in *International Zurich Seminar on Communications*, 2004.

[20] L. Larson, D. Laney and J. Jamp, “An overview of hardware requirements for uwb systems: interference issues and transceiver design implications,” in *IEEE Military Communications Conference, MILCOM 2003*, 2003.

[21] M. Larabel, “Linux 5.7 Staging Will Be ~28.7k Lines Of Code Lighter Thanks To Nuking WUSB + UWB,” linuxtoday, 2 February 2020. [Online]. Available: https://www.linuxtoday.com/developer/linux-5.7-staging-will-be-28.7k-lines-of-code-lighter-thanks-to-nuking-wusb-uwb.html. [Accessed 6 6 2020].

[22] M. Larabel, “Wireless USB + UWB Demotion Goes Ahead For Linux 5.4,” phoronix, 3 September 2019. [Online]. Available: https://www.phoronix.com/scan.php?page=news_item&px=Linux-5.4-Deprecates-WUSB-UWB. [Accessed 6 6 2020].

[23] Intel, “Thunderbolt™ for Developers,” Intel, [Online]. Available: https://www.intel.com/content/www/us/en/products/docs/io/thunderbolt/thunderbolt-technology-developer.html. [Accessed 6 6 2020].

[24] A. Oxford, “Whatever happened to Wireless USB & HDMI?,” techradar, 19 August 2011. [Online]. Available: https://www.techradar.com/news/computing/whatever-happened-to-wireless-usb-i-994212. [Accessed 6 6 2020].

[25] Ofcom, “Ultra Wideband,” Ofcom, 2005.

[26] T. Harrington, “Hearing on “Accountability and Oversight of the Federal Communications Commission”, Dec. 5, 2019; Ultra Wide Band Alliance Comments Regarding the FCC’s 6 GHz Proceeding,” Washington, 2019.

[27] D. Zito and D. Morche, “UWB Radios—The maturity age?,” in *14th IEEE International New Circuits and Systems Conference (NEWCAS)*, 2016.

[28] T. Wendt, F. Volk and E. Mackensen, “A benchmark survey of Long Range (LoRaTM) Spread-Spectrum-Communication at 2.45 GHz for safety applications,” in *IEEE 16th Annual Wireless and Microwave Technology Conference (WAMICON)*, 2015.

[29] Semtech, “SX1280/SX1281 Long Range, Low Power, 2.4 GHz Transceiver with Ranging Capability,” Semtech, 2020.

[30] NordicSemiconductor, “nRF52 Series SoC,” Nordic Semiconductor, 2019.

[31] S. Srinivasulu, M. Kavitha and C. S. Kolli, “Wireless Technology over Internet of Things,” in *Emerging Research in Data Engineering Systems and Computer Communications*, 2020.

[32] SONOFF, “SONOFF ZigBee Bridge. User manual V1.1,” SONOFF TECHNOLOGIES CO., LTD., 2020.

[33] Philips, “Philips Hue Bridge 2.0,” Philips, 2020.

[34] Tuya, “Smart Home Controller Pad,” Tuya Smart, 2020.

[35] A. Rahman, A. Nurhananie, M. H. Habaebi, M. M. Ahmad, S. Khan and M. Ismail, “Integrating ZigBee Modem into Android Platform,” in *International Conference on Computer and Communication Engineering*, 2014.

[36] ResearchAndMarkets, “802.15.4 IoT Markets,” Research and Markets, 2019.

[37] O. Bay, “850 Million IEEE 802.15.4 Chipsets to Ship in 2016, Despite Strong Competition from Bluetooth,” ABIresearch, 2 May 2012. [Online]. Available: https://www.abiresearch.com/press/850-million-ieee-802154-chipsets-to-ship-in-2016-d. [Accessed 6 6 2020].

[38] V. V. Garbhapu and S. Gopalan, “IoT based low cost single sensor node remote health monitoring system,” in *Procedia computer science*, 2017.

[39] V. D. Guchta, T. Blanckaert, J.-P. Goemaereb, C. Naessensc, S. Coola, K. C. Mertensa, A. V. Nuffela and J. Vangeytea, “Development of an open-source, low-cost and adaptable 3D accelerometer for monitoring animal motion,” in *International conference of Agricultural Engineering 2014 (AgEng 2014)*, 2014.

[40] Y. Wu, C. Shi, M. Ismail and H. Olsson, “Temperature compensation design for a 2.4 GHz CMOS low noise amplifier,” in *IEEE International Symposium on Circuits and Systems (ISCAS 2000)*, Geneva, 2000.

[41] G. G. Bannister Kenneth and S. K. Gupta, “Wireless sensor networking for hot applications: Effects of temperature on signal strength, data collection and localization,” in *Proceedings of the 5th Workshop on Embedded Networked Sensors (HotEmNets' 08)*, 2008.

[42] Y.-H. Chou and J.-F. Kiang, “Ducting and turbulence effects on radio-wave propagation in an atmospheric boundary layer,” *Progress In Electromagnetics Research,* vol. 60, pp. 301-315, 2014.

[43] S. I. Inácio and J. A. R. Azevedo, “Influence of meteorological parameters in the received signal of a 2.4 GHz wireless sensor network,” in *Loughborough Antennas & Propagation Conference 2018 (LAPC 2018)*, 2018.

[44] D. Bri, S. Sendra, H. Coll and J. Lloret, “How the atmospheric variables affect to the WLAN datalink layer parameters,” in *Sixth Advanced International Conference on Telecommunications*, 2010.

[45] B. Chandrasekaran, S. Gangadhar and J. M. Conrad, “A survey of multisensor fusion techniques, architectures and methodologies,” in *SoutheastCon 2017*, 2017.

[46] X. Zhao and D. Zhang, “A review of multi-sensor data fusion for traffic,” in *International Symposium on Intelligence Computation and Applications*, 2017.

[47] W. Elmenreich, “An introduction to sensor fusion (47/2001),” University of Technology, Vienna, 2002.

[48] A. Weckenmann, K.-D. S. X. Jiang, U. Neuschaefer-Rube, J. Seewig, L. Shaw and T. Estler, “Multisensor data fusion in dimensional metrology,” *CIRP annals,* vol. 58, no. 2, pp. 701-721, 2009.

[49] S. Bhanot, B. Singh and K. Singh, “Issues in multisensor fusion technology,” in *National conference in Trends in Industrial Electronics, Transducers, Controls and Communication*, 2000.

[50] H. B. Mitchell, Multi-sensor data fusion: an introduction, Springer Science & Business Media, 2007.

[51] J. Hightower and G. Borriello, “A survey and taxonomy of location systems for ubiquitous computing,” *IEEE computer,* vol. 34, no. 8, pp. 57-66, 2001.

[52] Z. Farid, R. Nordin and M. Ismail, “Recent advances in wireless indoor localization techniques and system,” *Journal of Computer Networks and Communications,* 2013.

[53] A. Corbacho Salas, “Indoor positioning system based on bluetooth low energy,” Universitat Politècnica de Catalunya, 2014.

[54] D. Bosnjak, “LG's VLC ZigBee Smartphone Connector Certified By The FCC,” Android, 2017. [Online]. Available: https://www.androidheadlines.com/2017/05/lgs-vlc-zigbee-smartphone-connector-certified-fcc.html. [Accessed 1 10 2018].

[55] S. Clark, “TazTag unveils first Android phone with NFC and ZigBee,” NFCW, 2012. [Online]. Available: https://www.nfcw.com/2012/02/26/313800/taztag-unveils-first-android-phone-with-nfc-and-zigbee/. [Accessed 1 10 2018].

[56] J. John, R. Saborio, S. A. Ghazanfar, D. Gebre-Egziabher and B. Davis, “Evaluation of Low-Cost, Centimeter-Level Accuracy OEM GNSS Receivers,” Minnesota Department of Transportation Research Services & Library, St. Paul, 2018.

[57] G. Oguntala, R. Abd-Alhameed, S. Jones, J. Noras, M. Patwary and J. Rodriguez, “Indoor Location Identification Technologies for Real-Time IoT-based Applications: An Inclusive Survey,” *Computer Science Review,* vol. 30, pp. 55-79, 2018.

[58] A. Yassin, Y. Nasser, M. Awad, A. Al-Dubai, R. Liu, C. Yuen, R. Raulefs and E. Aboutanios, “Recent advances in indoor localization: A survey on theoretical approaches and applications,” *IEEE Communications Surveys & Tutorials,* vol. 19, no. 2, pp. 1327-1346, 2017.

[59] E. Karlsson and A. Lagerbielke, Demonstrator Development for Phone as a Key Based on Bluetooth Low Energy, Linköping University, 2017.

[60] P. Huang and P. Zheng, “BlueID: Enabling robust in-car localization and on-demand personalization using Bluetooth.,” in *IEEE 28th Annual International Symposium on Personal, Indoor, and Mobile Radio Communications (PIMRC)*, 2017.

[61] Y. Cao, X. Lu, Z. Zhao, X. Ji, J. Yang and X. Pang, “A Comparative Study of BLE-based Fingerprint Localization for Vehicular Application,” in *IEEE Ubiquitous Positioning, Indoor Navigation and Location-Based Services (UPINLBS)*, 2018.

[62] Y. Cao, X. Lu, Z. Zhao, X. Ji and Y. Yan, “Distance Estimation Methods in Vehicular Application: An Experimental Study,” in *2018*, IEEE 18th International Conference on Control, Automation and Systems (ICCAS).

[63] R. D. Emmanuel, A. P. S. B., T. Melbin and T. Anshul, “Passenger Localization for In-Vehicle Personalization Using BLE Beacons,” in *IEEE 87th Vehicular Technology Conference (VTC Spring)*, 2018.

[64] B. I. Ahmad, P. M. Langdon, J. Liang, S. J. Godsill, M. Delgado and T. Popham, “Driver and Passenger Identification from Smartphone Data,” *IEEE Transactions on Intelligent Transportation Systems*, vol. 20, no. 4, pp. 1278-1288, 2018.

[65] L. W. S. Matthew P. Reed and L. L. Ricci, “Survey of auto seat design recommendations for improved comfort,” University of Michigan Transportation Research Institute , Michigan, 1994.

[66] K. Irene, “The influence of car-seat design on its character experience,” *Applied ergonomics*, vol. 43, no. 2, pp. 329-335, 2012.

[67] S. P. McEvoy, M. R. Stevenson and M. Woodward., “The contribution of passengers versus mobile phone use to motor vehicle crashes resulting in hospital attendance by the driver,” *Accident Analysis & Prevention*, vol. 39, no. 6, pp. 1170-1176, 2007.

[68] M. Hairulnizam, A. H. Omar, S. S. Yaacob, S. Kasim and M. F. M. Fudzee, “Minimizing heatstroke incidents for young children left inside vehicle,” in *IOP Conference Series: Materials Science and Engineering*, 2016.

[69] V. Aiello, P. N. Borazjani, E. Battista and M. Albanese, “Next-generation technologies for preventing accidental death of children trapped in parked vehicles,” in *Proceedings of the 2014 IEEE 15th International Conference*, 2014.

[70] J. White, C. Thompson, H. Turner, B. Dougherty and D. C. Schmidt, “WreckWatch: Automatic Traffic Accident Detection and Notification with Smartphones,” *Mobile Networks and Applications*, vol. 16, no. 3, p. 285, 2011.

[71] IEEE, “IEEE Standard 802.15.4: Wireless Medium Access Control (MAC) and Physi-cal Layer (PHY) Specifications for Low-Rate Wireless Personal Area Networks(LR-WPANs),” IEEE, 2003.

[72] H. Khudov, A. Fedorov, D. Holovniak and G. Misiyuk, “Improving the Efficiency of Radar Control of Airspace with the Multilateration System Use,” in *International Scientific-Practical Conference Problems of Infocommunications. Science and Technology (PIC S&T)*, 2018.

[73] A. Shayokh, U. A. Md and H. P. Partal., “Performance improvement techniques for RSSI based localization methods,” in *International Conference on Electrical Information and Communication Technology (EICT)*, 2013.

[74] S. Yiu, M. Dashti, H. Claussen and F. Perez-Cruz, “Wireless RSSI fingerprinting localization,” *Signal Processing*, vol. 131, pp. 235-244, 2017.

[75] S. Xia, Y. Liu, G. Yuan, M. Zhu and Z. Wang, “Indoor fingerprint positioning based on Wi-Fi: An overview,” *ISPRS International Journal of Geo-Information*, vol. 6, no. 5, p. 135, 2017.

[76] P. Bahl and V. N. Padmanabhan, “RADAR: An In-Building RF-based User Location and Tracking System,” 2000.

[77] A. Zanella, “Best Practice in RSS Measurements and Ranging,” *IEEE Communications Surveys & Tutorials* , vol. 18, no. 4, pp. 2662-2686, 2016.

[78] M. Singh, S. K. Bhoi and P. M. Khilar, “Omnidirectional Radio Propagation Antenna Using Organized Grouping of Monopole Antennas.,” *National Academy Science Letters*, vol. 42, no. 2, pp. 109-113, 2019.

[79] Y. Chen, Z. Liu, X. Fu, B. Liu and W. Zhao, “Theory underlying measurement of AOA with a rotating directional antenna,” in *Proceedings IEEE INFOCOM*, 2013.

[80] R. Zekavat and R. M. Buehrer, Handbook of Position Location: Theory, Practice, and Advances, vol. 27, John Wiley & Sons., 2011.

[81] H. Liu, H. Darabi, P. Banerjee and J. Liu, “Survey of wireless indoor positioning techniques and systems,” vol. 37, no. 6, pp. 1067-1080, 2007.

[82] C.-C. Pu, C.-H. Pu and H.-J. Lee, “Indoor location tracking using received signal strength indicator,” in *Emerging communications for wireless sensor networks. IntechOpen*, 2011.

[83] E. D. Manley, H. A. Nahas and J. S. Deogun, “Localization and tracking in sensor systems,” *IEEE International Conference on Sensor Networks, Ubiquitous, and Trustworthy Computing (SUTC'06)*, vol. 2, pp. 237-242, 2006.

[84] A. Roxin, J. Gaber, M. Wack and A. Nait-Sidi-Moh, “Survey of wireless geolocation techniques,” in *IEEE Globecom Workshops*, 2007.

[85] H. N. Mahjoub, A. Tahmasbi-Sarvestani, S. M. O. Gani and Y. P. Fallah, “Composite $\alpha-\mu $ Based DSRC Channel Model Using Large Data Set of RSSI Measurements,” *IEEE Transactions on Intelligent Transportation Systems,* vol. 20, no. 1, pp. 205-217, 2018.

[86] B. H. Liu, B. P. Otis, S. Challa, P. Axon, C. Chou and S. Jha, “The impact of fading and shadowing on the network performance of wireless sensor networks,” *International Journal of Sensor Networks,* vol. 3, no. 4, pp. 211-223, 2008.

[87] F. DellaRosa, M. Pelosi and J. Nurmi, “Human-induced effects on rss ranging measurements for cooperative positioning,” *International Journal of Navigation and Observation,* 2012.

[88] K. Kaemarungsi and P. Krishnamurthy, “Properties of indoor received signal strength for WLAN location fingerprinting,” in *The First Annual International Conference on Mobile and Ubiquitous Systems: Networking and Services,* 2004.

[89] S. Shukri, L. M. Kamarudin, G. C. Cheik, R. Gunasagaran, A. Zakaria, K. Kamarudin, S. S. Zakaria, A. Harun and S. N. Azemi, “Analysis of RSSI-based DFL for human detection in indoor environment using IRIS mote,” in *3rd international conference on electronic design (ICED),* 2016.

[90] A. Ruddle, L. Low, J. Rigelsford and R. Langley, “Variation of computed in-vehicle SAR with number and location of occupants at commonly used communications frequencies,” in *In 10th International Symposium on Electromagnetic Compatibility,* 2011.

[91] F.-K. Wang, T.-S. Horng, K.-C. Peng, J.-K. Jau, J.-Y. Li and C.-C. Chen, “Seeing through walls with a self-injection-locked radar to detect hidden people,” in *IEEE/MTT-S International Microwave Symposium Digest,* 2012.

[92] C. Debes, A. M. Zoubir and M. G. Amin, “Target detection in multiple-viewing through-the-wall radar imaging,” in *In IGARSS 2008-2008 IEEE International Geoscience and Remote Sensing Symposium,* 2008.

[93] R. Ravichandran, E. Saba, K.-Y. Chen, M. Goel, S. Gupta and S. N. Patel, “WiBreathe: Estimating respiration rate using wireless signals in natural settings in the home,” in *IEEE International Conference on Pervasive Computing an Conference on Pervasive Computing and Communications,* 2015.

[94] D. Obeid, S. Sadek, G. Zaharia and G. E. Zein, “Noncontact heartbeat detection at 2.4, 5.8, and 60 GHz: A comparative study,” *Microwave and Optical Technology Letters,* vol. 51, no. 3, pp. 666-669, 2009.

[95] S. Maity, K. Singha, P. Debnath and M. Singha, “Textiles in electromagnetic radiation protection,” *Journal of Safety Engineering,* vol. 2, no. 2, pp. 11-19, 2013.

[96] B. Kim, V. Koncar, E. Devaux, C. Dufour and P. Viallier, “Electrical and morphological properties of PP and PET conductive polymer fibers,” *Synthetic Metals,* vol. 146, no. 2, pp. 167-174, 2004.

[97] M. Hagan and H.-N. Teodorescu, “Intelligent clothes with a network of painted sensors,” in *IEEE E-Health and Bioengineering Conference (EHB),* 2013.

[98] G. Cho, Smart clothing: technology and applications, CRC press, 2009.

[99] J. Agbinya, M. C. Aguayo-Torres and R. Klempous, 4G Wireless Communication Networks: Design Planning and Applications, River Publishers, 2013.

[100] L. Xu, F. Yang, Y. Jiang, L. Zhang, C. Feng and N. Bao, “Variation of received signal strength in wireless sensor network,” in *3rd International Conference on Advanced Computer Control,* 2011.

[101] Y. Chapre, P. Mohapatra, S. Jha and A. Seneviratne, “Received signal strength indicator and its analysis in a typical WLAN system (short paper),” in *38th Annual IEEE Conference on Local Computer Networks,* 2013.

[102] N. Patwari and S. K. Kasera, “Temporal link signature measurements for location distinction,” *IEEE Transactions on Mobile Computing,* vol. 10, no. 3, pp. 449-462, 2010.

[103] K. H. M. Azmi, S. M. Berber and M. J. Neve., “The influence of received signal strength measurement methods on the accuracy of distance estimation in wireless sensor network.,” in *IEEE 4th International Conference on Smart Instrumentation,, Measurement and Application (ICSIMA),* 2017.

[104] I. G. Tudorache, I. Rasool and A. H. Kemp, “Indoor RSSI-based ranging consistency and error factors in wireless sensor networks,” in *IEEE 20th Telecommunications Forum,* 2012.

[105] B. J. Dil and P. J. Havinga., “RSS-based localization with different antenna orientations,” in *IEEE Australasian Telecommunication Networks and Applications Conference,* 2010.

[106] R. Rudd, K. Craig, M. Ganley and R. Hartless, “Building materials and propagation. Final Report. (2604/BMEM/R/3/2.0),” Ofcom, 2014.

[107] R. Wilson, “Propagation losses through common building materials 2.4 GHz vs 5 GHz. (E10589),” Magis Network, 2002.

[108] K. Bannister, G. Giorgetti and S. K. Gupta, “Wireless sensor networking for hot applications: Effects of temperature on signal strength, data collection and localization,” in *Proceedings of the 5th Workshop on Embedded Networked Sensors (HotEmN)*.

[109] J. Luomala and I. Hakala, “Effects of temperature and humidity on radio signal strength in outdoor wireless sensor networks,” in *IEEE Federated Conference on Computer Science and Information Systems (FedCSIS),*, 2015.

[110] P. Dhere, P. Chilveri, R. Vatti, V. Iyer and K. Jagdale, “Analysis of the Impact of Building Materials on ISM 2.4 GHz Band,” in *International Conference on Current Trends towards Converging Technologies (ICCTCT)*, 2018 .

[111] J. Fleury, L. Burnier, M. Lanini, M. D. Domenico, E. Zimmermann, C. Genoud, A. Salvadé and A. Schueler, “Novel microwave transparent low emissivity coating for energy-efficient glazing: towards 5G frequencies,” *Journal of Physics: Conference Series,* vol. 1343, no. 1, p. p. 012199, 2019.

[112] M. Gustafsson, A. Karlsson, A. P. P. Rebelo and B. Widenberg, “Design of frequency selective windows for improved indoor outdoor communication,” *IEEE transactions on antennas and propagation,* vol. 54, no. 6, pp. 1897-1900, 2006.

[113] Eurostat, “Majority of transport jobs held by men,” Eurostat, 2020.

[114] J. Garcia and C. Quintana-Domeque, “The evolution of adult height in Europe: a brief note,” *Economics & Human Biology,* vol. 5, no. 2, pp. 340-349, 2007.

[115] F. Naini, M. Cobourne, F. McDonald and A. Donaldson, “The influence of craniofacial to standing height proportion on perceived attractiveness,” *International journal of oral and maxillofacial surgery,* vol. 37, no. 10, pp. 877-885, 2008.

[116] E. Maghraby, M. A. Amr, O. Enany and M. Y. E. Nahas, “Detecting and Tracking of Multiple People in Video based on Hybrid Detection and Human Anatomy Body Proportion,” *International Journal of Computer Applications,* vol. 109, no. 17, pp. 10-14, 2015.

[117] Y. Hu, J. Wang, T. Jiang and S. Lin, “Semantic Feature Extraction of 3D Human Model from 2D Orthographic Projectio,” in *IEEE 5th International Conference on Digital Home*, 2014.

[118] C. D.-S. Liyange, “Audiovisual sensing of human movements for home-care and security in a smart environment,” *International Journal on Smart Sensing and Intelligent Systems,* vol. 1, no. 1, 2008.

[119] Y.-J. Liu, D.-L. Zhang and M. M.-F. Yuen, “A survey on CAD methods in 3D garment design,” *Computers in Industry,* vol. 61, no. 6, pp. 576-593, 2010.

[120] V. V. Yakovlev, “Examination of contemporary electromagnetic software capable of modeling problems of microwave heating,” in *Advances in Microwave and Radio Frequency Processing*, Berlin, 2006.

[121] D. Winske and N. Omidi, “Electromagnetic ion/ion cyclotron instability: Theory and simulations,” *Journal of Geophysical Research: Space Physics,* vol. 97, no. A10, pp. 14779-14799, 1992.

[122] A. Ewall-Wice, R. Bradley, D. Deboer, J. Hewitt, A. Parsons, J. Aguirre, Z. S. A. J., Z. Ali, J. Bowman, C. Cheng and P. N. Neben, “The hydrogen epoch of reionization array dish. ii. characterization of spectral structure with electromagnetic simulations and its science implications.,” *The Astrophysical Journal,* vol. 831, no. 2, p. 196, 2016.

[123] F. Bilotti and L. Sevgi, “Metamaterials: Definitions, properties, applications, and FDTD-based modeling and simulation,” *International Journal of RF and Microwave Computer-Aided Engineering ,* vol. 22, no. 4, pp. 422-438., 2012.

[124] M. Rutschlin and V. Sokol, “Reconfigurable antenna simulation: Design of reconfigurable antennas with electromagnetic simulation,” *IEEE Microwave Magazine,* vol. 14, no. 17, pp. 92-101, 2013.

[125] S. A. Cummer, “Modeling electromagnetic propagation in the Earth-ionosphere waveguide,” *IEEE Transactions on Antennas and Propagation,* vol. 48, no. 9, pp. 1420-1429, 2000.

[126] C. Yao, H. Wu, Y. Mi, Y. Ma, Y. Shen and L. Wang, "Finite difference time domain simulation of lightning transient electromagnetic fields on transmission lines," *IEEE Transactions on Dielectrics and Electrical Insulation,* vol. 20, no. 4, p. 1239, 2013.

[127] Y. Corre and Y. Lostanlen, "Three-dimensional urban EM wave propagation model for radio network planning and optimization over large areas," *IEEE Transactions on Vehicular Technology,* vol. 58, no. 7, pp. 3112-3123, 2009.

[128] N. Simonov, B.-R. Kim, K.-J. Lee, S.-I. Jeon and S.-H. Son, "Advanced fast 3-D electromagnetic solver for microwave tomography imaging," *IEEE Transactions on Medical Imaging,* vol. 36, no. 10, pp. 2160-2170, 2017.

[129] V. D. Giet, C. S. Michael, B. Schmulling and K. Hameyer, "Comparison of 2-D and 3-D coupled electromagnetic and structure-dynamic simulation of electrical machines," *IEEE Transactions on Magnetics,* vol. 44, no. 6, pp. 1594-1597, 2008.

[130] Y. Fu, M. Hate, J. McCalla, R. Langley and J. Rigelsford, "Variations in calculated whole body SAR for different ground coupling models," in *IEEE Loughborough Antennas & Propagation Conference*, Loughborough, 2011.

[131] A. Rosen, M. A. Stuchly and A. V. Vorst, "Applications of RF/Microwaves in Medicine," *Transactions on Microwave Theory and Techniques,* vol. 50, no. 3, pp. 963-974, 2002.

[132] G. Ala, M. C. D. Piazza, G. Tine, F. Viola and G. Vitale, "Evaluation of radiated EMI in 42-V vehicle electrical systems by FDTD simulation," *IEEE Transactions on Vehicular Technology,* vol. 56, no. 4, pp. 1477-1484, 2007.

[133] N. Mattew and O. Sadiku, Numerical techniques in electromagnetics with MATLAB, CRC Press, 2011.

[134] H. Baaser, Development and Application of the Finite Element Method based on MatLab, Springer Science & Business Media, 2010.

[135] S. Makarov, Antenna and EM Modeling with Matlab 1st Edition, New York: John Wiley & Sons Inc., 2002.

[136] T.-C. Poon and T. Kim, Engineering optics with Matlab®, World Scientific Publishing Co. Pte. Ltd, 2006.

[137] Q. Wang, W. Yao, J. Fang, X. Ai, J. Wen, X. Yang, H. Xie and X. Huang, "Dynamic modeling and small signal stability analysis of distributed photovoltaic grid-connected system with large scale of panel level DC optimizers," *Applied Energy,* vol. 259, p. 114132, 2020.

[138] M. Boban, J. Barrosy and O. K. Tonguz, "Geometry-Based Vehicle-to-Vehicle Channel Modeling for Large-Scale Simulation," *IEEE Transactions on Vehicular Technology,* vol. 63, no. 9, pp. 4146 - 4164, 2014.

[139] S. Bonafini and C. Sacchi, "Evaluation of Large Scale Propagation Phenomena on the Martian Surface: A 3D Ray Tracing Approach," in *IEEE 10th Advanced Satellite Multimedia Systems Conference and the 16th Signal Processing for Space Communication Workshop (ASMS/SPSC)*, 2020.

[140] L. Cheng, J. Casazza, J. Grace, F. Bai and D. D. Stancil, "Channel propagation measurement and modeling for vehicular in-cabin Wi-Fi networks," *IEEE Transactions on Antennas and Propagation,* vol. 64, no. 12, pp. 5424-5435, 2016.

[141] D. Didascalou, J. Maurer and W. Wiesbeck, "Subway tunnel guided electromagnetic wave propagation at mobile communications frequencies," *IEEE Transactions on Antennas and Propagation,* vol. 49, no. 11, pp. 1590-1596, 2001.

[142] Y. Ai, J. B. Andersen and M. Cheffena, "Path-loss prediction for an industrial indoor environment based on room electromagnetics," *IEEE Transactions on Antennas and Propagation,* vol. 65, no. 7, pp. 3664-3674, 2017.

[143] M. Sandip, K. Anil and R. Singh, "Computational Electromagnetics: Techniques and Applications," *International Journal for Research in Applied Science & Engineering Technology,* vol. 5, no. XI, pp. 122-125, 2017.

[144] L. H. Dieter, "The Origins of the Sampling Theorem," *IEEE Communications Magazine,* vol. 37, no. 4, pp. 106-108, 1999.

[145] M. Unser, "Sampling-50 years after Shannon," *Proceedings of the IEEE,* vol. 88, no. 4, pp. 569 - 587, 2000.

[146] M. Steffen, "Discretization Requirements: How many Elements per wavelength are necessary?," in *Computational Acoustics of Noise Propagation in Fluids - Finite and Boundary Element Methods*, Berlin Heidelberg, Springer, 2008, p. 309–332.

[147] Altair, “Numerical Methods in FEKO,” [Online]. Available: https://www.altair.com/resource/detail/4515. [Accessed 3 6 2019].

[148] A. I. Arbab, “Complex Maxwell’s equations,” *Chin. Phys. B,* vol. 22, no. 3, pp. 030301-1-030301-16, 2013.

[149] J. H. Bruce, “Oliver Heaviside: A first-rate oddity,” *Phys. Today,* vol. 65, no. 11, pp. 48-54, 2012.

[150] C. S. Helrich, “Chapter 2. Lagrangian Mechanics,” in *Analytical mechanics*, Springer, 2017, pp. 51-92.

[151] C. Jacoboni, “Survey of Classical Physics,” in *Theory of electron transport in semiconductors. A pathway from elementary physics to nonequilibrium Green function*, Springer, 2010, pp. 3-13.

[152] Y. Thomas, “Lagrangian formulation of the electromagnetic field,” 16 7 2012. [Online]. Available: http://math.uchicago.edu/~may/REU2012/REUPapers/Yu.pdf. [Accessed 12 12 2017].

[153] A. Wolski, “Theory of electromagnetic fields,” in *Proceedings of CAS ’10: RF for Accelerators*, Ebeltoft, 2010.

[154] R. Rumpf, “Maxwell ’ s Equations,” in *Computational Electromagnetics Courses, Lecture 2, EE 5337*, El Paso, 2017.

[155] J. Heinbockel, Introduction to Calculus Volume I, John H. Heinbockel , 2012.

[156] R. Courant, Introduction to Calculus and Analysis Vol1, Inderscience publishers, 1937.

[157] R. Courant, Differential and integral calculus Vol2, London: Blackie & Son Limitted, 1961.

[158] G. A. Osborne, Differential and integral calculus with example and applications, Boston: D. C. Heath & CO. Plublishers, 1906.

[159] H. Whitney, Geometric integration theory, New Jersey: Princeton University Press, 1957.

[160] K. Crane, F. de Goes, M. Desbrun and P. Schröder, “Digital geometry processing with discrete exterior calculus,” *SIGGRAPH Courses*, p. 7:1–7:126, 2013.

[161] B.-Y. Yaneer, Dynamics of Complex Systems, Massachusetts: Addison-Wesley, 1998.

[162] M. Baranger, “Chaos, complexity, and entropy; A physics talk for non-physicists,” Wesleyan University Physics Dept. Colloquium (2001), 2001. [Online]. Available: http://necsi.org/projects/baranger/cce.pdf. [Accessed 12 12 2017].

[163] J. D. Hoffman and S. Frankel, “Part III: Partial Differential Equations,” in *Numerical Methods for Engineers and Scientists. Second Edition*, New York, Marcel Dekker Inc., 2001, pp. 501-526.

[164] M. Kumar and G. Mishra, “An Introduction to Numerical Methods for the Solutions of Partial Differential Equations,” *Applied Mathematics,* vol. 2, pp. 1327-1338, 2011.

[165] A. S. John and M. B. Catherine, Modeling and simulation fundamentals Theoretical Underpinnings and Practical Domains, New Jersey: John Wiley & Sons, Inc., 2010.

[166] M. Törmä, Data Classification and Modelling in Remote Sensing (Maa-57.3210), Helsinki: Finnish Environment Institute, 2016.

[167] J. Frisch, Numerical modelling - Introductory approach (9th SimLab Course on parallel numerical simulation), Munich: Technical University of Munich, 2010.

[168] J. Spinnewijn, Lecture 9: Externalities (Lecture Notes for Ec426), London: London School of Economics, 2016.

[169] M. N. Sadiku, Numerical techniques in electromagnetics. Second edition, CRC press, 2001.

[170] J. D. Jackson, Classical electrodynamics, John Wiley & Sons, 1999.

[171] S. T. Chu and S. K. Chaudhuri, “Finite-difference timedomain method for optical waveguide analysis,” *Progress In Electromagnetics Research,* vol. PIER 11, pp. 255-300, 1995.

[172] S. Shinichi, T. Hideo and T. Masahiro, “Finite-Difference Time-Domain Method,” in *Computational Simulation in Architectural and Environmental Acoustics*, Tokyo, Springer, 2014, pp. 11-51.

[173] G. Anzaldi, P. J. Riu, F. Silva and R. Santos, “Finite difference time domain low cost modeling for automotive environments,” *Int. Symp. Electromagn. Compat. 2004,* vol. 3, pp. 775-780, 2004.

[174] U. T. Virk, K. Haneda, V. M. Kolmonen, P. Vainikainen and Y. Kaipainen, “Characterization of Vehicle Penetration Loss at wireless communication frequencies,” in *8th Eur. Conf. Antennas Propagation, EuCAP 2014*, 2014.

[175] W. Voit, W. Zapka, L. Belova and K. V. Rao, “Application of inkjet technology for the deposition of magnetic nanoparticles to form micron-scale structures,” *IEE Proc.-Sci. Meas. Technol*, vol. 150, no. 5, p. 252–256, 2003.

[176] P. Ankarson and J. Carlsson, “Fdtd-simulation of the electrical environment for vehicles by using cad-data,” in *3rd International Symposium on Electromagnetic Compatibility, 2002*, Beijing, 2003.

[177] G. Anzaldi, P. J. Rib, M. Fernandcz and F. Silva, “Validation procedure for final users applied to automotive environments,” in *IEE Seminar on Validation of Computational Electromagnetics*, Manchester, 2004.

[178] M. N. Sadiku, Numerical techniques in electromagnetics, Boca Raton: CRC Press LLC, 2001.

[179] A. Mihai, Efficient large electromagnetic simulation based on hybrid TLM and modal approach on grid computing and supercomputer, Toulouse: Institut National Polytechnique de Toulouse, 2012.

[180] R. Hocine, A. B. Stambouli and A. Saidane, “A Three-Dimensional TLM Simulation Method for Thermal Effect in PV-Solar Cells,” *International Journal of Energy and Power Engineering,* vol. 8, no. 6, pp. 911-915, 2014.

[181] M. El-Azeem and A. Hassan, “Using transmission line matrix method for metamaterial structures simulation,” *Journal of Advanced Vehicle System,* vol. 4, no. 1, pp. 7-11, 2017.

[182] G. L. Mats and B. Fredrik, The Finite Element Method: Theory, Implementation, and Practice, Springer, 2010.

[183] D. V. Hutton, Fundamentals of finite element analysis, Mc Graw Hill, 2003.

[184] I. Reguly and M. Giles, “Finite element algorithms and data structures on graphical processing units,” *International Journal of Parallel Programming,* p. 1–37, 2013.

[185] O. Castillo, J. DelaPuente, V. Puzyrev and J. M. Cela, “Assessment of edge-based finite element technique for geophysical electromagnetic problems: efficiency, accuracy and reliability,” in *Proceedings of the 1st Pan-American Congress on Computational Mechanics and XI Argentine Congress on Computational Mechanics. CIMNE*, Buenos Aires, 2015.

[186] A. R. Williams, P. J. Feibelman and N. D. Lang, “Green's-function methods for electronic-structure calculations,” *Physical Review,* vol. B 26, no. 10, p. 5433, 1982.

[187] T. Banov, Systematic Data Extractionin High-Frequency Electromagnetic Fields, Darmstadt: Technische Universität Darmstadt, 2014.

[188] R. Marklein, “The finite integration technique as a general tool to compute acoustic, electromagnetic, elastodynamic and coupled wave fields,” *Review of Radio Science 1999-2002,* vol. Review of radio science 1999–2002, pp. 201-244, 2002.

[189] S. Michael, “4. Finite Volume Methods,” in *Computational Engineering–Introduction to Numerical Methods*, Springer, 2006, pp. 77-105.

[190] L. Pedrotti, Basic Physical Optics, SPIE Press Book, 2008.

[191] P. Y. Ufimtsev, “Improved Physical Theory of Diffraction: Removal of the Grazing Singularity,” *IEEE Transactions on Antennas and Propagation,* vol. 54, no. 10, pp. 2698 - 2702, 2006.

[192] F. Vico, M. Ferrando, A. Valero, J. Herranz and E. Antonino, “Computational electromagnetics and fast physical optics,” *Waves,* vol. 1, pp. 155-161, 2009.

[193] J. B. Keller, “Geometrical Theory of Diffraction,” *Journal of the Optical Society of America,* vol. 52, no. 2, pp. 116-130, 1962.

[194] S. Sefi, Ray Tracing Tools for High Frequency Electromagnetics Simulations, Stockholm: Universitetsservice US AB, 2003.

[195] K. A. Remley, H. R. Anderson and A. Weisshar, “Improving the accuracy of ray-tracing techniques for indoor propagation modeling,” *IEEE transactions on vehicular technology,* vol. 49, no. 6, pp. 2350-2358, 2000.

[196] F. Xu and Y.-Q. Jin, “Bidirectional analytic ray tracing for fast computation of composite scattering from electric-large target over a randomly rough surface,” *IEEE Transactions on Antennas and Propagation,* vol. 57, no. 5, pp. 1495-1505, 2009.

[197] B. Engquist and O. Runborg, “Computational High Frequency Wave Propagation,” *Acta numerica,* vol. 12, pp. 181-266, 2003.

[198] T. Belytschko, Y. Krongauz, D. Organ, M. Fleming and P. Kryslc, “Meshless methods: An overview and recent developments,” *Comput Methods Appl Mech Eng,* vol. 139, no. 1-4, p. 3–47, 1996.

[199] Y. Chen, J. Lee and A. Eskandarian, “An Overview on Meshless Methods and Their Applications,” in *Meshless Methods in Solid Mechanics,* New York, Springer, 2006, pp. 55-67.

[200] L. B. Lucy, “A numerical approach to the testing of the fission hypothesis,” *Astron. J.,* vol. 82, p. 1013–1024, 1977.

[201] R. A. Gingold and J. J. Monaghan, “Smoothed particle hydrodynamics: theory and application to non-spherical stars,” *Monthly Notices R. Astron. Soc.,* vol. 181, p. 375–389, 1977.

[202] V. P. Nguyena, T. Rabczukb, S. Bordass and M. Duflotd, “Meshless methods: A review and computer implementation aspects,” *Mathematics and Computers in Simulation ,* vol. 79, p. 763–813, 2008.

[203] T. Belytschko, Y. Y. Lu and L. Gu, “Element-free Galerkin methods,” *Int. J. Numer. Methods Eng. ,* vol. 37, pp. 229-256, 1994.

[204] D. Yong, “A note on the meshless method using radial basis functions,” *Computers & Mathematics with Applications,* vol. 55, no. 1, pp. 66-75, 2008.

[205] P. Heckbert, “Fourier Transforms and the Fast Fourier Transform (FFT) Algorithm,” *Notes 3, Computer Graphics,* vol. 2, pp. 15-463, 1998.

[206] J. N. Edward, K. Herbert and K. Erwin, “Part C: Fourier Analysis. Partial Differential Equations (PDEs),” in *Advanced Engineering Mathematics, 10th Edition,* JOHN WILEY & SONS, INC, 2005, pp. 474-538.

[207] V. D. Maaten, E. P. Laurens and V.-d.-J. Herik, “Dimensionality reduction: a comparative,” *J Mach Learn Res,* vol. 10, no. 66-71, p. 13, 2009.

[208] I. K. Fodor, “A survey of dimension reduction techniques (UCRL-ID-148494),” Lawrence Livermore National Lab, 2002.

[209] Z. Hanbin and R. Serge, “Bottom-Up Assembly and Applications of Photonic Materials,” *Crystals,* vol. 6, no. 54, pp. 1-25, 2016.

[210] S. Robinson and R. Nakkeeran, “Photonic Crystal Ring Resonator Based Optical Filters,” *Light Interact. Matter,* vol. 1620, pp. 131-138, 2014.

[211] B. Weng, C. Chew and L. J. Jiang, “Overview of Large-Scale Computing : The Past , the Present , and the Future,” *Proceedings of the IEEE,* vol. 101, no. 2, pp. 227-241, 2013.

[212] P. Sumithra and D. Thiripurasundari, “A review on Computational Electromagnetics Methods,” *Advanced Electromagnetics,* vol. 6, no. 1, pp. 42-55, 2017.

[213] F. Reitich and K. K. Tamma, “State-of-the-art, trends, and directions in computational electromagnetics,” *Cmes,* vol. 5, no. 4, p. 287–294, 2004.

[214] T. Hubing, C. Su, H. Zeng and H. Ke, “Survey of Current Computational Electromagnetics Techniques and Software. CVEL-08-011.2,” The Calemson University Vehicular Electronics Laboratory, 2008.

[215] B. D. Davidson, Computational Electromagnetics for RF and Microwave Engineering, Cambridge: Cambridge University Press, 2005.

[216] M. S. Mollel and M. Kisangiri, “An Overview of Various Propagation Model for Mobile Communication,” 2014.

[217] J. I. Agbinya, M. C. Aguayo-Torres and R. Klempous, 4G Wireless Communication Networks: Design Planning and Applications, River Publishers, 2013.

[218] G. K. Karagiannidis, N. C. Sagias and P. Takis Mathiopoulos, “Nakagami: A Novel Stochastic Model for Cascaded Fading Channels,” vol. 55, no. 8, pp. 1453-1458.

[219] C.-C. Pu, C.-H. Pu and H.-J. Lee, “Indoor location tracking using received signal strength indicator,” 2011.

[220] E. C. Chan, G. Baciu and S. C. Mak, “Wi-Fi positioning based on Fourier descriptors,” vol. 3, 2010.

[221] S. Zhou, B. Wang, Y. Mo, X. Deng and L. T. .. Yang, “Indoor location search based on subarea fingerprinting and curve fitting,” 2013.

[222] P. K. Sharma, D. Sharma, P. C. Sau and A. Gupta, “Comparative analysis of propagation models in LTE networks with spline interpolation,” 2016.

[223] H. Zhao, B. Huang and B. Jia, “Applying kriging interpolation for WiFi fingerprinting based indoor positioning systems,” 2016.

[224] J. Yang and Y. Chen, “Indoor localization using improved RSS-based lateration methods,” 2009.

[225] H. W. Sorenson, “Least-squares estimation: from Gauss to Kalman,” vol. 7, no. 7, pp. 63-68, 1970.

[226] V. K. Ramachandra, Kalman filtering techniques for radar tracking, CRC Press, 2018.

[227] E. Brookner, Tracking and Kalman filtering made easy, New York: Wiley, 1998.

[228] S. Kurt and B. Tavli, “Path-Loss Modeling for Wireless Sensor Networks: A review of models and comparative evaluations,” vol. 59, no. 1, pp. 18-37, 2017.

[229] K. Roman, “Light and electromagnetic waves teaching in engineering education,” vol. 46, no. 4, pp. 343-353, 2009.

[230] S. Joseph, “Radiometry and the Friis transmission equation,” vol. 81, no. 1, pp. 33-37, 2013.

[231] H. Friis, “A note on a simple transmission formula,” vol. 34, no. 5, pp. 254-256, 1946.

[232] R. N. Pupala, “Introduction to wireless electromagnetic channels & large scale fading,” in *Lecture notes for Wireless Communication Technologies course* , Department of Electrical Engineering, Rutgers University, 2005.

[233] NXP, “Wireless Coexistence in the 2.4 GHz Band (AN5185),” NXP, 2015.

[234] ICCT, “European Vehicle Market Statistics, 2015–2016,” The International Council of Clean Transportation, 2015.

[235] T. Möller and B. Trumbore, “Fast, minimum storage ray/triangle intersection,” *ACM SIGGRAPH,* vol. Courses, no. ACM, p. 7, 2005.

[236] PulseLarsen, Tachnical data sheet: Series: Internal PCB Antenna PART NUMBER: W3538XXXXXSeries, PulseLarsen, 2009.

[237] NXP, Data Sheet: JN5168-001-Myy, NXP, 2013.

[238] H. Frederik, “A simple directional path loss model for a terminal inside a car,” in *IEEE 58th Vehicular Technology Conference. VTC 2003-Fall (IEEE Cat. No. 03CH37484),* 2003.

[239] J. Ilow, D. Hatzinakos and A. Venetsanopoulos, “Detection for binary transmission based on the empirical characteristic function,” in *Proceedings - ICASSP, IEEE International Conference on Acoustics, Speech and Signal Processing*, 1996.

[240] Q. Y. Kenny, “Indicator function and its application in two-level factorial designs,” *The Annals of Statistics,* vol. 31, no. 3, pp. 984-994, 2003.

[241] Y. Pang, H. Zhu, X. Li and J. Pan, “Motion blur detection with an indicator function for surveillance machines,” *IEEE Transactions on Industrial Electronics,* vol. 63, no. 9, pp. 5592-5601, 2016.

[242] R. P. Feynman, R. B. Leighton and M. Sands, The Feynman lectures on physics, Vol. I-II, London: Addision-Wesley Publishing Company INC., 1964.

[243] A. S. Glassner, An Introduction to Ray Tracing - Real-Time Rendering, San Diego: Elsevier, 1989.

[244] N. Jakica, "State-of-the-art review of solar design tools and methods for assessing daylighting and solar potential for building-integrated photovoltaics," *Renewable and Sustainable Energy Reviews,* vol. 81, pp. 1296-1328, 2018.

[245] M. E. Goss and K. Wu, "Study of supersampling methods for computer graphics hardware antialiasing," in *HP laboratories technical report HPL 121*, 2000.

[246] K. Beets and D. Barron, "Super-sampling anti-aliasing analyzed," 2000. [Online]. Available: http://citeseerx.ist.psu.edu/viewdoc/download?doi=10.1.1.91.1915&rep=rep1&type=pdf. [Accessed 3 6 2019].

[247] E. Delmelle, "Spatial Sampling," in *The SAGE handbook of spatial analysis*, 2009, pp. 165-186.

[248] G. Durgin, N. Patwari and T. S. Rappaport, "An advanced 3D ray launching method for wireless propagation prediction," in *IEEE 47th Vehicular Technology Conference. Technology in Motion*, 1997.

[249] A. S. Glassner, An Introduction to Ray Tracing - Real-Time Rendering, San Diego: Elsevier, 1989.

[250] Z. Zhang, Z. Yun and M. F. Iskander, "Ray tracing method for propagation models in wireless communication systems," *Electronics Letters,* vol. 36, no. 5, pp. 464-465, 2000.

[251] Microchip, "MRF24J40MA Data Sheet," Microchip, [Online]. Available: https://ww1.microchip.com/downloads/en/DeviceDoc/39776C.pdf. [Accessed 1 08 2019].

[252] Microchip, "PIC24F16KA102 Family Data Sheet," Microchip, [Online]. Available: http://ww1.microchip.com/downloads/en/devicedoc/39927c.pdf. [Accessed 1 08 2019].

[253] FTDI, "TTL-232RTTL to USB Serial Converter Range of Cables Datasheet," Future Technology Devices International Ltd, 2010.

[254] A. Kurusingal, A. Dhamdhere and V. Sivaraman., "Modeling signal strength of body-worn devices," in *IEEE Local Computer Network Conference*, 2010.

[255] B.-C. Min and E. T. Matson, "Robotic follower system using bearing-only tracking with directional antennas," *In Robot Intelligence Technology and Applications Springer,* vol. 2, no. Advances in Intelligent Systems and Computing 274, pp. 37-58, 2014.

[256] A. Elsts, R. Balass, J. Judvaitis, R. Zviedris, G. Strazdins, A. Mednis and L. Selavo, "SADmote: a robust and cost-effective device for environmental monitoring," in *International Conference on Architecture of Computing Systems*, 2012.

[257] J. Carroll, G. Paparisto and D. Vye, "The " Coffee-Can" Radar Redesigned as an Inexpensive RF PCB [Application Notes]," *IEEE Microwave Magazine,* vol. 17, no. 10, pp. 62-74, 2016.

[258] G. L. Charvat, A. J. Fenn and B. T. Perry, "The MIT IAP Radar Course: Build a Small Radar System Capable of Sensing Range, Doppler, and Synthetic Aperture (SAR) Imaging*," in *IEEE Radar Conference*, 2012.

[259] G. E. Coxson and E. Keyes, "The Coffee-Can radar at the naval academy," *The Journal of the Acoustical Society of America,* vol. 142, no. 4, pp. 2698-2698, 2017.

[260] H. E. M. Barlow, "Waveguide survey," *Electronics and Power,* vol. 10, no. 10, pp. 332-338, 1964.

[261] R. Duncan and F. Hinchey, "Cylindrical antenna theory," *J. Res,* vol. NBS D, no. 64, pp. 569-584, 1960.

[262] R. WP King and T. Wu, "The thick tubular transmitting antenna," *Radio Science,* vol. 2, no. 9, pp. 1061-1065, 1967.

[263] R. King and H. C., "Cylindrical shields," *IRE Transactions on Antennas and Propagation,* vol. 9, no. 2, pp. 166-170, 1961.

[264] B. Huang, M. Xu and D. Sharma, "Effects of antenna polarization on RSSI based location identification," in *11th International Conference on Advanced Communication Technology*, 2009.

[265] M. Malajner, P. Planinsic and D. Gleich, "Angle of arrival estimation using RSSI and omnidirectional rotatable antennas," *IEEE Sensors Journal,* vol. 12, no. 6, pp. 1950-1957, 2011.

[266] C.-H. Ko, "RFID 3D location sensing algorithms," *Automation in Construction,* vol. 19, no. 5, pp. 588-595, 2010.

[267] A. Kulaib, R. Shubair, M. Al-Qutayri and J. Ng, “An overview of localization techniques for wireless sensor networks,” 2011.

[268] H. Liu, H. Darabi, P. Banerjee and J. Liu, “Survey of wireless indoor positioning techniques and systems,” *IEEE Transactions on Systems, Man, and Cybernetics, Part C (Applications and Reviews),* vol. 37 , no. 6, pp. 1067-1080, 2007.

[269] S. Gezici, “A survey on wireless position estimation,” vol. 44, no. 3, pp. 263-282, 2008.

[270] B.-C. Liu, K.-H. Lin and J.-C. Wu, “Analysis of hyperbolic and circular positioning algorithms using stationary signal-strength-difference measurements in wireless communications,” vol. 55, no. 2, pp. 499-509, 2006.

[271] J. C. Lagarias, J. A. Reeds, M. H. Wright and P. E. Wright, “Convergence properties of the Nelder--Mead simplex method in low dimensions,” vol. 9, no. 1, pp. 112-147, 1998.

[272] G. Lui, T. Gallagher, B. Li, A. G. Dempster and C. Rizos, “Differences in RSSI readings made by different Wi-Fi chipsets: A limitation of WLAN localization,” in *International conference on localization and GNSS (ICL-GNSS)*, 2011.

[273] Z. Ma, S. Poslad, J. Bigham, X. Zhang and L. Men, “A BLE RSSI ranking based indoor positioning system for generic smartphones,” in *Wireless Telecommunications Symposium (WTS)*, 2017.

[274] J. Straub, “In search of technology readiness level (TRL) 10,” *Aerospace Science and Technology,* vol. 46, pp. 312-320, 2015.

[275] J. Lindh, “Bluetooth® low energy Beacons (SWRA475),” Texas Instruments, 2016.

[276] M. Herrera Vargas, Indoor navigation using bluetooth low energy (BLE) beacons., Turku University of Applied Sciences, 2016.

Annexes

Table A1. RF target located outside vehicle's cabin, the empirical data model calculations.

Empirical Results for Outside Location										
Sensor no	A(2D: 5.2m)					B(2D: 3.8m)				
	d[m]	Rd[m]	Md[m]	RMSE(d, Rd)	RMSE(d, Md)	d[m]	Rd[m]	Md[m]	RMSE(d, Rd)	RMSE(d, Md)
5	5.222	4.350	4.068	0.872	1.154	4.044	5.000	4.863	0.956	0.819
6	5.205	3.900	3.080	1.305	2.125	4.021	4.700	4.078	0.679	0.057
5	5.318	5.200				4.138	5.200			
6	5.320	1.750	2.841	3.570	2.479	4.140	3.050	3.804	1.090	0.336
RMSE Min				0.872	1.154				0.679	0.057
RMSE Max				3.570	2.479				1.090	0.819
Sensor no	C(2D: 2.6m)					D(2D: 1.4m)				
	d[m]	Rd[m]	Md[m]	RMSE(d, Rd)	RMSE(d, Md)	d[m]	Rd[m]	Md[m]	RMSE(d, Rd)	RMSE(d, Md)
5	2.883	3.300	3.212	0.417	0.329	1.775	1.200	1.240	0.575	0.535
6	2.851	3.100	2.544	0.249	0.308	1.723	2.200	1.921	0.477	0.198
5	2.973	2.800				1.855	2.900			
6	2.976	1.600	2.236	1.376	0.741	1.859	1.400	1.657	0.459	0.203
5	2.883	3.300	3.245	0.417	0.362	1.775	1.200	1.835	0.575	0.060
6	2.851	3.100	3.096	0.249	0.245	1.723	2.200	2.320	0.477	0.597
5	2.973	2.800	2.859	0.173	0.114	1.855	2.900	2.170	1.045	0.316
6	2.976	1.600				1.859	1.400			
5	2.883	3.300	3.157	0.417	0.273	1.775	1.200	1.914	0.575	0.138
6	2.851	3.100				1.723	2.200			
5	2.973	2.800	2.862	0.173	0.111	1.855	2.900	2.020	1.045	0.165
6	2.976	1.600	1.682	1.376	1.295	1.859	1.400	1.628	0.459	0.232
5	2.883	3.300				1.775	1.200			
6	2.851	3.100	2.540	0.249	0.311	1.723	2.200	1.955	0.477	0.232
5	2.973	2.800	2.730	0.173	0.243	1.855	2.900	2.779	1.045	0.924
6	2.976	1.600	2.222	1.376	0.754	1.859	1.400	1.758	0.459	0.102
5	2.883	3.300	3.204	0.417	0.321	1.775	1.200	1.826	0.575	0.051
6	2.851	3.100	2.543	0.249	0.308	1.723	2.200	1.778	0.477	0.055
5	2.973	2.800	2.809	0.173	0.164	1.855	2.900	2.058	1.045	0.203
6	2.976	1.600	2.234	1.376	0.742	1.859	1.400	2.064	0.459	0.204
RMSE Min				0.173	0.111				0.459	0.051
RMSE Max				1.376	1.295				1.045	0.924

Table A2. RF target located outside vehicle's cabin, the theoretical data model calculations**.**

Theoretical Results for Outside Location										
Sensor no	A(2D: 5.2m)					B(2D: 3.8m)				
	d[m]	Rd[m]	Md[m]	RMSE(d, Rd)	RMSE(d, Md)	d[m]	Rd[m]	Md[m]	RMSE(d, Rd)	RMSE(d, Md)
5	5.222	4.600	4.410	0.622	0.812	4.044	5.200			
6	5.205	3.500	3.202	1.705	2.003	4.021	4.050		0.029	
5	5.318	5.200				4.138	5.200			
6	5.320	2.550	3.034	2.770	2.285	4.140	2.700		1.440	
RMSE Min				0.622	0.812				0.029	0.000
RMSE Max				2.770	2.285				1.440	0.000
Sensor no	C(2D: 2.6m)					D(2D: 1.4m)				
	d[m]	Rd[m]	Md[m]	RMSE(d, Rd)	RMSE(d, Md)	d[m]	Rd[m]	Md[m]	RMSE(d, Rd)	RMSE(d, Md)
5	2.883	3.600	3.469	0.717	0.586	1.775	1.250	1.270	0.525	0.505
6	2.851	3.350	2.706	0.499	0.145	1.723	2.050	1.905	0.327	0.182
5	2.973	3.600				1.855	2.350			
6	2.976	1.650	2.415	1.326	0.561	1.859	1.500	1.634	0.359	0.225
5	2.883	3.600	3.600	0.717	0.717	1.775	1.250	1.608	0.525	0.167
6	2.851	3.350	3.350	0.499	0.499	1.723	2.050	2.122	0.327	0.399
5	2.973	3.600	3.600	0.627	0.627	1.855	2.350	1.939	0.495	0.084
6	2.976	1.650				1.859	1.500			
5	2.883	3.600	3.520	0.717	0.637	1.775	1.250	1.678	0.525	0.098
6	2.851	3.350				1.723	2.050			
5	2.973	3.600	3.279	0.627	0.306	1.855	2.350	1.829	0.495	0.025
6	2.976	1.650	2.050	1.326	0.926	1.859	1.500	1.636	0.359	0.224
5	2.883	3.600				1.775	1.250			
6	2.851	3.350	2.717	0.499	0.134	1.723	2.050	1.935	0.327	0.212
5	2.973	3.600	3.383	0.627	0.410	1.855	2.350	2.329	0.495	0.474
6	2.976	1.650	2.488	1.326	0.488	1.859	1.500	1.633	0.359	0.226
5	2.883	3.600	3.696	0.717	0.812	1.775	1.250	1.602	0.525	0.173
6	2.851	3.350	2.709	0.499	0.143	1.723	2.050	1.722	0.327	0.001
5	2.973	3.600	3.318	0.627	0.345	1.855	2.350	1.855	0.495	0.000
6	2.976	1.650	2.465	1.326	0.511	1.859	1.500	1.982	0.359	0.122
RMSE Min				0.499	0.134				0.327	0.000
RMSE Max				1.326	0.926				0.525	0.505

Table A3. RF target located inside vehicle's cabin, the empirical data model calculations.

Empirical Results for Inside Location										
Sensor no	AA(Right Front)					BB(Left Front)				
	d[m]	Rd[m]	Md[m]	RMSE(d, Rd)	RMSE(d, Md)	d[m]	Rd[m]	Md[m]	RMSE(d, Rd)	RMSE(d, Md)
1	0.574	0.850	0.850	0.276	0.276	1.276	1.200	1.200	0.076	0.076
2	1.463	2.350				1.855	2.150			
3	1.279	5.200				0.576	0.700	0.700	0.124	0.124
4	1.857	1.900				1.464	1.700	1.700	0.236	0.236
1	0.774	1.950				1.311	1.300			
2	1.503	1.100	1.100	0.403	0.403	1.839	1.800			
3	1.314	1.250	1.250	0.064	0.064	0.774	5.200			
4	1.840	2.700				1.503	2.250			
RMSE Min				0.064	0.064					
RMSE Max				0.403	0.403					
	CC(Right Rear)									
	d[m]	Rd[m]	Md[m]	RMSE(d, Rd)	RMSE(d, Md)					
1	1.680	2.000				1.276	1.200	1.200	0.076	0.076
2	1.348	0.600	0.710	0.748	0.637	1.855	2.150			
3	1.235	4.200				0.576	0.700	0.700	0.124	0.124
4	0.720	0.650	1.011	0.070	0.291	1.464	1.700			
1	1.539	3.000				1.311	1.300	1.300	0.011	0.011
2	1.376	2.400				1.839	1.800			
3	1.117	3.050				0.774	5.200			
4	0.880	1.450	1.120	0.570	0.239	1.503	2.250			
RMSE Min				0.070	0.239					
RMSE Max				0.748	0.637					
	DD(Left Rear)									
	d[m]	Rd[m]	Md[m]	RMSE(d, Rd)	RMSE(d, Md)					
1	1.235	0.900	0.933	0.335	0.301	1.276	1.200	1.200	0.076	0.076
2	0.719	1.700	1.515	0.981	0.796	1.855	2.150			
3	1.683	4.450				0.576	0.700			
4	1.351	2.250				1.464	1.700	1.700	0.236	0.236
1	1.117	2.950				1.311	1.300	1.300	0.011	0.011
2	0.880	1.100	1.281	0.220	0.402	1.839	1.800			
3	1.541	2.950				0.774	5.200			
4	1.379	1.800				1.503	2.250			
RMSE Min				0.220	0.301					
RMSE Max				0.981	0.796					
1						1.276	1.200			
2						1.855	2.150			
3						0.576	0.700	0.700	0.124	0.124
4						1.464	1.700	1.700	0.236	0.236
1						1.311	1.300	1.300	0.011	0.011
2						1.839	1.800			
3						0.774	5.200			
4						1.503	2.250			
1						1.276	1.200	1.188	0.076	0.088
2						1.855	2.150			
3						0.576	0.700	0.698	0.124	0.123
4						1.464	1.700	1.697	0.236	0.233
1						1.311	1.300	1.312	0.011	0.001
2						1.839	1.800			
3						0.774	5.200			
4						1.503	2.250			
RMSE Min									0.011	0.001
RMSE Max									0.236	0.236

Table A4. RF target located inside vehicle's cabin, the theoretical data model calculations.

Theoretical Results for Inside Location										
Sensor no	AA(Right Front)					BB(Left Front)				
	d[m]	Rd[m]	Md[m]	RMSE(d, Rd)	RMSE(d, Md)	d[m]	Rd[m]	Md[m]	RMSE(d, Rd)	RMSE(d, Md)
1	0.574	0.950	0.950	0.376	0.376	1.276	1.300	1.300	0.024	0.024
2	1.463	1.950				1.855	3.000			
3	1.279	5.200				0.576	0.800	0.800	0.224	0.224
4	1.857	1.600	1.600	0.257	0.257	1.464	2.050			
1	0.774	1.850				1.311	1.150	1.150	0.161	0.161
2	1.503	1.350	1.350	0.153	0.153	1.839	2.450			
3	1.314	1.200				0.774	5.200			
4	1.840	2.900				1.503	2.250			
RMSE Min									0.024	0.024
RMSE Max									0.224	0.224
						CC(Right Rear)				
						d[m]	Rd[m]	Md[m]	RMSE(d, Rd)	RMSE(d, Md)
1	0.574	0.950	0.950	0.376	0.376	1.680	2.300			
2	1.463	1.950				1.348	0.600	0.682	0.748	0.666
3	1.279	5.200				1.235	5.200			
4	1.857	1.600	1.600	0.257	0.257	0.720	0.700	0.928	0.020	0.207
1	0.774	1.850				1.539	2.600			
2	1.503	1.350				1.376	2.150			
3	1.314	1.200	1.200	0.114	0.114	1.117	2.750			
4	1.840	2.900				0.880	1.200	1.013	0.320	0.133
RMSE Min									0.020	0.133
RMSE Max									0.748	0.666
						DD(Left Rear)				
						d[m]	Rd[m]	Md[m]	RMSE(d, Rd)	RMSE(d, Md)
1	0.574	0.950	0.950	0.376	0.376	1.235	1.150		0.085	
2	1.463	1.950				0.719	2.050			
3	1.279	5.200				1.683	5.200			
4	1.857	1.600				1.351	2.300			
1	0.774	1.850				1.117	2.800			
2	1.503	1.350	1.350	0.153	0.153	0.880	1.300		0.420	
3	1.314	1.200	1.200	0.114	0.114	1.541	2.750			
4	1.840	2.900				1.379	2.450			
RMSE Min									0.085	0.000
RMSE Max									0.420	0.000
1	0.574	0.950								
2	1.463	1.950								
3	1.279	5.200								
4	1.857	1.600	1.600	0.257	0.257					
1	0.774	1.850								
2	1.503	1.350	1.600	0.153	0.097					
3	1.314	1.200	1.200	0.114	0.114					
4	1.840	2.900								
1	0.574	0.950	0.963	0.376	0.388					
2	1.463	1.950								
3	1.279	5.200								
4	1.857	1.600	1.618	0.257	0.239					
1	0.774	1.850								
2	1.503	1.350	1.587	0.153	0.084					
3	1.314	1.200	1.191	0.114	0.123					
4	1.840	2.900								
RMSE Min				0.114	0.084					
RMSE Max				0.376	0.388					